NASA SP-333

Design of Various Fixed-Geometry Water-Lubricated Hydrodynamic Journal Bearings for Maximum Stability

Schuller

NATIONAL AERONAUTICS AND SPACE ADMINISTRATION

NASA SP–333

Design of Various Fixed-Geometry Water-Lubricated Hydrodynamic Journal Bearings for Maximum Stability

Fredrick T. Schuller

Lewis Research Center

Prepared at Lewis Research Center

Scientific and Technical Information Office 1973
NATIONAL AERONAUTICS AND SPACE ADMINISTRATION
Washington, D.C.

PREFACE

This publication is the result of over 260 fractional-frequency-whirl stability tests on a variety of fixed-geometry journal bearings. It is intended principally as a guide in the selection and design of antiwhirl bearings that must operate at high speeds and low loads in low-viscosity fluids such as water or liquid metals. However, the various fixed-geometry configurations can be employed as well in applications where other lubricants, such as oil, are used and fractional-frequency whirl is a problem. The important parameters that affect stability are discussed for each bearing type, and design curves to facilitate the design of optimum-geometry bearings are included. A comparison of the stability of the different bearing configurations tested is also given.

Page intentionally left blank

Page intentionally left blank

CONTENTS

INTRODUCTION

The ability of a journal bearing to inhibit self-excited fractional-frequency whirl is of prime importance for successful operation of rotating machinery at conditions of high speed and low load with a low-viscosity fluid, such as water, as the lubricant. In this type of whirl, the journal center orbits the bearing center at an angular velocity about one-half that of the journal around its own center. Such whirling can fail a bearing, if the amplitude of whirl grows and is not limited. It is desirable, therefore, to select a bearing geometry that has a high degree of stability.

Tilting-pad bearings are exceptionally stable but are complex since they are composed of several parts and may be subject to pivot surface damage (ref. 1). Fixed-geometry bearings do not have the disadvantage of complexity, but they are not as stable as tilting-pad bearings. The tilting-pad bearing, because of its movable pads, directs the lubricant film reaction force of the bearing into the line of action of the applied load on the journal, and this force tends to stabilize the bearing. This stabilization is not possible with a fixed-geometry bearing. It is known, however, that discontinuous films, such as those produced by steps and grooves, tend to stabilize a bearing (ref. 2). One bearing that shows good stability properties is the herringbone journal mated with a plain bearing (fig. 1). The bearing acts as a viscous pump, pumping fluid along the grooves and increasing fluid pressure within the bearing. This self-pressurization effect can be used to control the attitude angle of the bearing and thereby improve bearing stability. Most of the theoretical and experimental work on herringbone journals has dealt with compressible lubricants (refs. 3 to 5), and there has been very little information available on incompressible lubricants (refs. 6 and 7). The experimental data presented in this report are for incompressible lubricants.

Theoretical analysis of the herringbone journal assumes an infinite number of grooves (ref. 5). It would be of interest to observe experimentally how bearing stability is affected by a variation in the finite number of grooves in such a bearing.

C-68-2882

Plain bearing

10 Partial grooves

20 Partial grooves

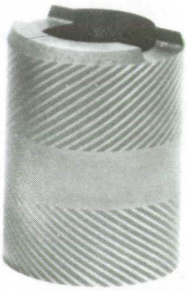

C-68-2881

40 Partial grooves

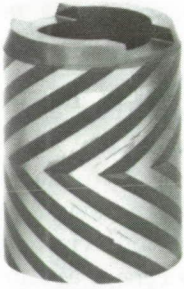

10 Full grooves

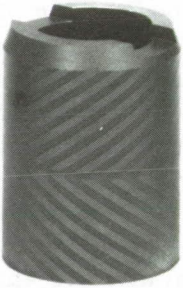

20 Full grooves

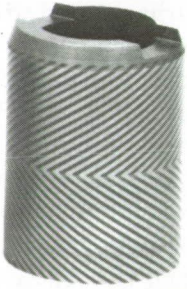

C-68-2880

40 Full grooves

(a) Configurations investigated.

Figure 1. - Herringbone-groove journals.

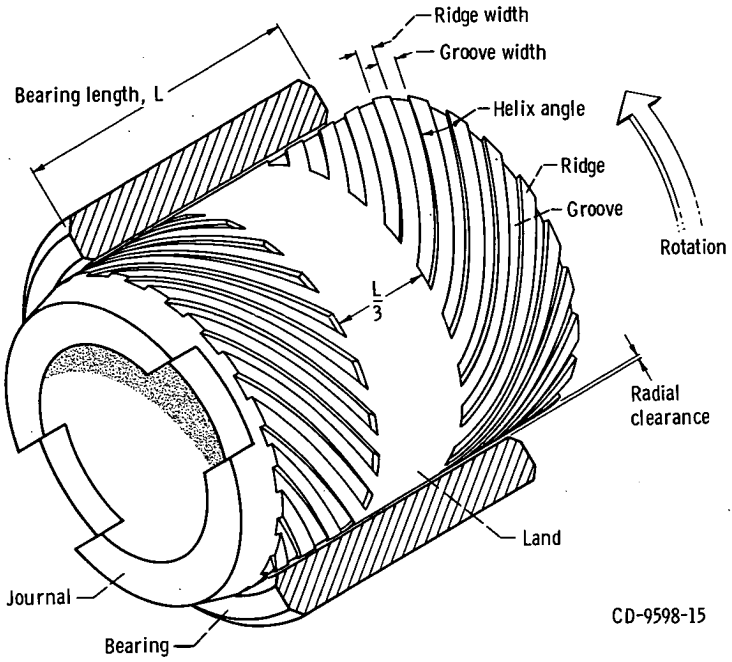

(b) Bearing assembly.

Figure 1. - Concluded.

Further, theory for incompressible flow predicts maximum stability at a film thickness ratio of 2.1 (ref. 5). Experimental verification of this prediction would be desirable. Film thickness ratio can be varied by either maintaining constant groove depth while varying the radial clearance or varying the groove depth while maintaining constant radial clearance. In these experiments, because of the strong influence of radial clearance on stability, both clearance and groove depth were varied so that the effects of varying film thickness ratio could be studied independently of radial clearance.

There is one fixed-geometry journal bearing configuration, the Rayleigh step bearing (fig. 2), that has had very little investigation as far as stability characteristics are concerned. For this reason and because analysis has shown that the single-step Rayleigh step journal bearing will carry a substantial load even though the bearing is in a concentric position (ref. 8), its stability characteristics were investigated experimentally. In this

report a pad is defined as a combination of feed groove and step and ridge regions. A segment is defined as an independently acting 360° region; it may incorporate one or more pads.

A Rayleigh step bearing with only a single pad in its circumference results in maximum load capacity (ref. 9). However, it has the disadvantage that the load capacity varies considerably with the direction of the applied load. In spite of this disadvantage, the stability of this type of bearing (see fig. 2(a)) was investigated. Two other Rayleigh step bearing configurations were also chosen for testing. One utilizes the single-pad configuration and is composed of three circumferential segments side by side (fig. 2(b)). Each segment, with a length one-third the entire bearing length, contains one pad and is displaced 120° circumferentially with respect to the other segments. The symmetry thus achieved largely eliminates the disadvantage of anisotropy. The other configuration consists of three pads extending the entire length of the bearing, as shown in figure 2(c). The ridge- to pad-arc ratio ψ is defined as the ratio of the arc subtended by the ridge to the arc subtended by the pad (fig. 2(d)). The trisymmetrical arrangements were selected mainly to enable direct comparison of stability data with three-lobe bearings also covered in this investigation.

Another fixed-geometry bearing that has shown promise is the lobed bearing (refs. 10 and 11), which has a marked simi-

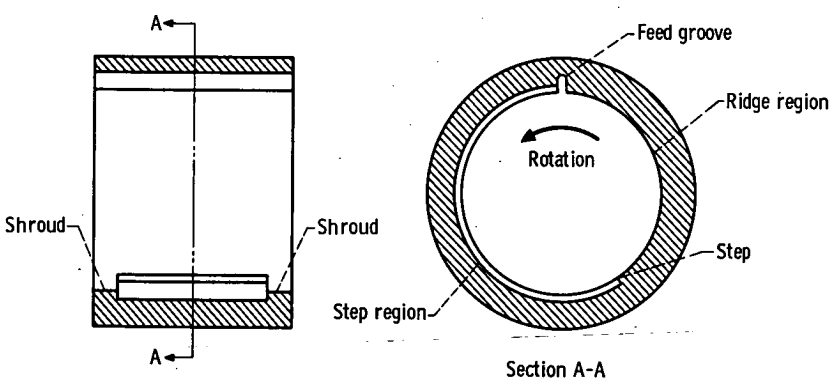

(a) One-segment, one-pad shrouded Rayleigh step journal bearing.

Figure 2. - Rayleigh step bearing.

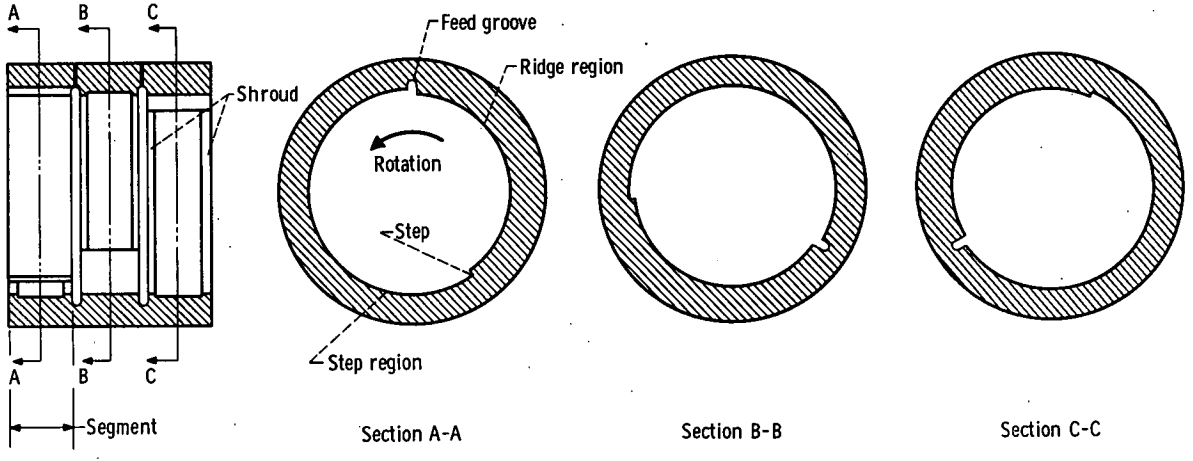

(b) Three-segment, one-pad shrouded Rayleigh step journal bearing.

Figure 2. - Continued.

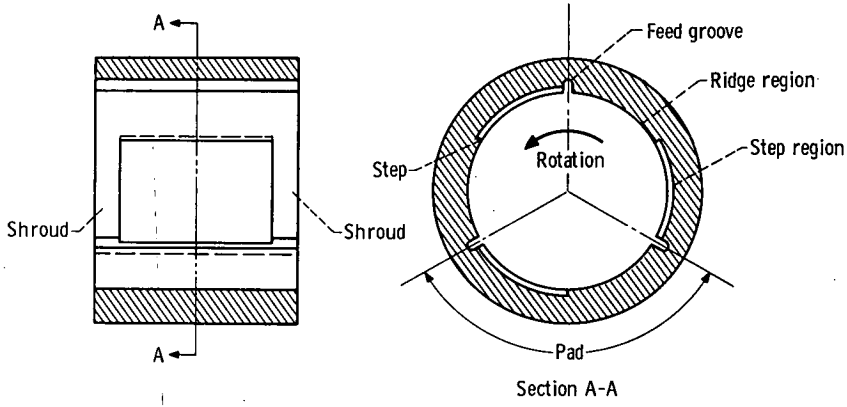

(c) One-segment, three-pad shrouded Rayleigh step journal bearing.

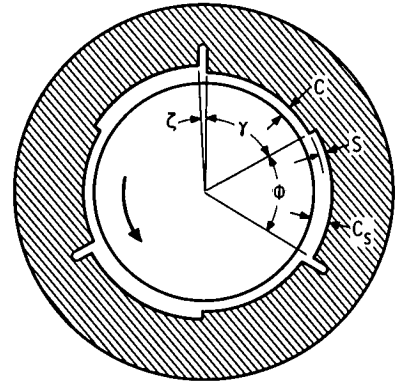

(d) Rayleigh step bearing geometry. Ridge-to pad-arc ratio $\psi = \gamma/(\gamma + \varphi + \zeta)$; film thickness ratio $k_r = C_s/C$.

Figure 2. - Concluded.

larity to the tilting-pad bearing except that its pads (lobes) are fixed in one position. Most of the research on lobed-bearing stability has been done with bearings that are centrally lobed (fig. 3), which result in converging-diverging films. In a centrally lobed bearing, only the converging-wedge position of the arc of each lobe is active in generating load capacity. If the lobe is tilted toward the shaft at the trailing edge of the lobe, as in figure 4(b), the minimum film thickness occurs nearer the trailing edge of the lobe, and a pressure profile is built up over a large portion of the lobe arc, which increases its load capacity (ref. 12). Reference 12 reports an improvement in the stability of a tilted-lobe bearing over those of centrally lobed bearings.

In the investigations on lobed bearings (refs. 10 to 12), the nonrotating member (the bearing) had the lobed contour and was run with a plain rotating journal. Reference 11 reports an analytical investigation of a centrally lobed rotor with three or more lobes running stably in a plain bearing. Also included are some experimental results for a three-central-lobe rotor, which verify the theoretical analysis. In the investigation described in this report, three-lobe journals with lobes tilted so that the minimum film thickness occurs at their trailing edges (fig. 5(a)) and centrally lobed journals (fig. 5(b)) were run with plain bearings. Tilted-lobe journals were tested because of previous reports that tilted-lobe bearings had increased stability over those of centrally lobed bearings run with plain journals (ref. 12).

The objectives of this study were (1) to determine the important parameters that affect the stability of the various fixed-geometry bearings tested, (2) to generate design curves to facilitate the design of optimum-geometry bearings, and (3) to compare the stability of the different bearing configurations.

This work was originally reported in references 13 to 18.

The following types of fixed-geometry journal bearings were tested: (1) herringbone journals mated with plain bearings, (2) Rayleigh step bearings, (3) three-lobe bearings, and (4) three-lobe journals mated with plain bearings.

The test bearings had a nominal 3.8-centimeter (1.5-in.) diameter and a length-diameter ratio L/D of unity. They were submerged in water at an average temperature of 300 K (80° F) and were operated hydrodynamically with zero load.

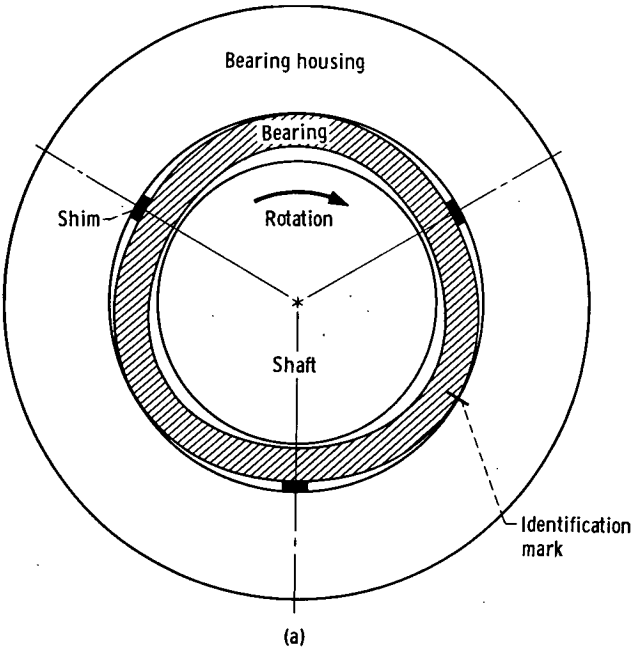

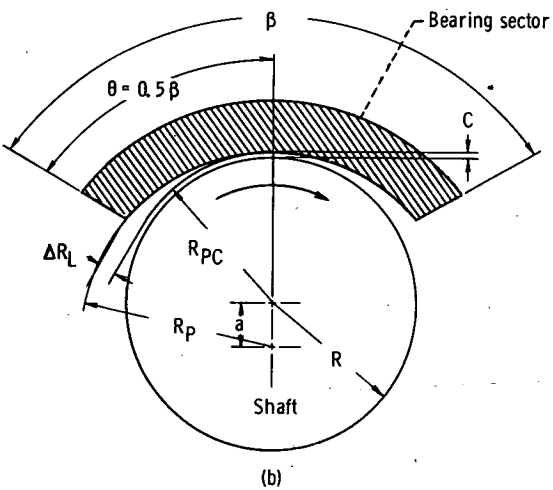

(a) Bearing assembly.

(b) Bearing geometry. Offset factor $\alpha = \theta/\beta = 0.5$.

Figure 3. - Three-central-lobe bearing.

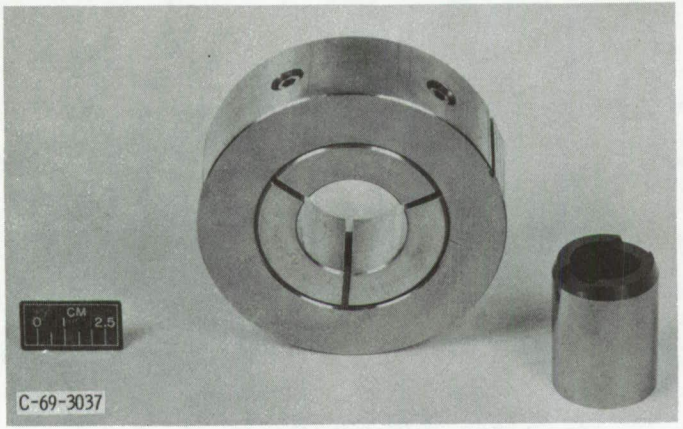

(a) Assembled bearing configuration.

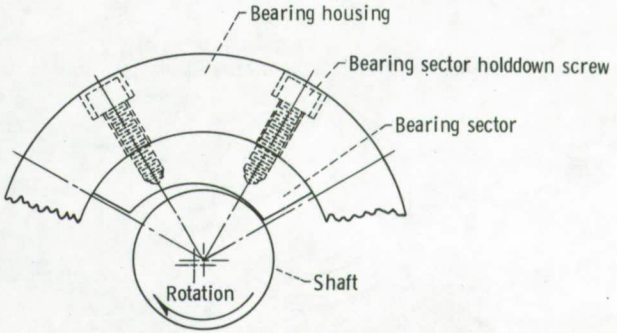

(b) Bearing sector assembly.

Figure 4. - Three-tilted-lobe bearing.

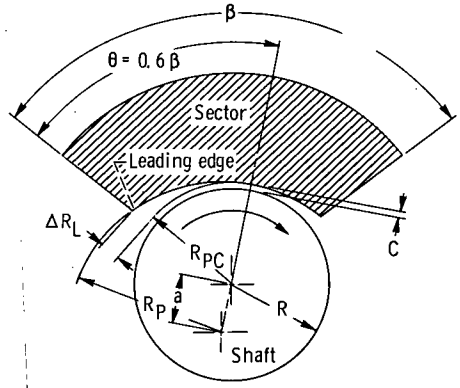

(c) Converging-diverging configuration. Offset factor $\alpha = \theta/\beta = 0.6$.

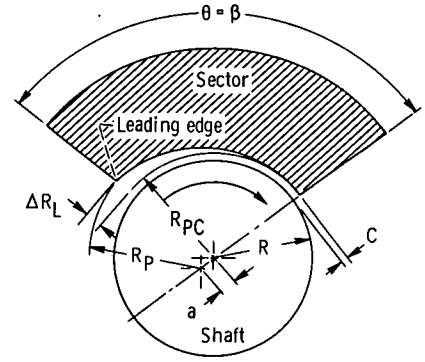

(d) Wholly converging configuration. Offset factor $\alpha = \theta/\beta = 1.0$.

Figure 4. - Concluded.

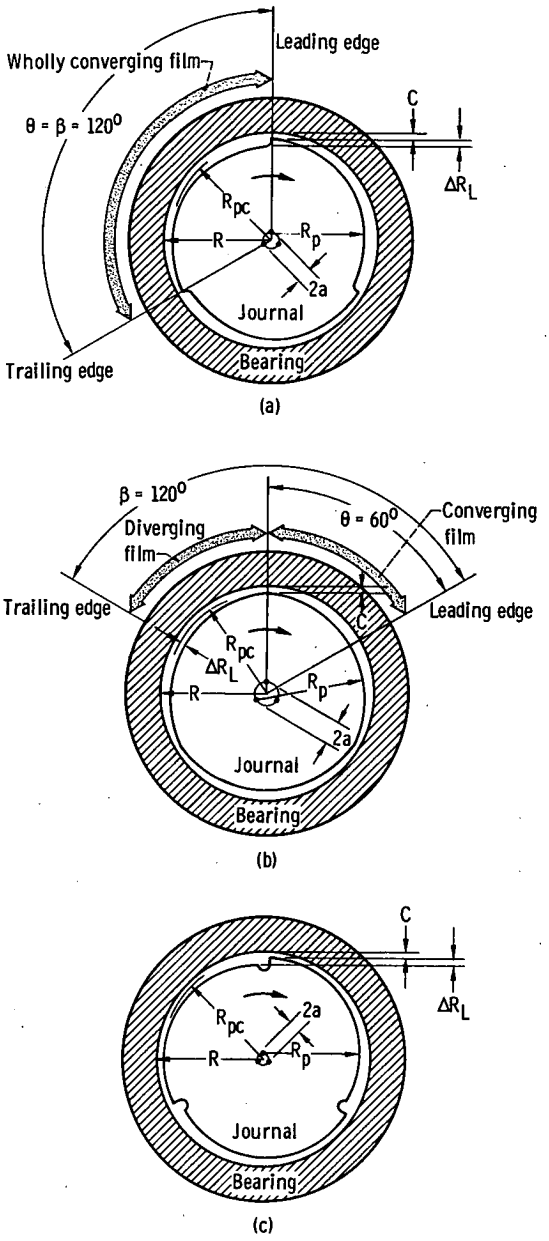

(a) Tilted-lobe (wholly converging) configuration. Offset factor $\alpha = \theta/\beta = 1.0$.

(b) Centrally lobed (converging-diverging) configuration. Offset factor $\alpha = \theta/\beta = 0.5$.

(c) Tilted-lobe (wholly converging) configuration with three axial grooves.

Figure 5. - Three-lobe journal geometry.

SYMBOLS

a	preload (ellipticity), mm; in.
C	bearing radial clearance, mm; in.
C_s	radial clearance in step region when bearing and journal are concentric, C + S, mm; in.
C_0	bearing radial clearance at zero preload, $R_P - R$, mm; in.
D	journal diameter, cm; in.
g	gravitational constant, m/sec^2; in. $/sec^2$
H	herringbone-groove film thickness ratio, ratio of groove clearance to ridge clearance, h_g/C
H_L	lobe height, cm; in.
h_g	groove clearance, C + S, mm; in.
k	film thickness ratio for tilted-lobe bearings and journals, $1 + \Delta R_L/C$
k_c	film thickness ratio for centrally lobed bearings, $1 + H_L/C$
k_r	film thickness ratio for Rayleigh step bearings, C_s/C
L	bearing length, cm; in.
L_1	length of grooved portion of bearing, cm; in.
M	rotor mass per bearing, W_r/g, kg; $(lb)(sec^2)/in.$
$\overline{M}$	dimensionless mass parameter, $MP_a(C/R)^5/2\mu^2L$
$\overline{M}_0$	dimensionless rotor mass parameter, $C_0MN_S/\mu DL(R/C_0)^2$ (ref. 10)
N_S	journal speed, rps
N_W	journal fractional-frequency-whirl onset speed at zero load, rpm
P_a	atmospheric pressure, N/m^2; psia
R	journal or bearing radius, cm; in.
ΔR_L	leading-edge entrance wedge thickness, mm; in.
R_P	lobe radius, cm; in.
R_{PC}	radius of pitch circle, cm; in.
S	depth of herringbone groove or Rayleigh step, mm; in.
W_r	total weight of test vessel (rotor), N; lb
α	offset factor, θ/β

β sector arc length, deg

Γ dimensionless speed parameter, $6\mu\omega R^2/P_a C^2$

γ angle subtended by ridge in Rayleigh step bearing, deg

δ preload coefficient, $a/(R_P - R)$

ζ angle subtended by lubrication groove in Rayleigh step bearing, deg

θ arc length from leading edge of sector to line along which lobe is preloaded radially, deg

μ lubricant dynamic viscosity, $(N)(sec)/m^2$; $(lb)(sec)/in.^2$

φ angle subtended by step region in Rayleigh step bearing, deg

ψ ratio of ridge angle to total angle of ridge-step-groove combination, ridge- to pad-arc ratio in Rayleigh step bearing, $\gamma/(\gamma + \varphi + \zeta)$

ω journal angular speed, rad/sec

APPARATUS

Test Bearings and Journals

The assembled bearing in all cases had a nominal 3.8-centimeter (1.5-in.) diameter and an L/D of unity. The inside surfaces of the bearings and the outside surfaces of the journals were machined to a root-mean-square finish of 0.1 to 0.2 micrometer (4 to 8 μin.). The journals were made of stainless steel or Stellite material and the bearings of bronze. Run-out of the journals on the test shaft average 5 micrometers (200 μin.).

Herringbone journals mated with plain bearings. - Herringbone journals of six configurations, three journals having 10, 20, and 40 full grooves and three having 10, 20, and 40 partial grooves (fig. 1), were evaluated. Grooving extended beyond the bearing sleeves at each end to ensure an adequate lubricant supply. The partially grooved journals had a circumferential land centrally located along the length of the bearing. The width of the circumferential land was one-third the length of the bearing (fig. 1(b)). The fully grooved journals had herringbone grooves that met midway along the axial length of the bearing. Circumferential surface profile traces were made of each jour-

nal outside diameter in two planes along the length of the journal to obtain the average groove depths listed in table I. A typical surface profile trace is shown in figure 6. To reduce the number of new journals required, the outside surfaces of the journals with large groove depths were ground after testing to reduce the groove depths, and the journals were reused. Surface profile traces were made after each grinding operation to determine the new average groove depth.

The herringbone-groove journal helix angle and groove- to ridge-width ratio (table I) were set at those values which yield a maximum radial force at a compressibility number of zero for a compressible lubricant (ref. 5), which approximated the conditions existing with an incompressible lubricant. Because of manufacturing difficulties, the maximum number of grooves was set at 40 for this investigation.

TABLE I. - HERRINGBONE-GROOVE JOURNAL GEOMETRIES

[Helix angle, 33°.]

Journal	Groove depth, S		Groove type	Number of grooves	Groove width		Ridge width	
	mm	μin.			mm	in.	mm	in.
1	0.015	590	Partial	40	0.813	0.032	0.813	0.032
2	.016	620	Full					
3	.035	1380	Full					
4	.043	1700	Partial					
5	0.010	410	Partial	20	1.626	0.062	1.626	0.062
6	.018	700	Full					
7	.036	1400	Partial					
8	.042	1640	Full					
9	0.009	340	Partial	10	2.438	0.128	2.438	0.128
10	.018	700	Partial					
11	.024	960	Full					
12	.032	1280	Partial					
13	.036	1420	Full					
14	.034	1350	Full					
15	.068	2660	Partial					
16	.085	3350	Partial					

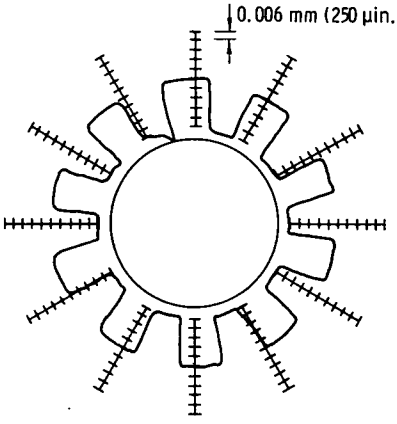

Figure 6. - Herringbone-groove circumferential surface profile trace of journal 12.

Rayleigh step bearings. - Terms which will be used in the description of the Rayleigh step bearing are defined as follows:

Configuration	Relative disposition of pads and segments (figs. 2(a) to (c))
Feed groove	Axial groove that runs the length of the segment and feeds lubricant to the bearing (fig. 2(c); although not shown in this figure, the depth of the feed groove is orders of magnitude deeper than the film thickness)
Geometry	Arc lengths and step depths that describe the step and ridge regions (fig. 2(d))
Pad	A combination of feed groove and step and ridge regions (fig. 2(c))
Ridge region	Raised area of pad not including the shrouds (fig. 2)
Segment	An independently acting 360° region; it may incorporate one or more pads (fig. 2(b))
Shroud	Side rails at the axial ends of the segment in the step region that act as a dam (fig. 2)
Step region	Relieved area of a pad (fig. 2)

Rayleigh step bearings of four different configurations were evaluated (fig. 2). One consisted of one segment running the

length of the bearing with one pad in its circumference, as shown in figure 2(a). Another consisted of three circumferential segments of equal length, side by side, separated from each other by grooves, as shown in figure 2(b). Each segment contained one pad that was displaced 120° circumferentially with respect to the others to achieve symmetry in the bearing. The length of each segment was one-third the total length of the bearing. One set of such bearings had a ridge- to pad-arc ratio ψ (fig. 2(d)) of 0.40, and another set had a ψ of 0.49. These ridge- to pad-arc ratios were selected on the basis of the load capacity results of reference 8. Since the load capacity curve of reference 8 has a rather flat peak, both arc ratios represent conditions which yield maximum load capacity for a single-pad Rayleigh step bearing at the small eccentricity ratios (ϵ = 0 to 0.3) that can be expected with a bearing under zero load.

The third Rayleigh step bearing configuration that was evaluated is shown in figure 2(c). It consisted of three pads extending the entire length of the bearing. One set of such bearings had a ridge- to pad-arc ratio ψ of 0.27, and another set had a ψ of 0.45. The ratios chosen were based on analytical work on load capacity for three-pad Rayleigh step bearings at an eccentricity ratio of 0.1 reported in reference 19.

One of the one-segment, three-pad bearings with shrouds and a ridge- to pad-arc ratio ψ of 0.45 had its shrouds machined off after it was tested. It was then rerun without shrouds. This was the fourth configuration tested.

The width of the shroud was 1.5 millimeters (0.06 in.) for the three-segment, single-pad bearing and 4.8 millimeters (0.19 in.) for the one-segment, three-pad bearings and the one-segment, one-pad bearings. The bottom corners of the steps in the bearings were not sharp but had a machined radius of approximately 0.97 centimeter (0.38 in.).

Figure 2(d) shows the parameters that define the Rayleigh step bearing geometry. The angle γ is defined as the angle subtended by the ridge region; φ, the angle subtended by the step region; and ζ, the angle subtended by the lubrication groove. The angle ζ is included since it was used in the analysis of references 8 and 9. Although this angle is normally small and may not be important for the one- and three-step configurations employed in this investigation, it can become important in an analysis of a Rayleigh step bearing with a large

number of pads. The symbol C in figure 2(d) is the radial clearance between the journal and the ridge region, and C_s is the radial clearance in the step region when the journal is in a concentric position in the bearing. The depth of the step S is then $C_s - C$.

Three-central-lobe bearings. - Three-lobe bearings with and without axial grooves separating the lobes were evaluated. The bearings were lobed by the use of shims in a unique manner, as presented in a recent patent disclosure (ref. 20) and shown in figure 3(a). The procedure for fabricating a shimmed, lobed bearing is as follows:

(1) A plain cylindrical bearing is assembled without shims into a housing (fig. 3(a)), with a light interference fit by cooling the bearing or heating the housing and depositing the bearing in the housing.

(2) The bearing is machined in place to a predetermined round inside diameter, and an identification mark is scribed on the top surface of the bearing and housing.

(3) The bearing is removed from its housing by cooling the assembly. (If the expansion coefficient of the housing is greater than that of the bearing, heat can be used for the disassembly operation.)

(4) Equally spaced metal shims approximately 3 millimeters (1/8 in.) wide are placed axially around the inside diameter of the housing and are tack-welded or taped to the top and bottom of the bearing housing to prevent their dislocation. The thickness of the shims depends upon the lobe height desired.

(5) The bearing is assembled into the shimmed housing by cooling the bearing or heating the housing and placing the bearing in the housing with the identification marks on the bearing and housing lined up with each other.

(6) When the bearing and housing have reached thermal equilibrium, a profile trace of the inside diameter will indicate accurately what size lobing has been attained. The amount of lobing will depend upon the thickness of the shims and the physical properties of the bearing housing, shim stock, and bearing materials used.

A typical bearing assembly used in this report had the following dimensions:

Housing (stainless steel)	
Outside diameter, cm (in.)	10.79 (4.250)
Inside diameter, cm (in.)	5.0411 (1.9847)
Bearing (bronze)	
Outside diameter, cm (in.)	5.0419 (1.9850)
Inside diameter, cm (in.)	3.8199 (1.5039)
Interference fit between bearing and housing, mm (μin.)	0.008 (300)
Shim (steel)	
Width, mm (in.)	3 (1/8)
Thickness, mm (in.)	0.025 (0.0010)
Resultant lobe height of bearing, mm (in.)	0.025 (0.0010)

A typical circumferential profile trace of the inside surface of the shimmed test bearing is shown in figure 7. The height of the lobes H_L was determined from similar traces for each of the test bearings used in this study.

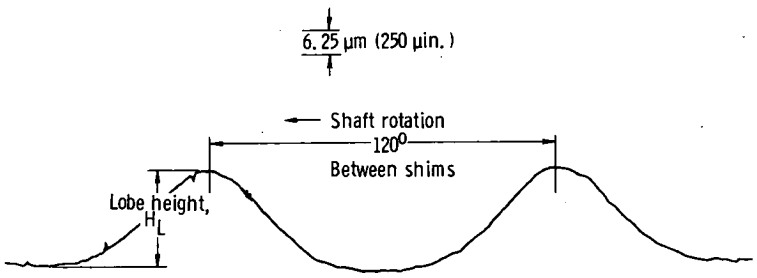

Figure 7. - Typical circumferential profile trace of inside surface of shimmed bearing.

Figure 3(b) shows the parameters which define the centrally lobed bearing geometry employed in this investigation. The angle θ is defined as the arc length from the leading edge of a sector to the line along which the lobe is preloaded radially. In this case $\theta = 0.5\,\beta$. The offset factor $\alpha = \theta/\beta$ for the centrally lobed bearing is, therefore, 0.5. The preload coefficient δ is equal to the preload a divided by the difference between the radius of the lobe and the radius of the journal $\delta = a/(R_P - R)$. In conventionally lobed bearings the lobe is machined in. However, in this case the lobe was generated by distortion of the bearing

wall, so the radius of the lobe R_P had to be calculated from the values of lobe height H_L obtained from the profile traces (fig. 7) of each bearing tested.

Three-tilted-lobe bearings. - Three-tilted-lobe bearings, consisting of three 115° sectors mounted in a solid housing by holddown screws (figs. 4(a) and (b)), were evaluated. Each sector of one particular bearing assembly was ground to its specified contour while it was the only sector assembled in the housing. Three sectors with identical internal contours were then assembled in a common housing to form a three-tilted-lobe bearing, as shown in figure 4(a).

Two different contours were employed in the bearing sectors to give one bearing a converging-diverging film (fig. 4(c)) in operation and another bearing a wholly converging film (fig. 4(d)). The converging-diverging contour was designed with the minimum radial clearance at a point approximately 60 percent of the sector arc length from the leading edge of each sector (fig. 4(c)). The wholly converging contour had a minimum radial clearance at the trailing edge of each sector (fig. 4(d)). Circumferential profile traces were made of the internal surface of each sector in each bearing assembly in three planes along the length of the bearing to obtain the leading-edge entrance wedge thicknesses ΔR_L (fig. 4). Typical surface profile traces are shown in figure 8, which illustrates how the ΔR_L values were obtained.

Three-lobe journals. - Basically two different contours were used in the journals to give one a wholly converging film profile in operation (fig. 5(a), offset factor α of 1.0) and another a converging-diverging film (fig. 5(b), offset factor of 0.5). A third configuration was obtained by machining three axial grooves in the journal with the wholly converging film (fig. 5(c)). Figure 5 also shows the parameters which define the wholly converging, or tilted-lobe, journal and the converging-diverging, or centrally lobed, journal. The angle θ is defined as the arc length from the leading edge of a lobe (sector) to the line along which the lobe is preloaded radially. The symbol β is defined as the lobe arc length. In the case of the tilted-lobe journal, $\theta = \beta$ (fig. 5(a)). The offset factor $\alpha = \theta/\beta$ is, therefore, 1.0. The offset factor for the centrally lobed journal is $\theta/\beta = 60^\circ/120^\circ = 0.5$ (fig. 5(b)). All axial grooves were 0.236 centimeter (0.093 in.) wide and equally as deep.

Circumferential profile traces were made of the external surface of each journal in two planes along the length of the journal to

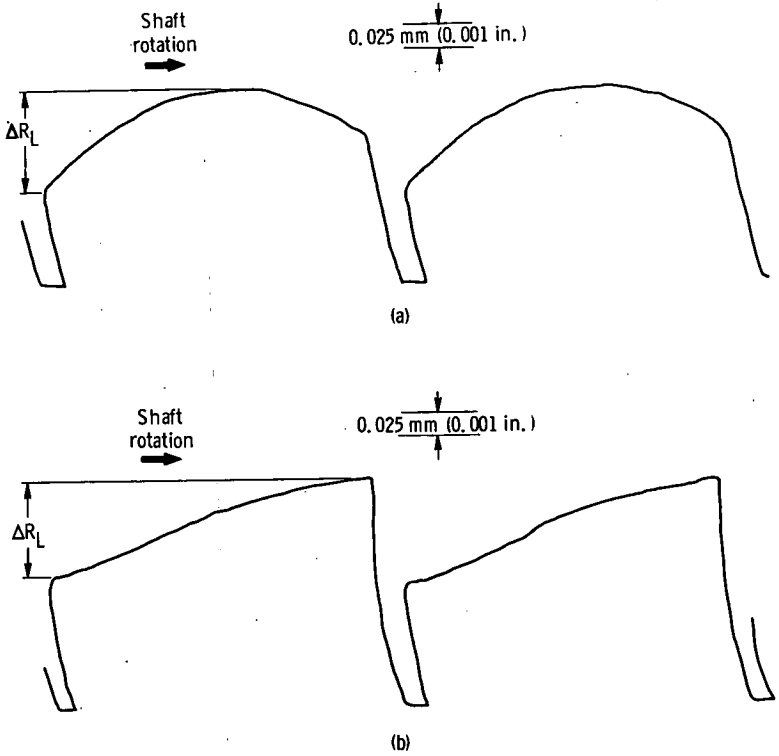

(a) Converging-diverging configuration.

(b) Wholly converging configuration.

Figure 8. - Typical circumferential profile traces of inside surfaces of bearing sectors.

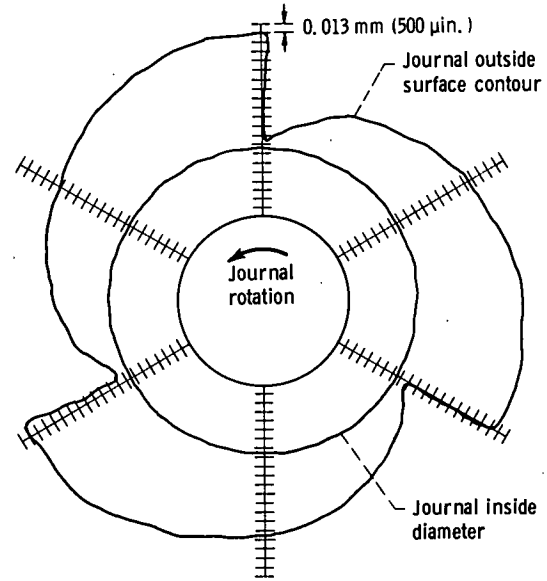

Figure 9. - Circumferential surface profile trace of tilted-lobe journal 5.

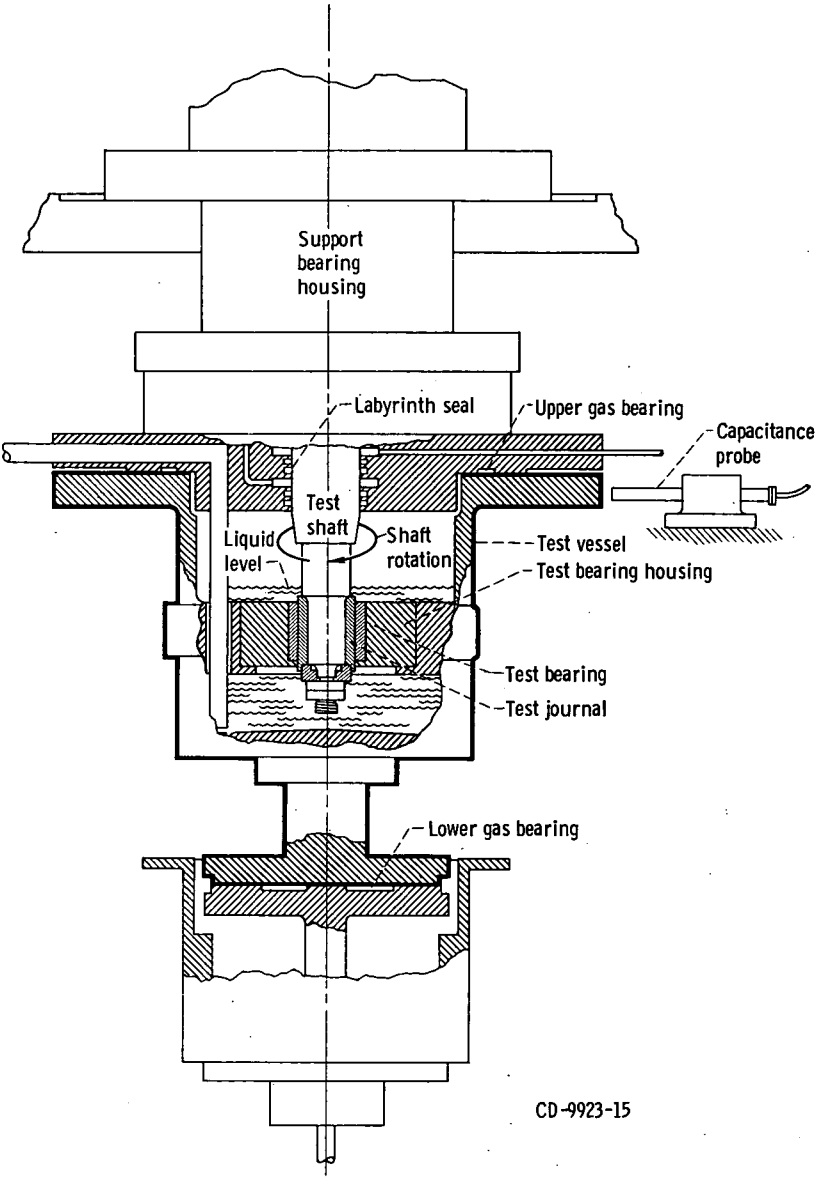

Figure 10. - Bearing test apparatus.

obtain the leading-edge entrance wedge thickness ΔR_L (fig. 5). Typical surface profile traces are shown in figure 9, which illustrates how the ΔR_L values were obtained. A trace of the inside diameter of the journal was also made to ensure that the lobe contour was concentric with the inside diameter of the journal to within 5 micrometers (200 μin.).

Bearing Test Apparatus

The test apparatus and its associated parts are shown in figure 10. The shaft is positioned vertically so that gravity forces do not load the bearing. The test vessel, which also serves as the test bearing housing, floats between the upper and lower gas bearings. Bearing torque is measured by a force transducer attached to the floating test vessel. The test shaft was mounted on two support ball bearings that were preloaded to about 890 newtons (200 lb) by a wave spring. This preload was necessary to ensure a minimum amount of shaft runout.

Two capacitance probes, which measured the movement of the test vessel during a test, were mounted outside the test vessel on the stationary vessel cover 90° from each other. The signal from the probes was fed through displacement meters to an X, Y-display on an oscilloscope, where the actual pattern of motion of the test vessel could be observed and photographed. The orbital frequency of the test vessel motion was measured by a frequency counter.

The temperature of the water in the test vessel was monitored by a thermocouple that extended into the liquid. Test-shaft speed was measured with a magnetic pickup head mounted close to a six-tooth gear on the shaft. The signal from the pickup was displayed on a four-channel frequency counter.

TEST PROCEDURE

Test-shaft speed was increased in increments ranging from 100 rpm in some tests to 1000 rpm in others. The bearings were run at zero load throughout the entire test. Onset of whirl was noted by observing the bearing housing motion on the oscilloscope screen (fig. 11). Shaft speed was recorded at this time. Damage to the test bearing and journal due to fractional-frequency

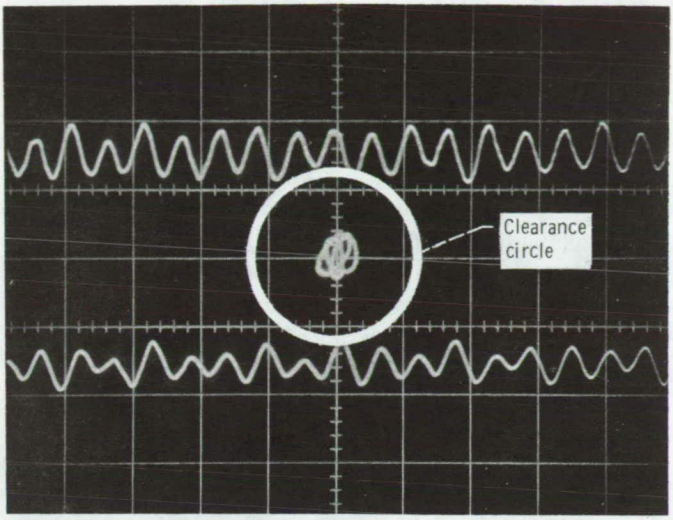

(a) Stable operation at 5600 rpm.

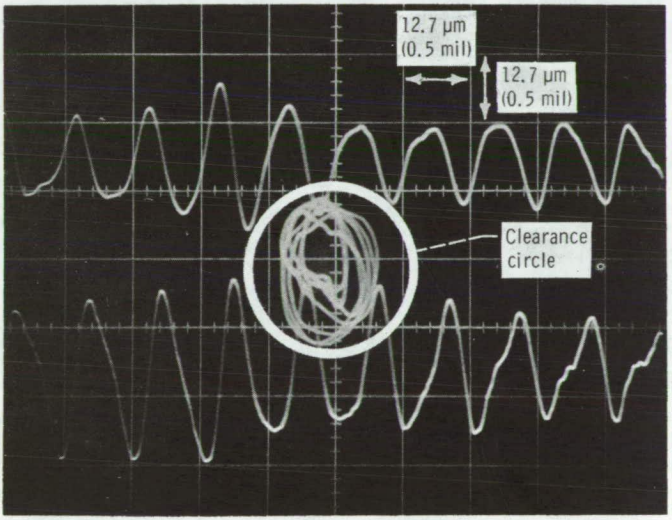

(b) Unstable operation (fractional-frequency whirl) at 5770 rpm.

Figure 11. - Bearing motion of shrouded three-pad Rayleigh step bearing in water. Bearing 11; zero load; radial clearance, 15 micrometers (600 μin.); horizontal time trace, 20 milliseconds per major division.

whirl was prevented by reducing the speed immediately after photographing the whirl pattern on the oscilloscope screen.

Usually, in any bearing stability investigation, the motion of the test shaft is monitored. However, in the experiments described in this report, the motion of the bearing with its massive housing (45.4 kg, 100 lb) was monitored. In order to establish the validity of the stability data obtained in this investigation, a three-axial-groove bearing, under light radial loads, was run in water with a plain journal. The results were compared with the theoretical curve for a 100° partial-arc bearing (ref. 21), as shown in figure 12. (The 100° partial-arc bearing has stability characteristics similar to those of the three-axial-groove bearing.) Excellent correlation was obtained between theoretical and experimental data, which indicated that the test apparatus and its monitoring system were highly reliable.

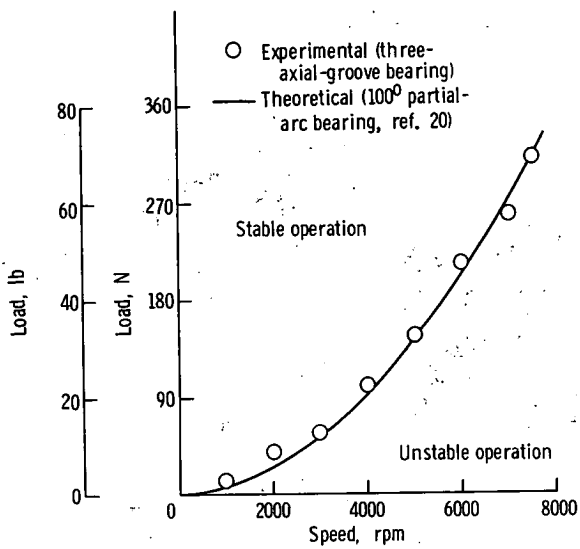

Figure 12. - Comparison of theoretical stability characteristics of 100° partial-arc bearing with experimental data for three-axial-groove bearing. Length-diameter ratio, 1; radial clearance, 0.020 millimeter (800 μin.).

RESULTS AND DISCUSSION

Herringbone Journals Mated With Plain Bearings

Experimental results obtained with six journals having different groove geometries are shown in table II and figures 13 to 20. Fifteen different groove depths were investigated. These were obtained by regrinding the outside surface of the original journals. The reworked journals were then used to obtain data for a journal having the same geometry as the original but a lesser groove depth. A total of 67 bearing stability tests were conducted at radial clearances ranging from 0.008 to 0.046 millimeter (300 to 1800 μin.) and groove depths ranging from 0.009 to 0.085 millimeter (340 to 3350 μin.).

Effect of number of grooves on stability. - The experimental results obtained with herringbone journals having 40, 20, and 10 partial grooves and full grooves are shown in figures 13(a) and (b), respectively. The experimental curve represents the stability limits of the bearings tested and indicates a zero-load threshold of stability. The area to the left of the curve represents conditions of stable operation under zero load, while the area to the right of the curve represents conditions that produce fractional-frequency whirl. The theoretical stability analysis of a journal bearing in reference 13 showed that the important parameters to consider are the dimensionless mass parameter $\overline{M}$ and the dimensionless speed parameter Γ, as shown in figure 13. A smooth curve was drawn through the collective data points for partially grooved journals with grooves 0.032 to 0.043 millimeter (1280 to 1700 μin.) deep and fully grooved journals with grooves 0.035 to 0.042 millimeter (1380 to 1640 μin.) deep in figures 13(a) and (b). Although there are some individual differences in some of the data points, these differences are minimal. Thus, for the range of groove numbers investigated in partially and fully grooved herringbone journals, the number of grooves does not seem to affect stability significantly.

Effect of partial and full grooves on stability. - The partially grooved journals, because of the circumferential land centrally located along the length of the bearing, have a total groove length two-thirds that of the fully grooved journals. How this difference in groove length affects stability is shown in figure 14. A study of this figure shows that the stability

TABLE II. - TEST RESULTS FOR HERRINGBONE JOURNALS WITH 40, 20, AND 10 GROOVES

(a) 40 Grooves

Journal	Groove depth, S		Groove type	Bearing	Radial clearance, C		Film thickness ratio, H	Fractional-frequency-whirl onset speed at zero load, N_W, rpm
	mm	μin.			mm	μin.		
1	0.015	590	Partial	1	0.014	550	2.1	9 000
				2	.023	900	1.7	5 500
				3	.028	1100	1.5	3 900
				4	.041	1600	1.4	1 000
2	0.016	620	Full	5	0.013	500	2.2	11 300
				6	.015	600	2.0	7 500
				7	.019	750	1.8	7 500
				8	.025	1000	1.6	4 600
				9	.036	1400	1.4	1 700
4	0.043	1700	Partial	10	0.013	500	4.4	7 000
				11	.020	800	3.1	6 000
				12	.043	1700	2.0	2 900
3	0.035	1380	Full	8	0.008	300	5.6	11 500
				9	.016	650	3.1	11 200
				13	.028	1100	2.3	4 800
				14	.037	1450	2.0	2 000
				15	.046	1800	1.8	1 500

TABLE II. - Continued. TEST RESULTS FOR HERRINGBONE JOURNALS WITH 40, 20, AND 10 GROOVES

(b) 20 Grooves

Journal	Groove depth, S		Groove type	Bearing	Radial clearance, C		Film thickness ratio, H	Fractional-frequency-whirl onset speed at zero load, N_W, rpm
	mm	μin.			mm	μin.		
7	0.036	1400	Partial	10	0.008	300	5.7	7800
				11	.018	700	3.0	6500
				16	.024	950	2.5	5300
				17	.032	1250	2.1	4000
8	0.042	1640	Full	18	0.016	650	3.5	6500
				19	.020	800	3.0	6000
				20	.027	1050	2.6	7000
				21	.034	1350	2.2	3000
5	0.010	410	Partial	2	0.011	450	1.9	7800
				3	.016	650	1.6	6000
				22	.024	950	1.4	3000
				23	.034	1350	1.3	1200
6	0.018	700	Full	24	0.019	750	1.9	9800
				25	.025	1000	1.7	5000
				26	.029	1150	1.6	4300
				27	.034	1350	1.5	2000
				28	.041	1600	1.4	1500

TABLE II. - Continued. TEST RESULTS FOR HERRINGBONE JOURNALS WITH 40, 20, AND 10 GROOVES

(c) 10 Grooves

Journal	Groove depth, S		Groove type	Bearing	Radial clearance, C		Film thickness ratio, H	Fractional-frequency-whirl onset speed at zero load, N_W, rpm
	mm	μin.			mm	μin.		
16	0.085	3350	Partial	8	0.011	450	8.5	4300
				9	.020	800	5.2	3200
				13	.032	1250	3.7	2600
				14	.041	1600	3.1	1300
15	0.068	2660	Partial	29	0.011	450	6.9	5300
				5	.020	800	4.3	4000
				8	.032	1250	3.1	3000
				9	.042	1650	2.6	1500
12	0.032	1280	Partial	8	0.011	450	3.8	7000
				9	.020	800	2.6	6000
				13	.032	1250	2.0	3800
				14	.041	1600	1.8	1800
10	0.018	700	Partial	29	0.009	350	3.0	7500
				30	.014	550	2.3	7000
				5	.019	750	1.9	6500
				8	.029	1150	1.6	3300
				9	.039	1550	1.4	1200

TABLE II. - Concluded. TEST RESULTS FOR HERRINGBONE JOURNALS WITH 40, 20, AND 10 GROOVES

(c) Concluded. 10 Grooves

Journal	Groove depth, S		Groove type	Bearing	Radial clearance, C		Film thickness ratio, H	Fractional-frequency-whirl onset speed at zero load, N_W, rpm
	mm	μin.			mm	μin.		
9	0.009	340	Partial	31	0.013	500	1.7	6 500
				32	.024	950	1.4	4 000
				7	.033	1300	1.3	1 000
[a]14	0.034	1350	Full	33	0.019	750	2.8	9 500
				34	.030	1200	2.1	7 500
				35	.036	1400	2.0	6 200
				36	.042	1650	1.8	5 400
13	0.036	1420	Full	8	0.010	400	4.6	10 000
				9	.020	800	2.8	5 800
				13	.030	1200	2.2	4 600
				14	.039	1550	1.9	2 000
11	0.024	960	Full	5	0.013	500	2.9	7 500
				6	.015	600	2.6	7 500
				7	.019	750	2.3	7 000
				8	.025	1000	2.0	5 300
				9	.036	1400	1.7	1 600

[a]Bearing tests with one-third the housing mass of other bearings.

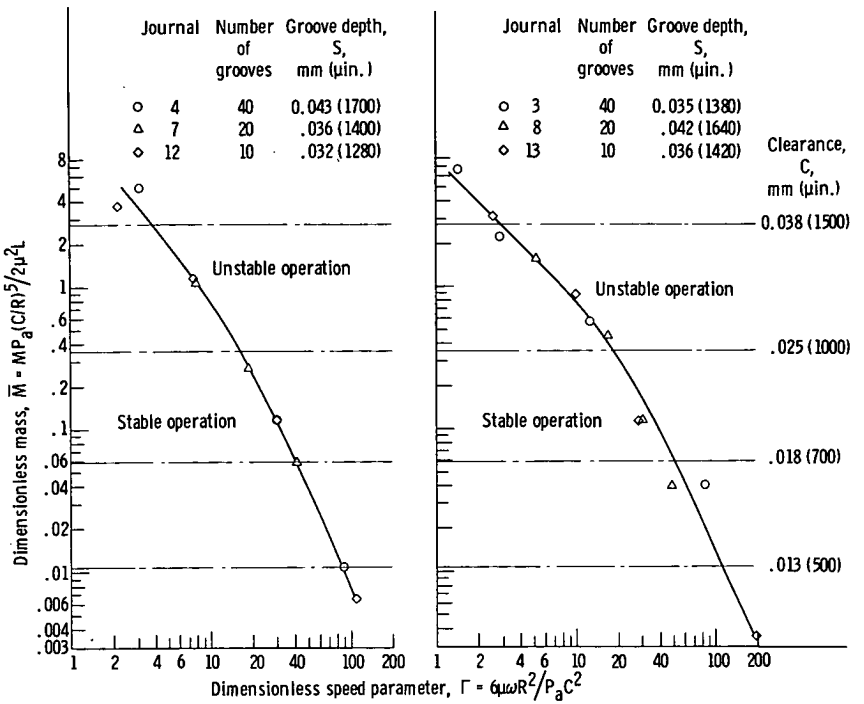

(a) Partially grooved journals. (b) Fully grooved journals.

Figure 13. - Effect of number of grooves on stability of water-lubricated herringbone journals having 40, 20, and 10 grooves.

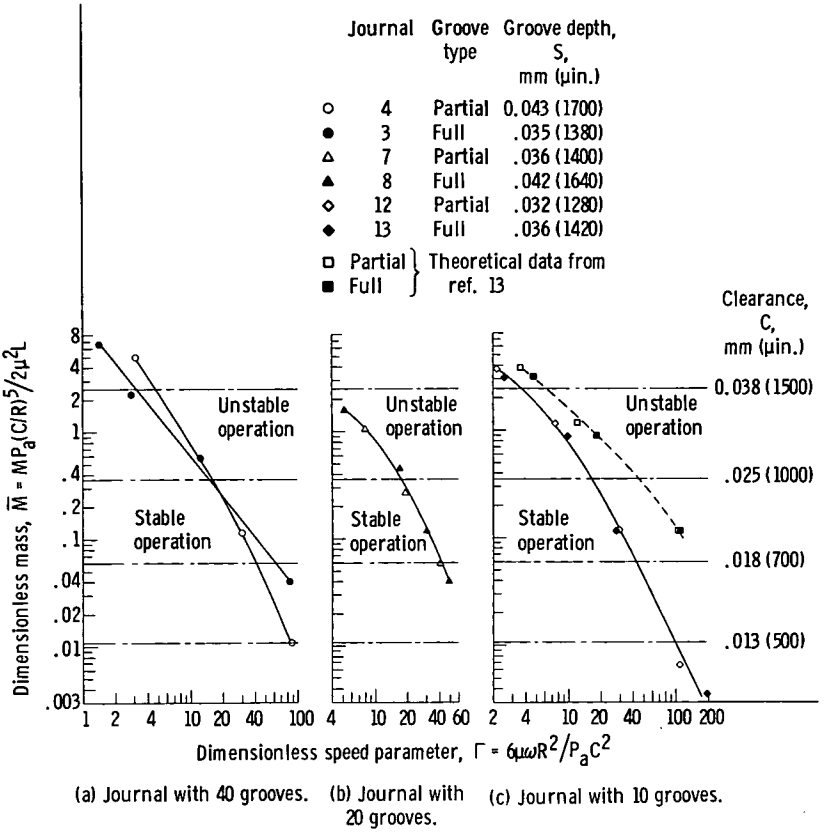

Figure 14. - Effect of partial and full grooves on stability of water-lubricated herringbone journals.

characteristics of only the 40-groove journals are appreciably affected by groove length. In figure 14(a), at $\overline{M}$ values above 0. 25, the journal with the shorter grooves (partially grooved) had better stability than the one with the longer grooves (fully grooved). At $\overline{M}$ values less than 0. 25, however, the opposite was true.

For the journals with 20 and 10 partial and full grooves, the effect of groove length on stability was negligible (figs. 14(b) and (c)). Figure 14(c) also shows a theoretical data curve (the dashed curve), with open square symbols representing partial-groove journals and solid square symbols full-groove journals. These points were obtained from an analytical study in reference 13 and show that the effect of groove length on stability is

also negligible in theory for the range of dimensionless parameters considered in this report.

As has been pointed out, there are individual differences in the stability characteristics of herringbone-groove journals when the effects of number of grooves and groove length are considered. However, these differences are minimal when all the data are grouped to form one stability plot. Such a curve is shown in figure 15, where a smooth curve is drawn through the collective data for all journal bearings having 40, 20, and 10 partial and full grooves ranging in depth from 0.032 to 0.043 millimeter (1280 to 1700 μin.).

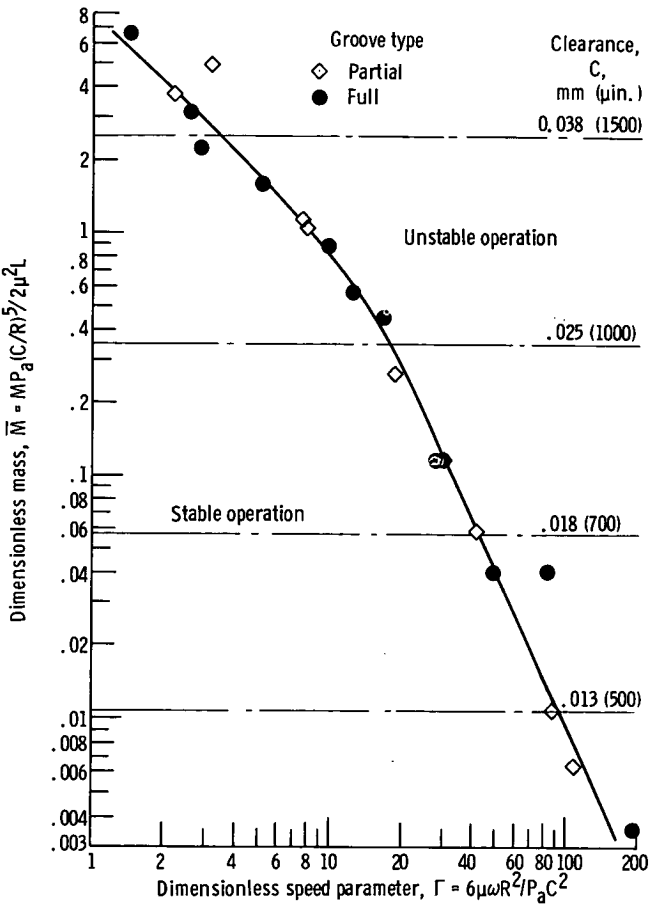

Figure 15. - Mean stability of herringbone journals with 10, 20, and 40 partial and full grooves. Range of groove depth, 0.032 to 0.043 millimeter (1280 to 1700 μin.).

Effect of groove depth on stability. - The effect of groove depth on stability is shown in figure 16. Figure 16(a) shows the effect of reducing the groove depth for journals having 40, 20, and 10 partial and full grooves from an average of 0.038 millimeter (1490 μin.) to an average of 0.017 millimeter (660 μin.). The dashed curve is the curve of figure 15 and represents journals with an average groove depth of 0.038 millimeter (1490 μin.), and the solid curve shows the mean stability of a group of herringbone-groove bearings with groove depths ranging from 0.010 to 0.024 millimeter (410 to 960 μin.) and averaging 0.017 millimeter (660 μin.). Stability decreased with a decrease in

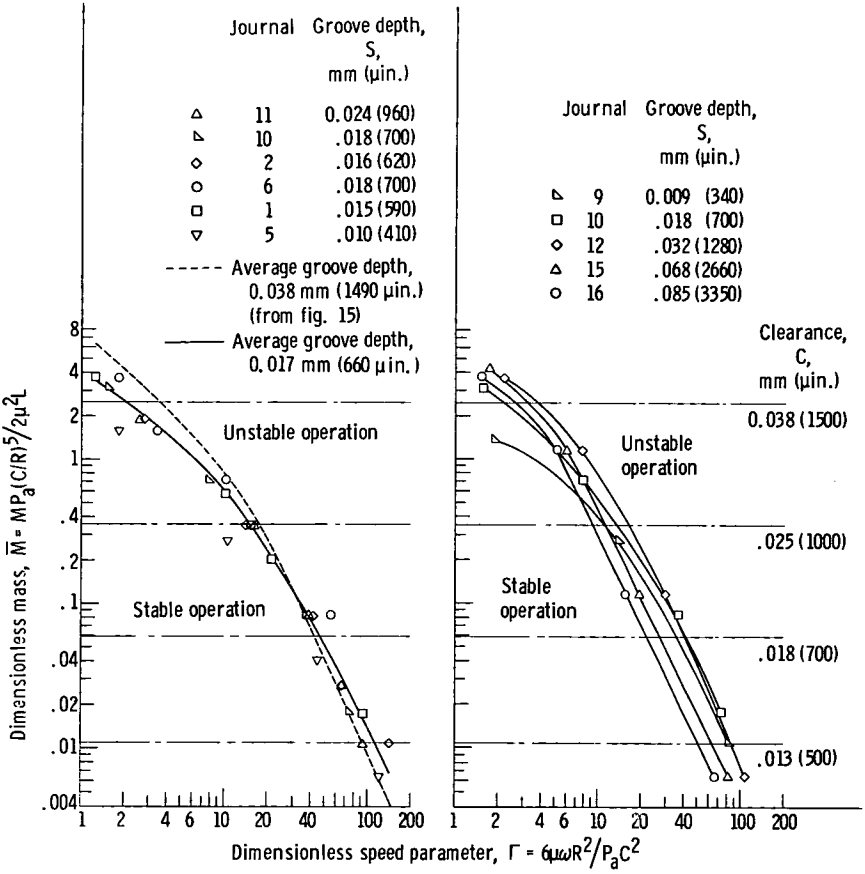

(a) Journals with 10, 20, and 40 partial and full grooves.

(b) Journal with 10 partial grooves.

Figure 16. - Effect of groove depth on stability of water-lubricated herringbone journals.

groove depth for bearings with $\overline{M}$ values above 0.12 and increased slightly with a decrease in groove depth for bearings with $\overline{M}$ values below 0.12.

In general, figure 16(a) shows that the optimum groove depth depends on clearance. The optimum groove depth changes with $\overline{M}$ and Γ, both of which are dependent on the clearance; a larger clearance requires a larger groove depth for maximum stability.

Figure 16(b) shows the stability limits of a journal having 10 partial grooves at five groove depths. As the groove depth was increased from 0.009 to 0.032 millimeter (340 to 1280 μin.), the stability increased. Then, as the groove depth was further increased from 0.032 millimeter (1280 μin.) to a maximum value of 0.085 millimeter (3350 μin.), the stability gradually decreased. Maximum stability occurred at a groove depth of 0.032 millimeter (1280 μin.).

Effect of film thickness ratio on stability. - The herringbone-journal helix angle and groove- to ridge-width ratio (table I) were set at those values which yield a maximum radial

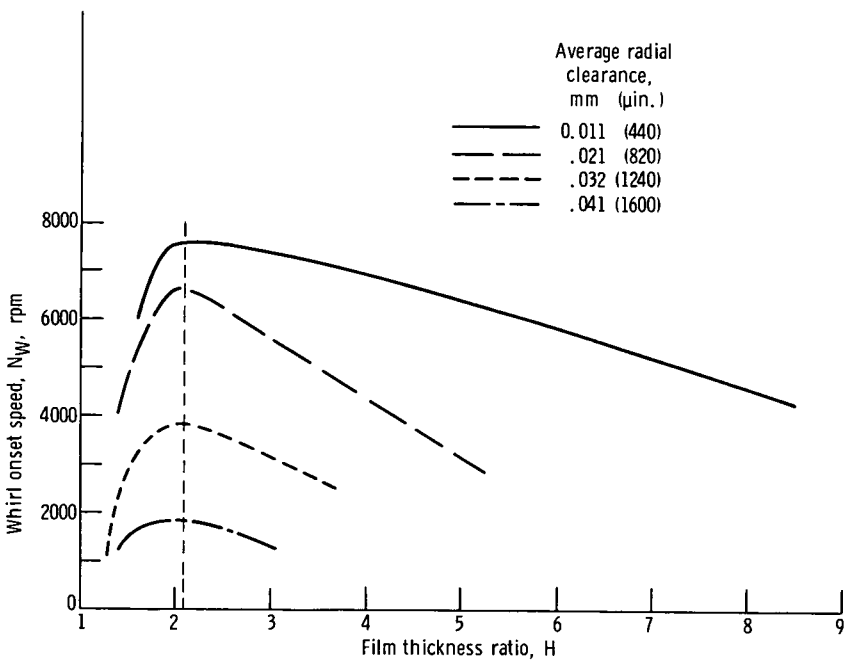

Figure 17. - Effect of film thickness ratio on stability of herringbone journal with 10 partial grooves in water. Zero load.

force as calculated from reference 5 at a compressibility number of zero for a compressible lubricant. This approximates the conditions existing with an incompressible lubricant. The optimum film thickness ratio H is 2.1 for this condition (ref. 5). An optimization program, utilizing the analysis in reference 5, is developed in reference 7 to determine groove configurations to maximize radial load capacity. Results are applicable for operating conditions ranging from an incompressible solution to a highly compressible solution and for bearing length-diameter ratios of 1/4 to 2. The optimum film thickness ratio H calculated by this program is 2.2. Figure 17 shows plots of H against zero-load whirl onset speed at four clearance values. The zero-load whirl onset speed at each clearance reached a maximum at an H value very close to 2.1, which indicated that this value of H is also optimum for stability. These curves were obtained from data on a herringbone journal having 10 partial grooves.

Figure 18 shows a dimensionless plot of H against $\overline{M}\Gamma$, which was the stability parameter used in the theoretical stability analysis in reference 13. The data from partially and fully grooved journals with 40, 20, and 10 grooves were combined to obtain the five dashed curves shown, which represent five clearances. Although the data show some scatter caused by minor variations in the stability limits of the different journal configurations, the curves all tend to peak at a value of H very close to 2.1.

Once a value for radial clearance has been chosen for a particular herringbone journal mated with a plain bearing, the groove depth for maximum stability can be reliably determined from the H = 2.1 value for incompressible flow.

The theoretical curves for a herringbone journal having partial and full grooves are also shown in figure 18 as the solid and long-dash curves, respectively. Data for these curves were obtained from the computer program in reference 13. These two curves also peak at an H value of 2.1. This indicates that maximum stability is predicted to occur at the same H value as the maximum radial force at a compressibility number of zero (for a compressible lubricant), namely, at H = 2.1 (ref. 5). Figure 18 also shows that theory predicts a larger range of stable operation than that observed experimentally. Similar results were reported in reference 4, which indicates that there may be an important parameter missing in the theoretical analysis.

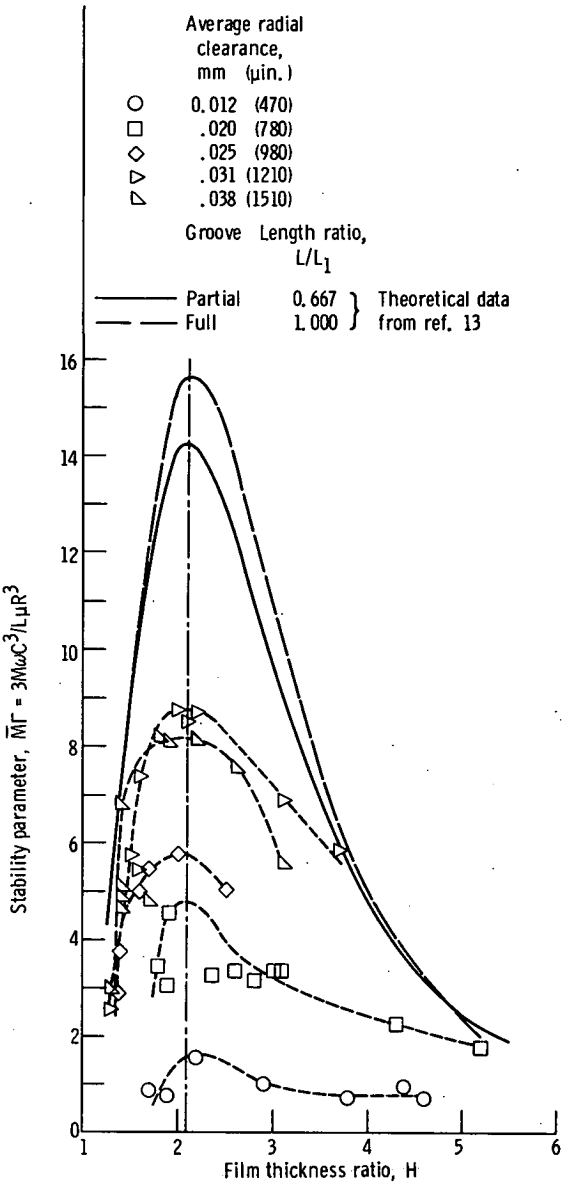

Figure 18. - Comparison of theoretical and experimental stability data for herringbone journal. Helix angle, 33^0; groove-width ratio, 0.5; length-diameter ratio, 1.

The data in figure 18 are repeated in figure 19 with a different stability parameter ($3MC^{3/2}/LR^{3/2}$) in an effort to bring the experimental curves closer together. Stability thresholds fall within a narrower range of this parameter.

Effect of changes in housing mass. - The mass of the test housing (rotor mass per bearing) M that was used in all but four stability tests in this investigation was 45.4 kilograms (0.286 (lb)(sec^2)/in.). The remaining four tests were run with a plastic test housing which had a mass of 13.3 kilograms (0.084 (lb)(sec^2)/in.), or 30 percent of the mass of the heavier test

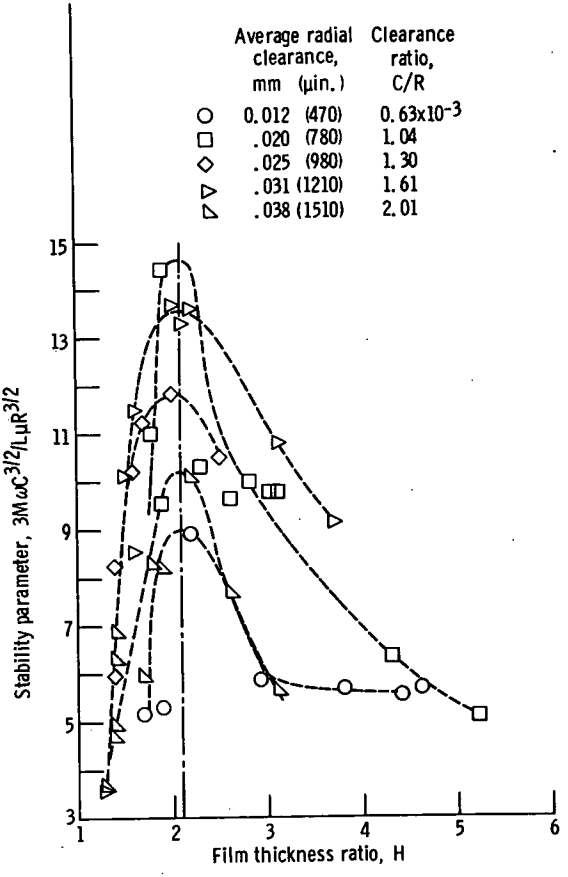

Figure 19. - Experimental stability data for herringbone journal. Helix angle, 33°; groove-width ratio, 0.5; length-diameter ratio, 1.

housing. Stability curves are shown in figure 20 for a herringbone journal having 10 full grooves run at the two different mass conditions. The close correlation of the data for the two curves demonstrates the validity of the chosen dimensionless parameters $\overline{M}$ and Γ.

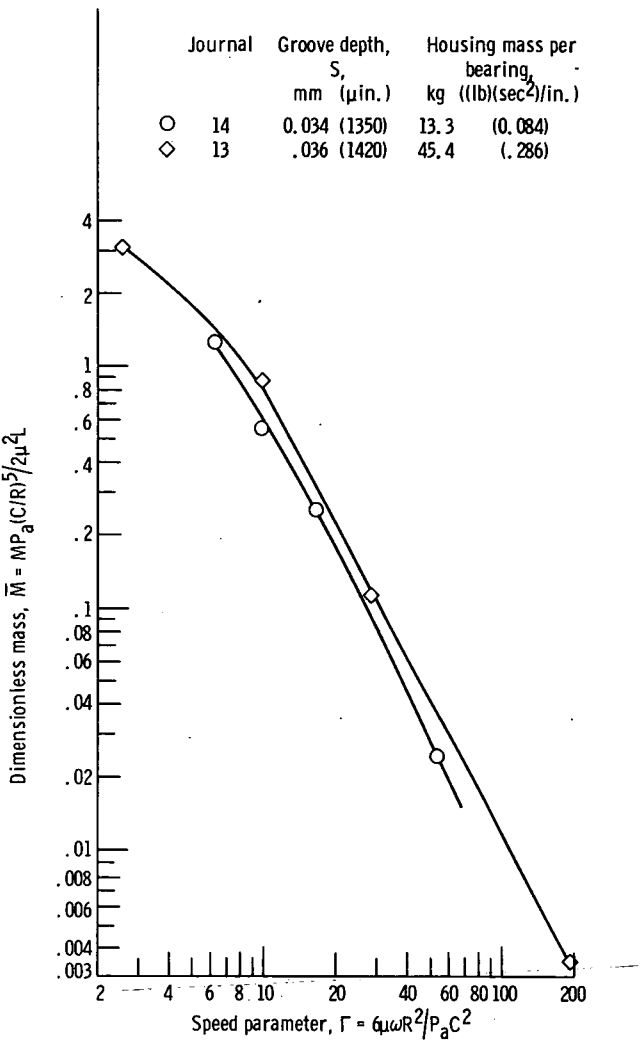

Figure 20. - Stability data for herringbone journal having 10 full grooves run with plain bearing at two rotor mass values.

Rayleigh Step Bearings

Experimental results obtained with three-segment, one-pad shrouded Rayleigh step bearings (fig. 2(b)) with values of ridge-to pad-arc ratio ψ of 0.40 and 0.49 are shown in table III. Test results for one-segment, three-pad shrouded bearings (fig. 2(c)) with ψ equal to 0.27 and 0.45 are shown in table IV. Table V lists the results for a similar bearing with a ψ of 0.45 but without shrouds. Test results for a Rayleigh step bearing

TABLE III. - TEST RESULTS FOR THREE-SEGMENT, ONE-PAD SHROUDED RAYLEIGH STEP JOURNAL BEARINGS

(a) Ridge- to pad-arc ratio ψ, 0.40

Bearing	Depth of step, S		Radial clearance at ridge, C		Radial clearance at step, $C_s = C + S$		Film thickness ratio, $k_r = C_s/C$	Fractional-frequency-whirl onset speed at zero load, N_w, rpm
	mm	μin.	mm	μin.	mm	μin.		
1	0.023	900	0.013	500	0.036	1400	2.80	5700
			.025	1000	.048	1900	1.90	1230
			.038	1500	.061	2400	1.60	420
			.051	2000	.074	2900	1.45	200
2	0.041	1600	0.013	500	0.053	2100	4.20	5200
			.025	1000	.066	2600	2.60	920
			.038	1500	.079	3100	2.07	360
			.052	2050	.093	3650	1.73	210
3	0.053	2100	0.013	500	0.066	2600	5.20	5300
			.025	1000	.079	3100	3.10	1320
			.038	1500	.091	3600	2.40	450
			.051	2000	.104	4100	2.05	280
4	0.094	3700	0.013	500	0.107	4200	8.41	3800
			.024	950	.118	4650	4.90	1100
			.037	1450	.131	5150	3.55	300
			.050	1950	.144	5650	2.90	100

with a single segment extending the length of the bearing and one pad in its circumference and ψ equal to 0.4 are listed in table VI. A total of 80 bearing stability tests were conducted at a radial clearance C ranging from 0.010 to 0.052 millimeter (400 to 2050 μin.) and step depths S ranging from 0.015 to 0.094 millimeter (600 to 3700 μin.).

TABLE III. - Concluded. TEST RESULTS FOR THREE-SEGMENT, ONE-PAD SHROUDED RAYLEIGH STEP JOURNAL BEARINGS

(b) Ridge- to pad-arc ratio ψ, 0.49

Bearing	Depth of step, S		Radial clearance at ridge, C		Radial clearance at step, $C_s = C + S$		Film thickness ratio, $k_r = C_s/C$	Fractional-frequency-whirl onset speed at zero load, N_w, rpm
	mm	μin.	mm	μin.	mm	μin.		
5	0.029	1100	0.010	400	0.038	1500	3.75	5840
			.024	950	.052	2050	2.16	1200
			.037	1450	.065	2550	1.76	370
			.051	2000	.079	3100	1.55	190
6	0.036	1400	0.011	450	0.047	1850	4.12	5600
			.025	1000	.061	2400	2.40	1200
			.038	1500	.074	2900	1.93	390
			.052	2050	.088	3450	1.68	230
7	0.053	2100	0.013	500	0.066	2600	5.20	5300
			.025	1000	.079	3100	3.10	1410
			.038	1500	.091	3600	2.40	440
			.052	2050	.105	4150	2.03	200
8	0.089	3500	0.013	500	0.102	4000	8.00	4100
			.024	950	.113	4450	4.69	1000
			.037	1450	.126	4950	3.41	150
			.050	1950	.138	5450	2.80	100

TABLE IV. - TEST RESULTS FOR ONE-SEGMENT, THREE-PAD SHROUDED RAYLEIGH STEP JOURNAL BEARINGS

(a) Ridge- to pad-arc ratio ψ, 0.27

Bearing	Depth of step, S		Radial clearance at ridge, C		Radial clearance at step, $C_s = C + S$		Film thickness ratio, $k_r = C_s/C$	Fractional-frequency-whirl onset speed at zero load, N_w, rpm
	mm	μin.	mm	μin.	mm	μin.		
9	0.015	600	0.014	550	0.029	1150	2.09	5700
			.024	950	.039	1550	1.63	4300
			.042	1650	.057	2250	1.37	2100
			.051	2000	.066	2600	1.30	500
10	0.030	1200	0.013	500	0.043	1700	3.40	6300
			.024	950	.055	2150	2.26	4400
			.038	1500	.069	2700	1.80	2800
			.052	2050	.083	3250	1.59	1300
11	0.048	1900	0.015	600	0.064	2500	4.18	5600
			.025	1000	.074	2900	2.90	4400
			.037	1450	.085	3350	2.31	3000
			.051	2000	.099	3900	1.95	1200
12	0.064	2500	0.018	700	0.081	3200	4.58	4200
			.024	950	.088	3450	3.64	4100
			.037	1450	.100	3950	2.72	3000
			.052	2050	.116	4550	2.22	600
13	0.091	3600	0.017	650	0.108	4250	6.54	3500
			.023	900	.114	4500	5.01	3000
			.036	1400	.127	5000	3.57	2100
			.051	2000	.142	5600	2.80	500

TABLE IV. - Concluded. TEST RESULTS FOR ONE-SEGMENT, THREE-PAD SHROUDED RAYLEIGH STEP JOURNAL BEARINGS

(b) Ridge- to pad-arc ratio ψ, 0.45

Bearing	Depth of step, S		Radial clearance at ridge, C		Radial clearance at step, $C_s = C + S$		Film thickness ratio, $k_r = C_s/C$	Fractional-frequency-whirl onset speed at zero load, N_w, rpm
	mm	μin.	mm	μin.	mm	μin.		
14	0.020	800	0.011	450	0.032	1250	2.78	6000
			.022	850	.042	1650	1.95	4300
			.039	1550	.060	2350	1.52	2800
			.050	1950	.069	2700	1.42	600
15	0.025	1000	0.011	450	0.037	1450	3.23	5600
			.024	950	.050	1950	2.05	4100
			.036	1400	.061	2400	1.71	3000
			.050	1950	.075	2950	1.51	1020
16	0.048	1900	0.015	600	0.064	2500	4.18	5700
			.025	1000	.074	2900	2.90	4200
			.037	1450	.085	3350	2.31	3200
			.051	2000	.099	3900	1.95	1200
17	0.066	2600	0.017	650	0.083	3250	5.00	5000
			.023	900	.089	3500	3.89	3700
			.036	1400	.102	4000	2.86	2300
			.051	2000	.117	4600	2.30	800
18	0.089	3500	0.015	600	0.104	4100	6.84	4100
			.022	850	.110	4350	5.12	3300
			.034	1350	.123	4850	3.59	1500
			.050	1950	.138	5450	2.79	600

TABLE V. - TEST RESULTS FOR ONE-SEGMENT,

THREE-PAD UNSHROUDED RAYLEIGH

STEP JOURNAL BEARING

[Ridge- to pad-arc ratio ψ, 0.45; bearing 19; depth of step S, 0.066 mm (2600 μin.).]

Radial clearance at ridge, C		Radial clearance at step, $C_s = C + S$		Film thickness ratio, $k_r = C_s/C$	Fractional-frequency-whirl onset speed at zero load, N_W, rpm
mm	μin.	mm	μin.		
0.013	500	0.079	3100	6.20	4300
.024	950	.090	3550	3.74	1400
.037	1450	.103	4050	2.79	1000
.050	1950	.116	4550	2.33	650

TABLE VI. - TEST RESULTS FOR ONE-SEGMENT,

ONE-PAD SHROUDED RAYLEIGH STEP

JOURNAL BEARING

[Ridge- to pad-arc ratio ψ, 0.40; bearing 20; depth of step S, 0.066 mm (2600 μin.).]

Radial clearance at ridge, C		Radial clearance at step, $C_s = C + S$		Film thickness ratio, $k_r = C_s/C$	Fractional-frequency-whirl onset speed at zero load, N_W, rpm
mm	μin.	mm	μin.		
0.015	600	0.081	3200	5.33	3900
.027	1050	.093	3650	3.47	3000
.043	1700	.109	4300	2.53	720
.052	2050	.118	4650	2.27	700

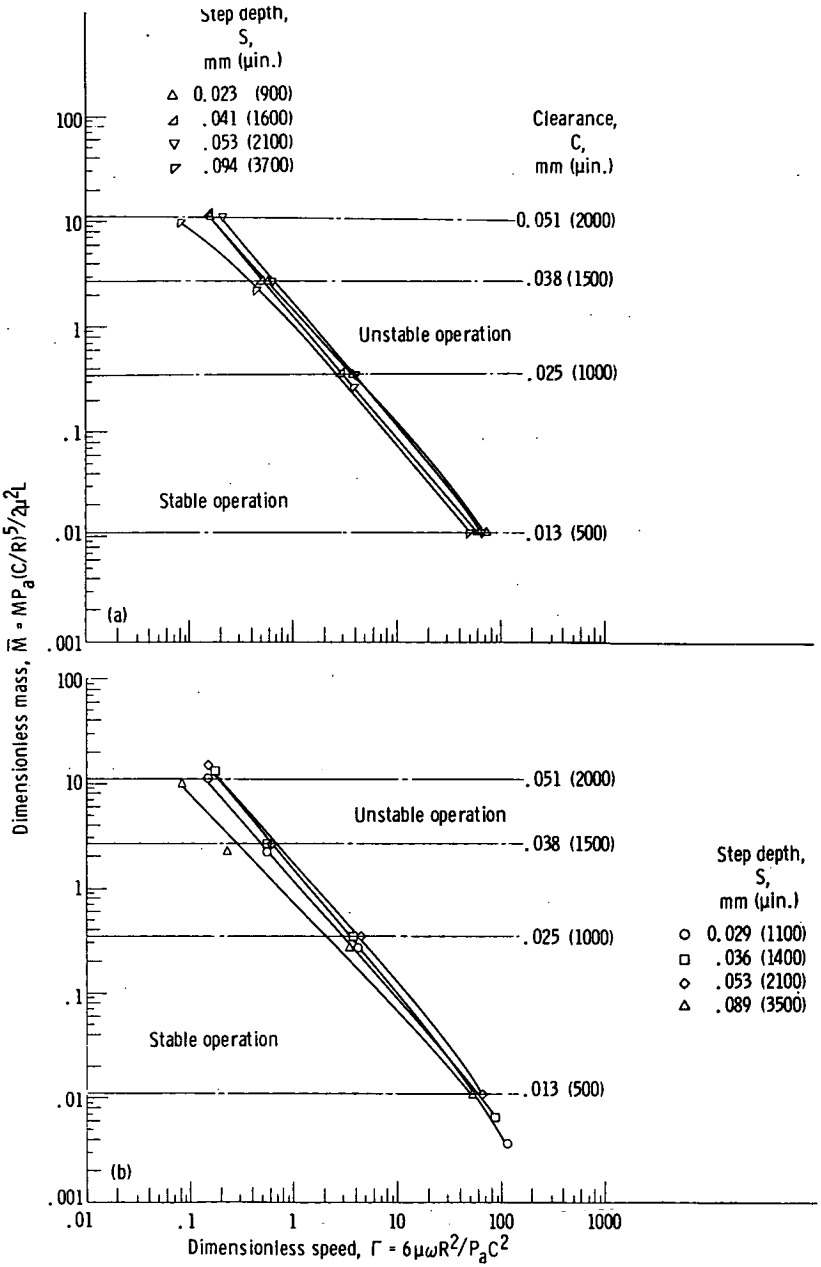

(a) Ridge- to pad-arc ratio, 0.40.

(b) Ridge- to pad-arc ratio, 0.49.

Figure 21. - Effect of step depth on stability of three-segment, one-pad shrouded Rayleigh step bearing.

Effect of step depth on stability. - The experimental results obtained with three-segment, one-pad shrouded Rayleigh step bearings are shown in figure 21. Figure 21(a) shows the stability limits of a three-segment, one-pad shrouded Rayleigh step bearing with a ridge- to pad-arc ratio of 0.40 at four step depths. Maximum stability occurred at a step depth of 0.053 millimeter (2100 μin.) as the step depth was varied over a range of 0.023 to 0.094 millimeter (900 to 3700 μin.). This was also the case for similar bearings with a ψ of 0.49 (fig. 21(b)), where maximum stability occurred at a step depth of 0.053 millimeter (2100 μin.) as the step depth was varied over a range of 0.029 to 0.089 millimeter (1100 to 3500 μin.).

The experimental results obtained with one-segment, three-pad shrouded Rayleigh step bearings are shown in figure 22. Threshold of stability curves for the bearings with a ψ of 0.27 are shown in figure 22(a). The stability characteristics remained essentially the same for bearings with a range of step

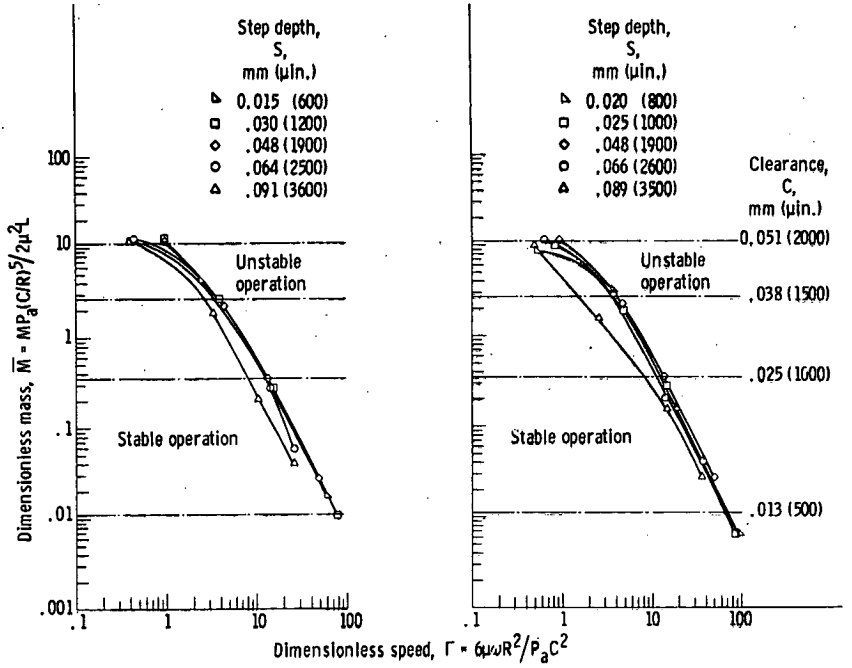

(a) Ridge- to pad-arc ratio, 0.27. (b) Ridge- to pad-arc ratio, 0.45.

Figure 22. - Effect of step depth on stability of one-segment, three-pad shrouded Rayleigh step bearing.

depths from 0.015 to 0.064 millimeter (600 to 2500 μin.) at $\overline{M}$ values below 5.0. A noticeable drop in stability occurred when the step depth was increased to 0.091 millimeter (3600 μin.). This was also true for similar bearings with a ψ of 0.45 (fig. 22(b)), where stability was little affected by increased step depth at $\overline{M}$ values below 5.0 until a value of 0.089 millimeter (3500 μin.) was reached. Experimental data points for values of dimensionless mass $\overline{M}$ above 5.0 for the bearings with ψ equal to 0.27 (fig. 22(a)) and 0.45 (fig. 22(b)) represent bearings with large clearances ranging from 0.048 to 0.052 millimeter (1900 to 2050 μin.). There is a greater variation in stability at these large clearances for both bearing types (ψ of 0.27 and 0.45) as the step depths are varied over their respective ranges.

Effect of ridge- to pad-arc ratio on stability. - The effect of ridge- to pad-arc ratio ψ on stability of the three-segment, one-pad shrouded Rayleigh step bearing is shown in figure 23. The solid and dashed curves were obtained from figures 21(a) and (b), respectively, and represent the stability characteristics of a three-segment, one-pad shrouded bearing at two ψ values (0.40 and 0.49) but at the same step depth of 0.053 millimeter (2100 μin.). A study of figure 23 shows that the stability of the three-segment, one-pad shrouded Rayleigh step bearing was not appreciably affected by a change in ridge- to pad-arc ratio ψ from 0.40 to 0.49, since the two curves are in such close proximity to one another.

The two curves shown in figure 24 for a one-segment, three-pad shrouded Rayleigh step bearing were obtained in a manner similar to that for the curves in figure 23. The solid and dashed curves represent the stability characteristics of a one-segment, three-pad shrouded bearing at ψ equal to 0.27 and 0.45, respectively, at a step depth of 0.048 millimeter (1900 μin.) obtained from figures 22(a) and (b). As in the case of the three-segment, one-pad bearing, the stability characteristics of the one-segment, three-pad bearing were not appreciably affected by a change in ψ even though this change in ψ (0.27 to 0.45) was much greater than that for the three-segment, one-pad bearing (0.40 to 0.49).

Effect of bearing configuration on stability. - Comparison of the stability curves for the three-segment, one-pad bearing (fig. 23) with those for the one-segment, three-pad bearing (fig. 24) shows that the latter bearing configuration is the more stable of the two. For example, at a dimensionless mass $\overline{M}$ of 1.0, the dimensionless speed Γ is 1.6 for the three-segment,

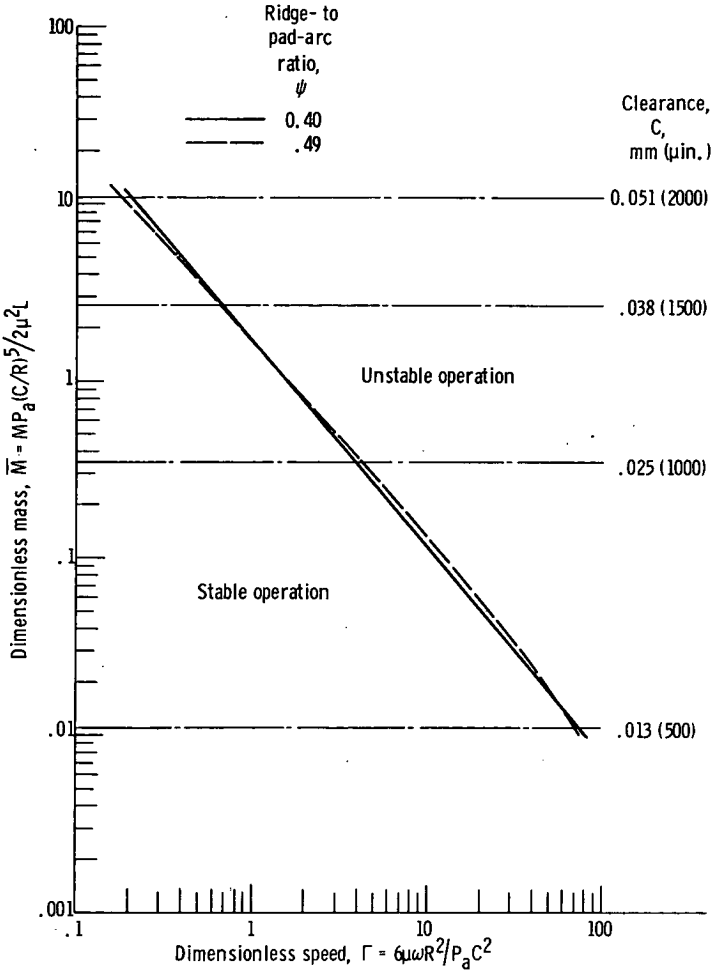

Figure 23. - Effect of ridge- to pad-arc ratio on stability of three-segment, one-pad shrouded Rayleigh step bearing. Step depth, 0.053 millimeter (2100 μin.).

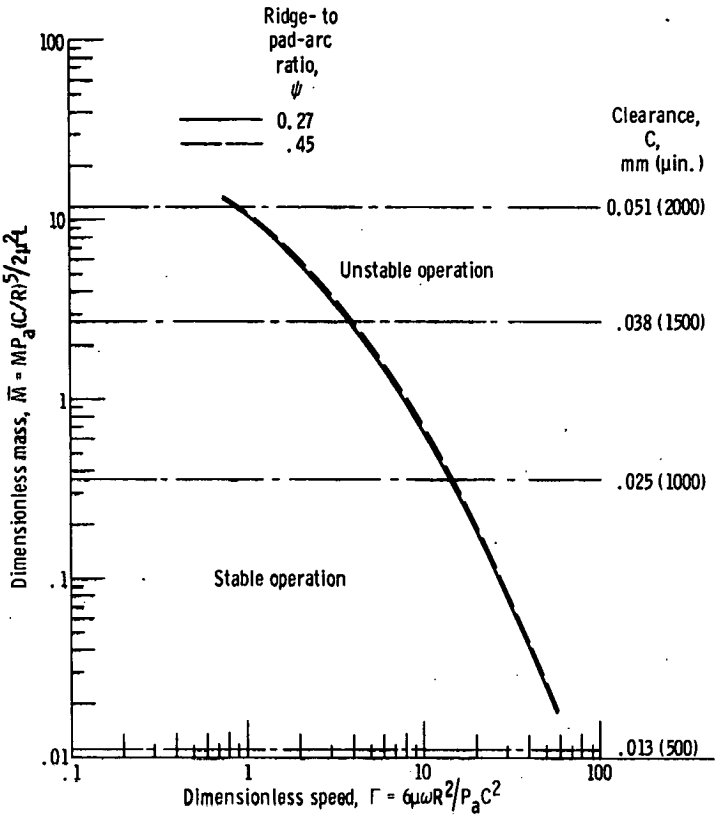

Figure 24. - Effect of ridge- to pad-arc ratio on stability of one-segment, three-pad shrouded Rayleigh step bearing. Step depth, 0.048 millimeter (1900 μin.).

one-pad bearing (fig. 23) and 7, 8 for the one-segment, three-pad bearing (fig. 24), which indicates a substantial gain in stability with the one-segment, three-pad configuration. However, it must be remembered that the single-pad bearing is composed of three separate bearings (segments), each with a length-diameter ratio L/D of 1/3, whereas the three-pad bearing has an L/D of 1. It may be that this difference in L/D between the two bearing configurations accounts for the main difference in their stability characteristics.

The main purpose for testing the one-segment, one-pad bearing (fig. 2(a)) was to determine if it had any stability whatsoever. The results of the tests showed that this configuration does have very good stability characteristics even though it has

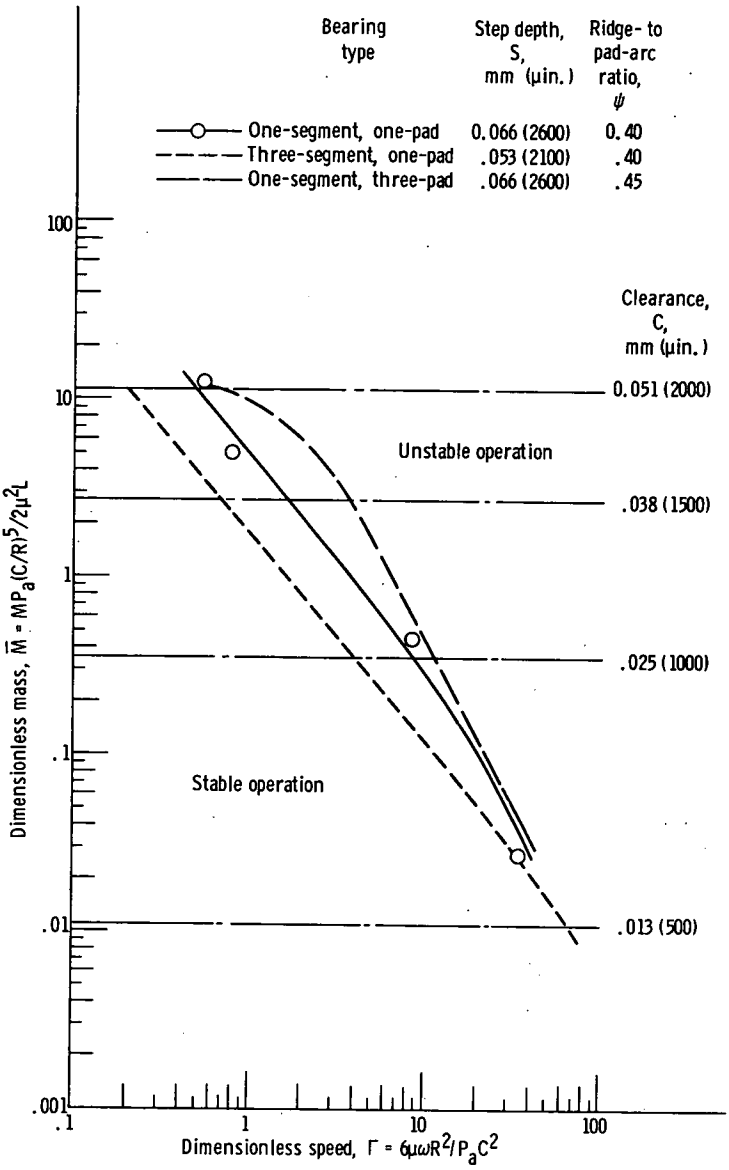

Figure 25. - Comparison of stability of shrouded Rayleigh step bearings of three different configurations.

the disadvantage of a preferential loading direction. Figure 25 shows a comparison of stability characteristics of the one-segment, one-pad bearing with those of the three-segment, one-pad bearing and the one-segment, three-pad bearing. Bearings with approximately the same step depth S and ridge- to pad-arc ratio ψ were employed for this comparison. Figure 25 shows that the one-segment, three-pad configuration is the most stable of the three, followed by the one-segment, one-pad bearing. The three-segment, one-pad bearing was the least stable. The increase in stability of the one-segment, one-pad and the one-segment, three-pad bearings over that of the three-segment, one-pad bearing in all probability is due to the larger L/D ratio of the first two bearing configurations.

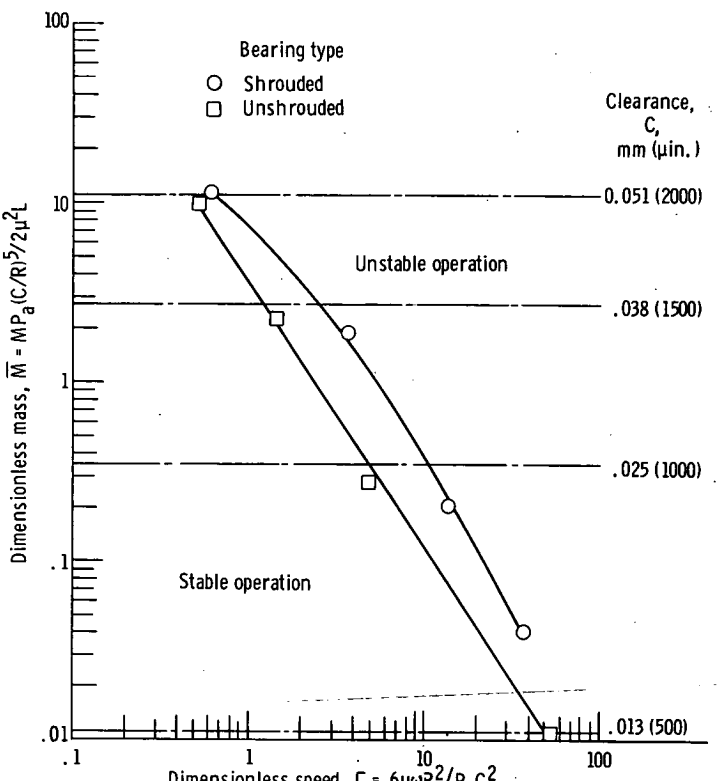

Figure 26. - Comparison of stability of shrouded and unshrouded one-segment, three-pad Rayleigh step bearing. Ridge- to pad-arc ratio, 0.45; step depth, 0.066 millimeter (2600 μin.).

Comparison of stability of a shrouded and an unshrouded Rayleigh step bearing. - The two curves in figure 26 show the threshold of stability of shrouded and unshrouded one-segment, three-pad bearings with ψ equal to 0.45. The data for both were obtained from the same bearing (number 17, table IV(b)), which was first run with shrouds. The shrouds were then machined off, and the bearing was renumbered 19 (table V) and rerun without shrouds. Figure 26 shows that a substantial increase in stability can be gained by using shrouds since the dimensionless mass $\overline{M}$ for the shrouded bearing is always greater than that for the unshrouded bearing over the entire range of dimensionless speed Γ tested.

Effect of clearance on stability. - Figure 27 is a plot of whirl speed against film thickness ratio k_r at four clearances. At the larger clearances, 0.025 and 0.048 millimeter (1000 and 1900 μin.), the one-segment, three-pad shrouded bearing is clearly the most stable of the four Rayleigh step bearings tested. However, at the smallest clearance value, 0.010 to 0.015 millimeter (400 to 600 μin.), the stability of all four configurations tends to approach equal magnitude. In fact, the three-segment, one-pad shrouded bearing shows greater stability than the other three configurations at high film thickness ratios (above 5.2), which is the opposite of their performance at the larger clearance value, 0.025 to 0.048 millimeter (1000 to 1900 μin.). This difference is possibly due to some slight angular misalinement of the bearing axis with the journal axis which tends to preload the bearings and gives them a stability which might not be present under more ideal alinement conditions (see ref. 22). Reference 17 reports a plain bearing and journal running stably in water at a radial clearance of 0.009 millimeter (350 μin.) to a speed of 6200 rpm apparently because of preloading of the bearing by misalinement. For the Rayleigh step bearings (in fig. 27) at clearances above 0.015 millimeter (600 μin.), this preload is too small to affect the bearings and results in a more accurate measure of their true stability. In light of the preceding discussion, the four Rayleigh step bearing configurations of this investigation can be rated in order of diminishing stability as follows: (1) one-segment, three-pad shrouded bearing, (2) one-segment, one-pad shrouded bearing, (3) one-segment, three-pad unshrouded bearing, and (4) three-segment, one-pad shrouded bearing.

Rayleigh step bearing design curves. - The data for the one-segment, three-pad shrouded Rayleigh step bearing with

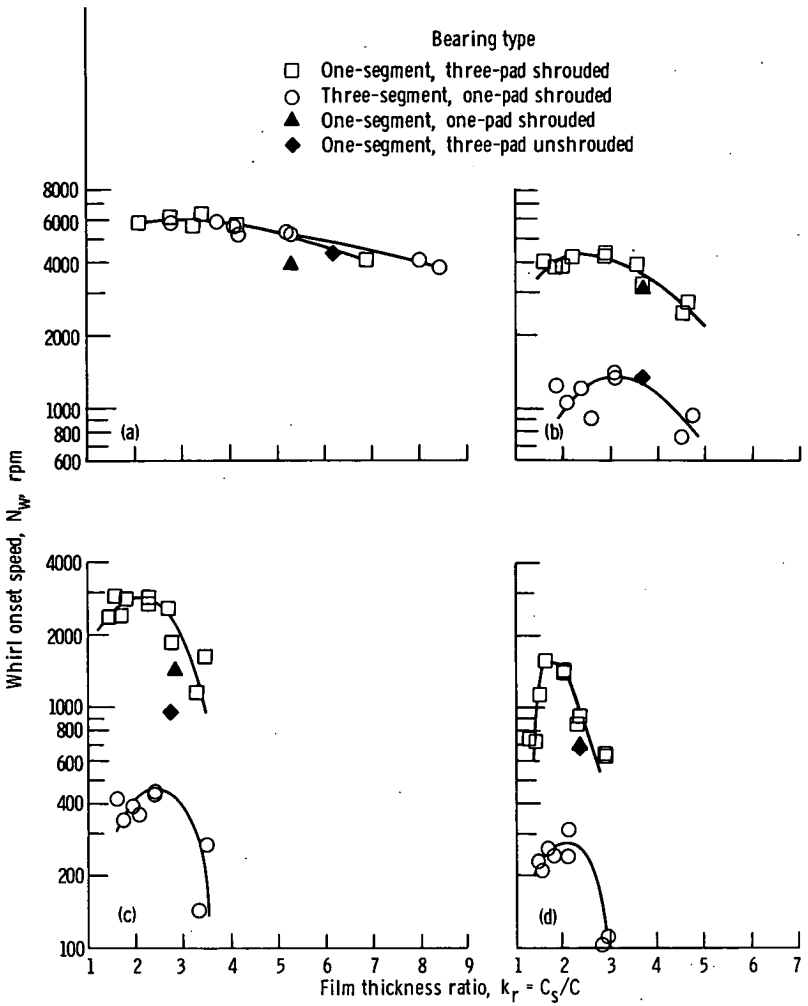

(a) Radial clearance in ridge region, 0.010 to 0.015 millimeter (400 to 600 μin.).

(b) Radial clearance in ridge region, 0.025 millimeter (1000 μin.).

(c) Radial clearance in ridge region, 0.038 millimeter (1500 μin.).

(d) Radial clearance in ridge region, 0.048 millimeter (1900 μin.).

Figure 27. - Whirl onset speed as function of film thickness ratio at various radial clearances.

a ψ of 0.27 were replotted in slightly different form in order to facilitate the design of optimum-geometry bearings. Because of the close similarity of the stability data for the bearings with ψ equal to 0.27 and 0.45 (fig. 24), the design curves discussed in this section can be applied to either. Design curves for the three-segment, one-pad shrouded bearing were not considered in this report because of their relatively low stability. The one-segment, one-pad configuration was not considered because of its limitation of preferential loading direction and the fact that insufficient stability data were available.

Whirl onset speed is plotted against radial clearance in figure 28 for five values of step depth for the one-segment, three-

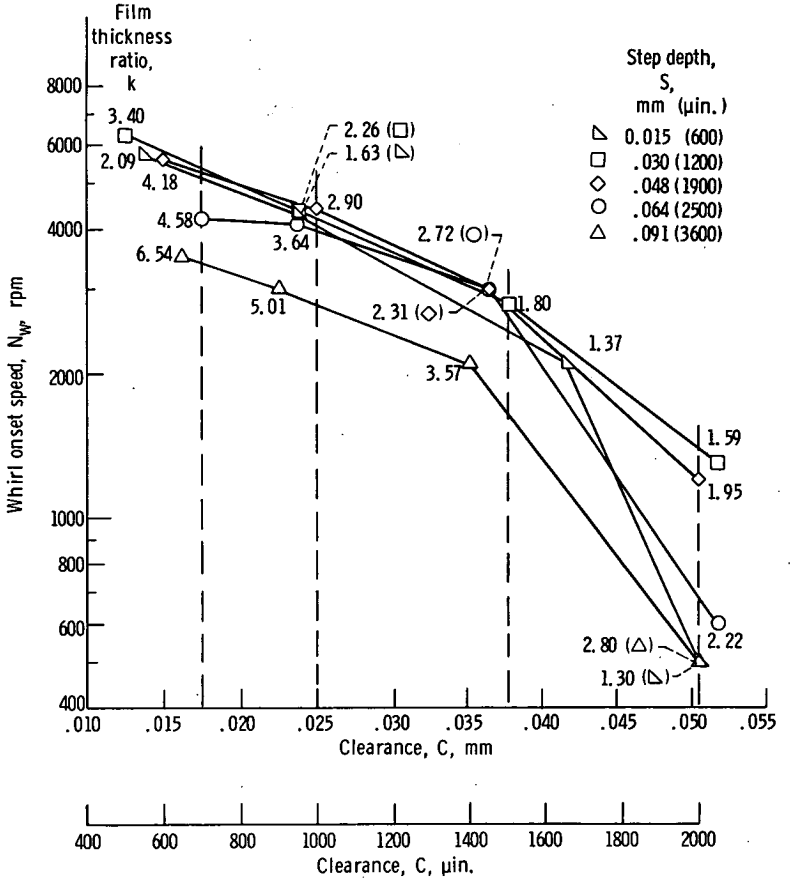

Figure 28. - Whirl onset speed as function of radial clearance for one-segment, three-pad shrouded Rayleigh step bearing at various film thickness ratios. Ridge- to pad-arc ratio, 0.27.

pad shrouded bearings. The values of the film thickness ratio $k_r = C_s/C$ (table IV(a)) are given for each data point and represent the ratio of the clearance at the step region to the clearance at the ridge region of each bearing when the shaft is concentric in the bearing (see fig. 2(d)). The four vertical dashed lines, drawn at arbitrary clearance values of 0.018, 0.025, 0.038, and 0.051 millimeter (700, 1000, 1500, and 2000 μin.), intersect the stability curves at various values of whirl onset speed. The curves in figure 29 were obtained by cross plotting the data in figure 28 at the four values of clearance with whirl onset speed N_W and film thickness ratio k_r as variables. Simple straight line interpolation was used for the cross plot. In figure 29 there is an optimum value of k_r at any given C, and this optimum is a function of C. Figure 29 shows that stability becomes more sensitive to k_r as C increases, which makes it more difficult to achieve an optimum. The figure also shows that the optimum film thickness ratio k_r decreases from 2.8 to 1.6 as the clearance increases from 0.018 to 0.051 millimeter (700 to

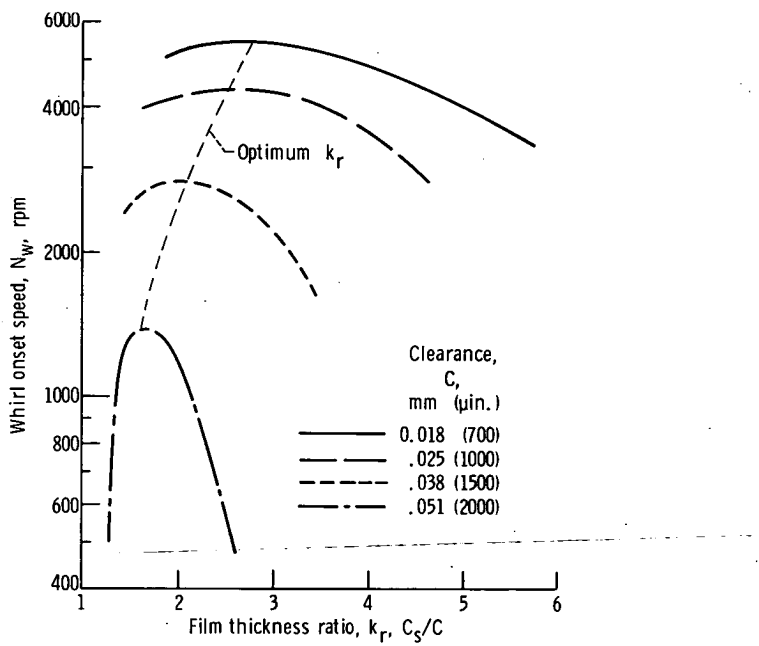

Figure 29. - Whirl onset speed as function of film thickness ratio for one-segment, three-pad shrouded Rayleigh step bearing. Ridge- to pad-arc ratio, 0.27.

2000 μin.). For eccentricity ratios less than 0.2, an optimum film thickness ratio of 1.7, obtained by using the criterion of load capacity, was reported in reference 9. The optimum k_r value is, therefore, generally higher (1.6 to 2.8) when the criterion of stability is used rather than load capacity.

From figure 29 the step height for maximum stability at each of four clearances can be calculated. It is approximately 36 millimeters (1400 μin.) over the range of clearances investigated. A ratio of step height to radius $(C_s - C)/R$ of 0.0019 will, therefore, yield the most stable one-segment, three-pad

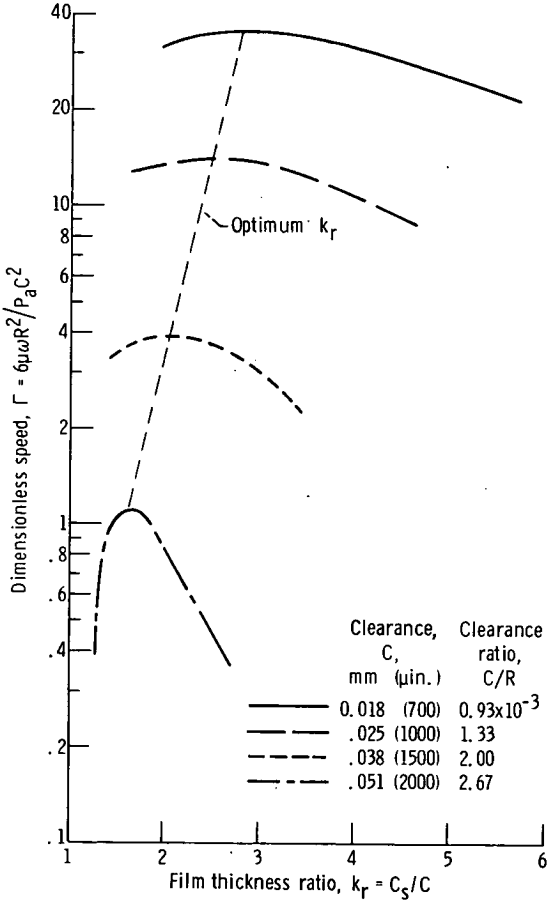

Figure 30. - Dimensionless speed as function of film thickness ratio for one-segment three-pad shrouded Rayleigh step bearing. Ridge- to pad-arc ratio, 0.27.

shrouded Rayleigh step bearing at any clearance value.

Figure 30 is essentially a repetition of figure 29 except that the ordinate is the dimensionless speed γ rather than the dimensional speed N_W. Values of C/R as well as C have also been listed in an attempt to make this figure of wider applicability in the design of a Rayleigh step bearing of optimum stability.

Three-Central-Lobe Bearings

Experimental results obtained with 10 bearings having different lobe heights are shown in tables VII to X. Test results for three-lobe bearings with three axial grooves are shown in table VII, and results for bearings with no axial grooves are shown in table X. Table VIII lists the results for a three-axial-groove bearing with no lobing, and table IX the results for a plain bearing with no grooves and no lobing. Journals of different diameters were used to obtain the different clearances shown for any particular bearing tested. A total of 39 bearing stability tests were conducted at values of radial clearance C ranging from 0.009 to 0.052 millimeter (350 to 2050 μin.) and lobe heights ranging from 0 to 0.102 millimeter (0 to 4000 μin.).

Effect of lobe height on stability. - Figure 31(a) shows the stability limits of a three-lobe, three-axial-groove bearing at five lobe heights. As the lobe height was increased from 0 to 0.25 millimeter (0 to 1000 μin.), the stability increased. (The bearing having a lobe height of zero is actually a plain (unlobed) bearing with three axial grooves.) As the lobe height was further increased from 0.025 to 0.066 millimeter (1000 to 2600 μin.), the stability decreased. Maximum stability occurred at a lobe height of 0.025 millimeter (1000 μin.).

Figure 31(b) shows the stability limits of three-lobe bearings with no axial grooves at five lobe heights. Maximum stability occurred at a lobe height of 0.025 millimeter (1000 μin.) for the limited data recorded. (There were no data obtained at lobe heights below 0.025 mm (1000 μin.).) An increase in lobe height above 0.025 millimeter (1000 μin.) caused a decrease in stability.

Range of stability of three-central-lobe bearing with and without axial grooves. - It is interesting to note that stable operation at a clearance value above 0.018 millimeter (700 μin.) was impossible to attain with the three-central-lobe bearing

TABLE VII. - TEST RESULTS FOR THREE-CENTRAL-LOBE BEARINGS WITH THREE AXIAL GROOVES

[Offset factor α, 0.5.]

Bearing	Lobe height, H_L		Preload (ellipticity), a		Minimum radial clearance, $C = R_{PC} - R$		Radial clearance before preload, $C_0 = R_P - R$		Fractional-frequency-whirl onset speed at zero load, N_W, rpm	Film thickness ratio, $k_c = 1 + \frac{H_L}{C}$	Preload coefficient, $\delta = \frac{a}{R_P - R}$
	mm	μin.	mm	μin.	mm	μin.	mm	μin.			
1	0.015	600	0.030	1200	0.014	550	0.044	1750	5000	2.09	0.685
					.020	800	.051	2000	670	1.75	.600
					.025	1000	.056	2200	300	1.60	.545
					.039	1550	.070	2750	200	1.39	.438
					.052	2050	.083	3250	90	1.29	.367
2	0.025	1000	0.051	2000	0.015	600	0.066	2600	4900	2.67	0.770
					.024	950	.076	3000	2000	2.06	.680
					.039	1550	.091	3600	500	1.65	.565
					.052	2050	.104	4100	160	1.49	.494
3	0.046	1800	0.091	3600	0.013	500	0.104	4100	5000	4.60	0.878
					.022	850	.114	4500	2200	3.12	.810
					.037	1450	.130	5100	390	2.24	.713
					.050	1950	.142	5600	100	1.92	.648
4	0.066	2600	0.132	5200	0.010	400	0.142	5600	4300	7.50	0.930
					.024	950	.158	6200	1300	3.74	.848
					.037	1450	.170	6700	200	2.79	.782
					.047	1850	.180	7100	130	2.41	.738

TABLE VIII. - TEST RESULTS FOR THREE-AXIAL-GROOVE BEARING WITH NO LOBING

[Bearing 5; film thickness ratio, 1.0.]

Radial clearance, C		Fractional-frequency-whirl onset speed at zero load, N_W, rpm
mm	μin.	
0.009	350	7000
.023	900	500
.033	1300	250
.046	1800	70

TABLE IX. - TEST RESULTS FOR A PLAIN BEARING (NO GROOVES, NO LOBING)

[Bearing 6.]

Radial clearance, C		Fractional-frequency-whirl onset speed at zero load, N_W, rpm
mm	μin.	
0.009	350	6200
.018	700	(a)

[a]Bearing unstable at minimum operating speed (70 rpm).

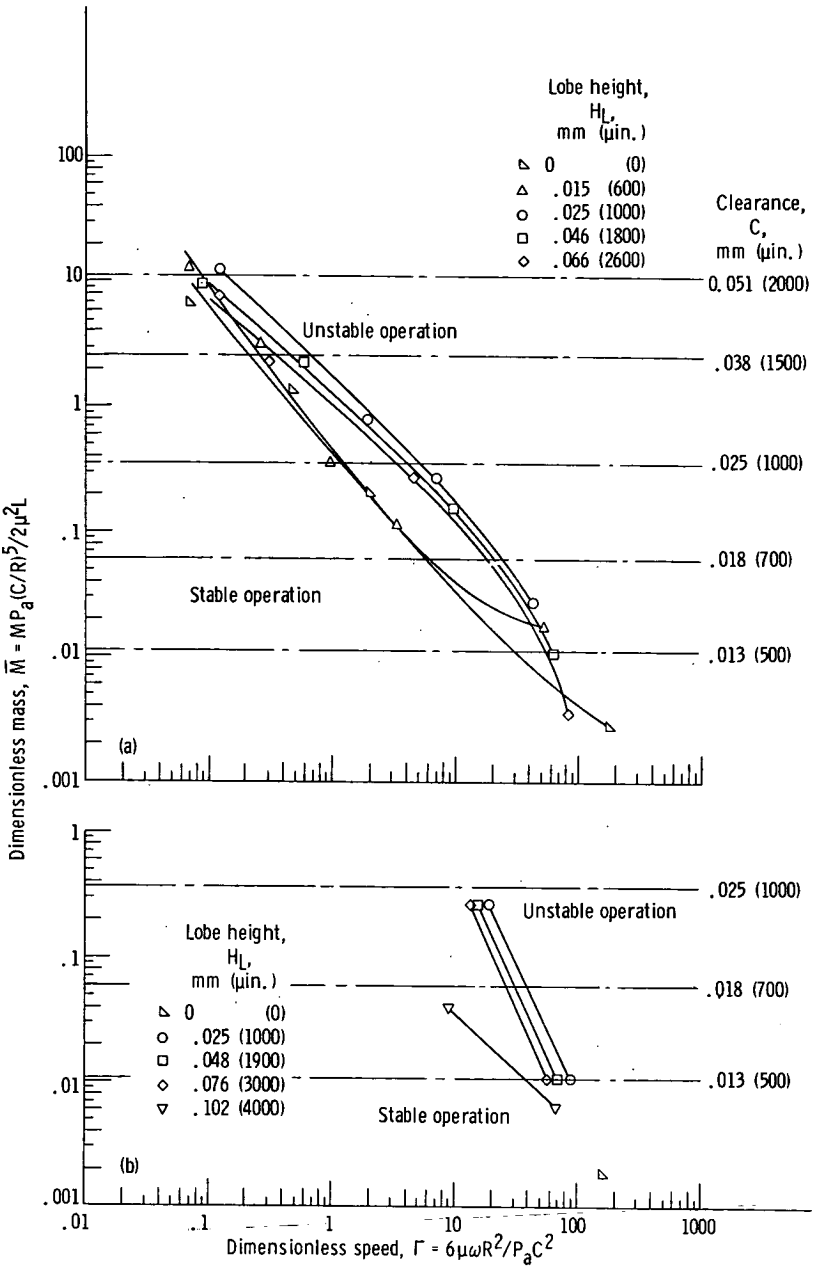

(a) With three axial grooves.

(b) Without grooves.

Figure 31. - Effect of lobe height on stability of three-central-lobe bearing.

without the three axial grooves (table X). It appears that at the tighter clearances, 0.013 to 0.018 millimeter (500 to 700 μin.), the lobes of the bearing without grooves are effective in keeping the bearing stable. However, as the clearance is increased above 0.013 millimeter (700 μin.), the lobes lose their effectiveness, and the bearing no longer acts as a plain bearing with a uniformly distorted contour. An attempt was made to run a plain cylindrical bearing with no grooves and zero lobe height, which represented a minimum condition of lobe height for the bearings without grooves. This bearing ran stable at a clearance of 0.009 millimeter

TABLE X. - TEST RESULTS FOR THREE-CENTRAL-LOBE BEARINGS WITH NO GROOVES

[Offset factor α, 0.5.]

Bearing	Lobe height, H_L		Minimum radial clearance, $C = R_{PC} - R$		Fractional-frequency-whirl onset speed at zero load, N_W, rpm
	mm	μin.	mm	μin.	
7	0.025	1000	0.013	500	7000
			.018	700	5400
			.023	900	(a)
			.032	1250	(a)
8	0.048	1900	0.013	500	5500
			.018	700	4400
			.023	900	(a)
			.032	1250	(a)
9	0.076	3000	0.013	500	4500
			.018	700	3800
			.023	900	(a)
			.032	1250	(a)
10	0.102	4000	0.011	450	4300
			.016	650	1200
			.025	1000	(a)
			.029	1150	(a)

[a]Bearing unstable at minimum operating speed (70 rpm).

(350 μin.) to a speed of 6200 rpm but was completely unstable at a clearance of 0.018 millimeter (700 μin.)(table IX). Since an unloaded plain journal bearing will whirl at all speeds and clearances, the one stable point at 0.009 millimeter (350 μin.) was probably due to a slight misalinement of the bearing with the journal. This would tend to preload the bearing and give it some stability (ref. 22). At higher clearances, above 0.009 millimeter (350 μin.), the preload was too small to preload the bearing effectively and keep it running stably.

From the results of the present investigation it is apparent that a three-central-lobe bearing with three axial grooves is stable over a larger range of clearances than one without grooves when operating hydrodynamically while immersed in a low-viscosity lubricant such as water.

Comparison of theoretical and experimental stability data for three-central-lobe, three-axial-groove bearings. - The solid curves shown in figure 32 are from reference 10 and show the theoretical stability threshold of three-lobe bearings that are centrally lobed. Since the Reynolds number of the experimental points presented in this report fell within the range of 0 to 2000, both curves have been included. The experimental data were plotted by using the parameters of reference 10 and show fair agreement with the theoretical values for the centrally lobed bearing (offset factor $\alpha = 0.5$). Theory predicts a larger range of stable operation than was observed experimentally.

Conventionally the lobe radius is machined into the bearings, and this radius is then measured. Using shims to obtain the lobes, as was done here, results in a lobe contour that is not exactly a true circular arc. Therefore, a radius which approximates the curvature of the lobes had to be calculated from the lobe heights. Figure 33 shows the difference in lobe contour between a lobe that has been machined in and a lobe that has been generated by a shim. The contour of the shimmed lobe is shown as a solid curve and was traced from a profile trace of one of the test bearings. The dashed curve illustrates what the contour would look like if it were machined in and generated from the 120° arc to the right of the curves. Both lobes have the same height, 0.025 millimeter (1000 μin.). The effect that differences in lobe contour might have on stability could only be determined if the results of these shimmed-lobe bearing tests were compared with those for machined-lobe bearings of equal offset factor and dimensions.

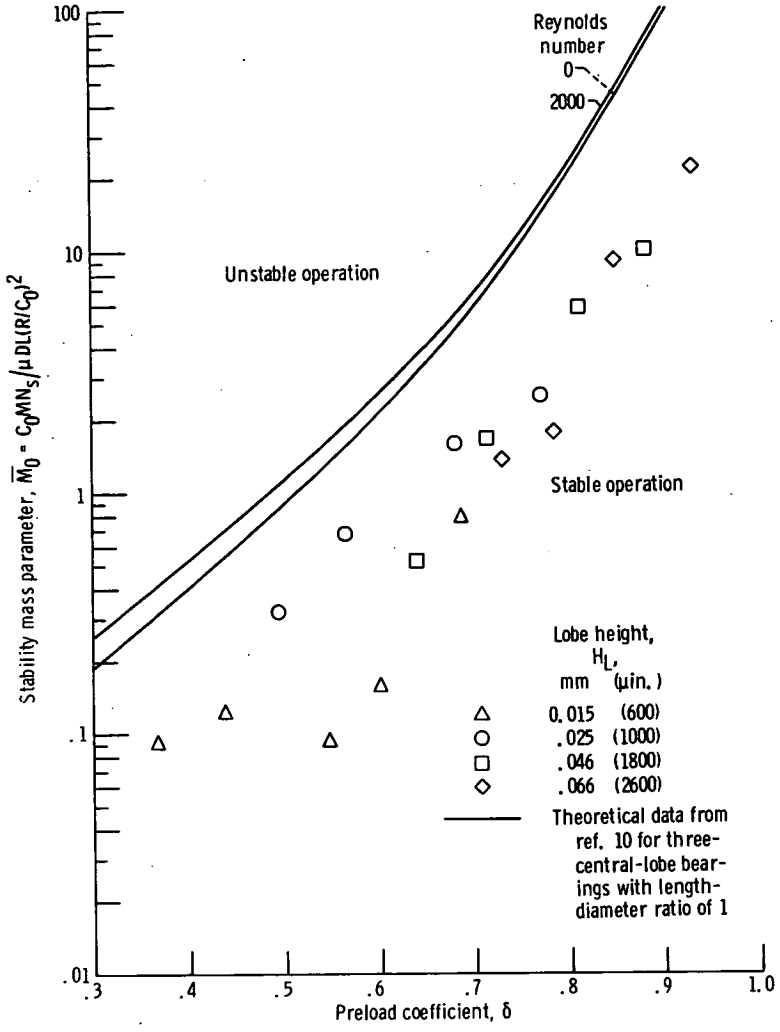

Figure 32. - Comparison of theoretical and experimental data using dimensionless parameters of reference 10.

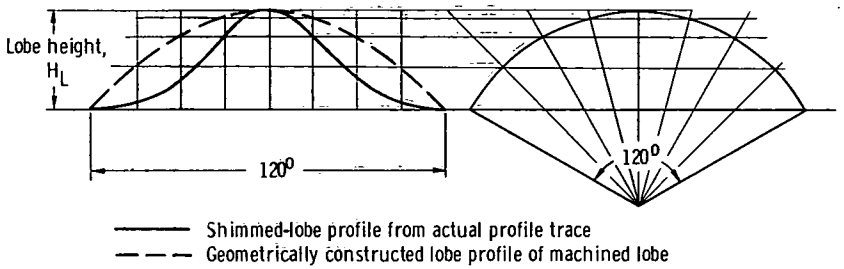

Figure 33. - Comparison of profiles of shimmed and machined lobes. Lobe height, 0.025 millimeter (1000 μin.).

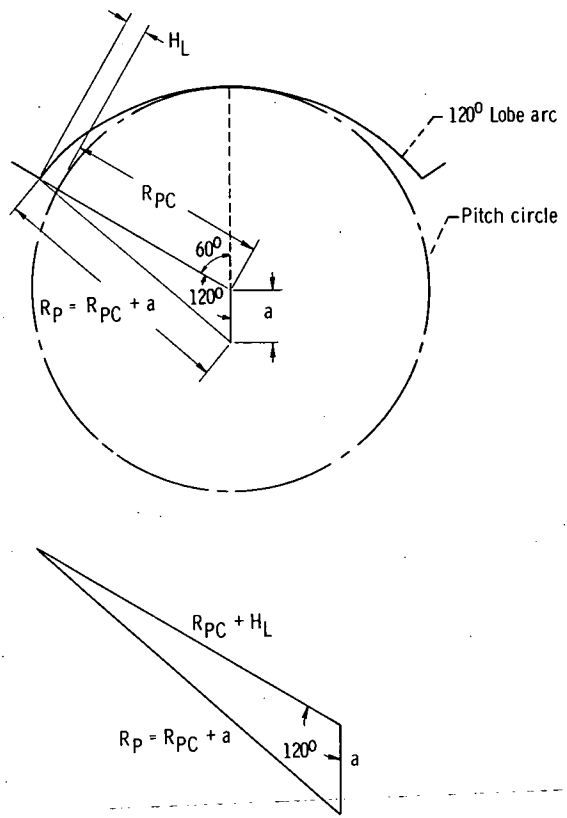

Figure 34. - Method of calculating preload a, lobe radius R_P, and preload coefficient δ from measured value of lobe height H_L. Three-central-lobe bearing.

The calculated lobe radius R_P is the radius that would be used to machine a lobe of the same height as the shimmed lobe. A sample calculation follows to show how the measured lobe height of the shimmed bearings H_L was used to obtain R_P. Figure 34 is an illustration of the pitch circle of a three-lobe bearing and one of the centrally lobed sectors. The pitch circle is defined as a circle that touches each lobe at its minimum film thickness location (the midpoint of each lobe arc for centrally lobed bearings). A triangle based on the relation between the pitch circle and lobe radii is constructed as shown. From the law of cosines

$$(R_{PC} + a)^2 = (R_{PC} + H_L)^2 + (a)^2 - 2(R_{PC} + H_L)(a)(\cos 120^\circ) \quad (1)$$

In this example the lobe height H_L was measured to be 0.025 millimeter (1000 μin.), and the pitch circle radius R_{PC} was measured to be 1.909 centimeters (0.7514 in.). Substituting these known values into equation (1) results in a value of 0.050 millimeter (2000 μin.) for the preload a. The lobe radius R_P is the sum of the pitch circle radius R_{PC} and the preload a, or in this case 1.909 + 0.0050 = 1.914 centimeters (0.7514 + 0.0020 = 0.7534 in.). The preload coefficient is then obtained from $\delta = a/(R_P - R)$ and would be the same for a machined lobe of equal height.

Three-central-lobe bearing design curves. - Whirl onset speed is plotted against radial clearance in figure 35 for the four values of lobe height H_L for the three-lobe axial-groove bearings. The values of film thickness ratio $k_c = 1 + (H_L/C)$ and preload coefficient $\delta = a/(R_P - R)$ (table VII) are given for each data point. Figure 36, obtained from figure 35, shows that there is an optimum value of k_c and δ at any given C and that this optimum is a function of C. It also shows that stability becomes more sensitive to k_c as C increases, although this is not readily apparent because of the nonlinear scale used in plotting k_c in this figure.

Figure 37 is essentially a repetition of figure 36 except that it was plotted by using the dimensionless speed parameter Γ instead of whirl onset speed as the ordinate. It is included because it is more useful as a design parameter than the curves of figure 36.

From figure 36 the lobe height for maximum stability at each of four clearances can be calculated. It is approximately 28 millimeters (1080 μin.) over the range of clearances investigated.

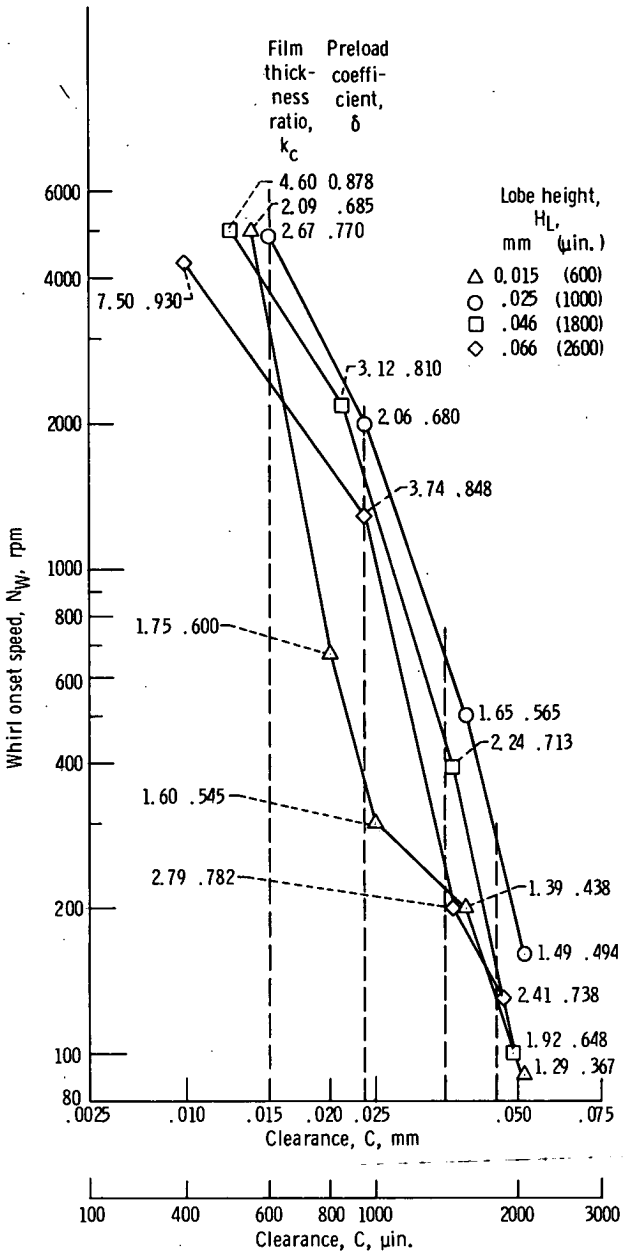

Figure 35. - Whirl onset speed as function of radial clearance at various film thickness ratios and preload coefficients for three-central-lobe bearing with axial grooves.

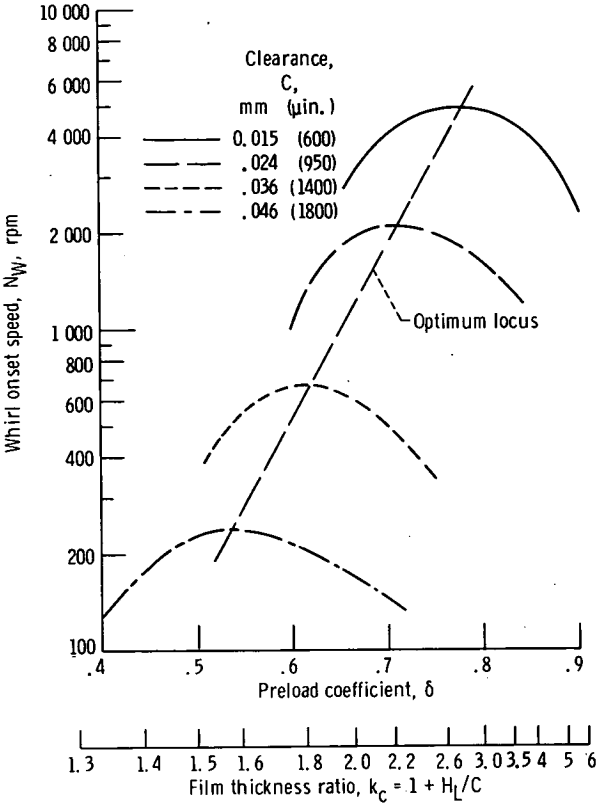

Figure 36. - Whirl onset speed as function of preload coefficient and film thickness ratio for three-central-lobe bearings with axial grooves.

A ratio of lobe height to radius H_L/R of 0.0014 will, therefore, yield the most stable three-central-lobe bearing with axial grooves, at any clearance.

Preload coefficient is a more universal term used in lobed-bearing design than is film thickness ratio. Lobe height is used in this report only because it was the dimension that was measured, and from it the radius of the sector R_P was calculated to arrive at the preload coefficient $\delta = a/(R_P - R)$. For this reason both preload coefficient δ and film thickness ratio k_c appear as coordinates in figures 36 and 37.

Figures 36 and 37 show that the preload coefficient, at the points of optimum locus, increases from about 0.54 to 0.78 and

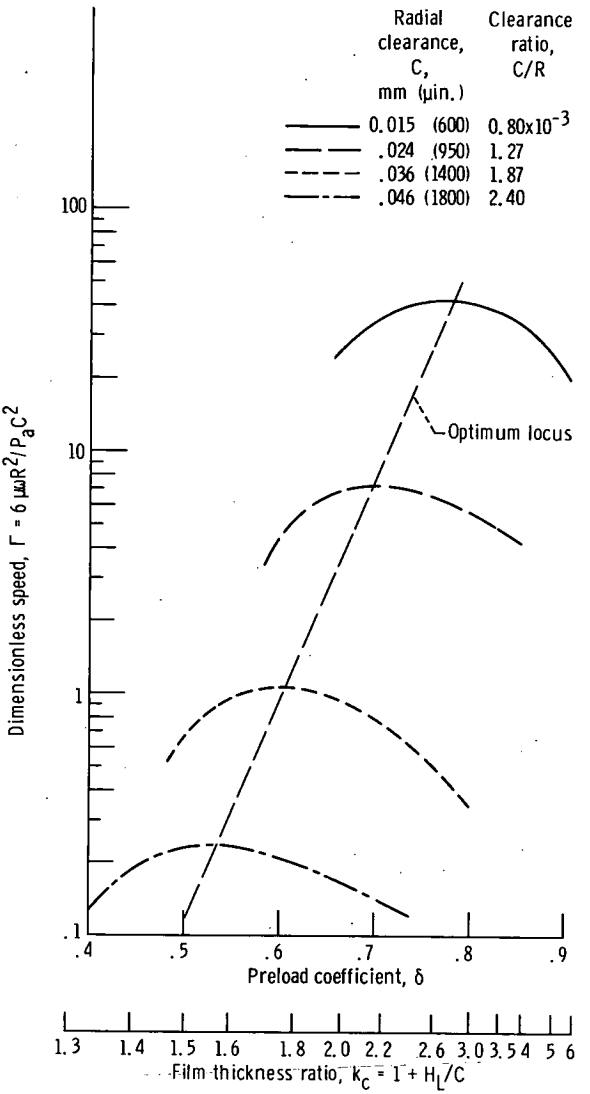

Figure 37. - Dimensionless speed as function of preload coefficient and film thickness ratio for three-central-lobe bearings with axial grooves.

the film thickness ratio from 1.57 to 2.78 as the clearance is reduced from 0.046 to 0.015 millimeter (1800 to 600 μin.).

Three-Tilted-Lobe Bearings

The results of 32 stability tests that covered a range of ΔR_L from 0.013 to 0.108 millimeter (500 to 4200 μin.) are shown in tables XI and XII and in figures 38 to 45.

In these experiments, the leading-edge entrance wedge thickness ΔR_L (figs. 4 and 8) was used as a parameter for comparing the stability characteristics of converging-diverging bearings with wholly converging-film three-sector bearings. Both types of bearings were run at four values of radial clearance C for each of four values of ΔR_L.

The preload coefficient δ of a converging-diverging-film bearing is different from that of a wholly converging-film bearing when both have the same ΔR_L and clearance, as shown in figure 38. For example, at a ΔR_L value of 0.076 millimeter (3000 μin.), the preload coefficient for a converging-diverging-film bearing at a radial clearance C of 0.053 millimeter (2100 μin.) is 0.71, while for a wholly converging-film bearing the preload coefficient is only 0.54. In this report, therefore, the preload coefficient is used only when experimental data are compared with referenced theoretical data for which the preload coefficient was used as one of the parameters.

Effect of bearing configuration on stability. - The experimental results obtained with three-sector bearings having a converging-diverging-film ($\alpha = 0.6$) and a wholly converging-film geometry ($\alpha = 1.0$) are shown in figure 39. The smallest average leading-edge entrance wedge thickness ΔR_L was 0.014 millimeter (550 μin.) for the converging-diverging-film and wholly converging-film bearings (the stability curves for which are depicted in fig. 39(a)). At this value of ΔR_L, the bearings of the two different film geometries had essentially the same stability characteristics.

A study of figure 39 shows that the wholly converging-film bearing is more stable for all ΔR_L values ranging from 0.037 to 0.103 millimeter (1450 to 4050 μin.), with one possible exception. In figure 39(d), at a ΔR_L of 0.103 millimeter (4050 μin.) and an $\overline{M}$ of 0.11, the curve representing the converging-diverging-film bearing appears to cross over that for the wholly

TABLE XI. - TEST RESULTS FOR THREE-TILTED-LOBE BEARINGS WITH CONVERGING-DIVERGING-FILM GEOMETRY

[Offset factor α, 0.6.]

Bearing	Leading-edge entrance wedge thickness, ΔR_L		Preload (ellipticity), a		Minimum radial clearance, $C = R_{PC} - R$		Radial clearance before preload, $C_0 = R_P - R$		Preload coefficient, $\delta = \frac{a}{R_P - R}$	Fractional-frequency-whirl onset speed at zero load, N_W, rpm	Film thickness ratio, $k = 1 + \frac{\Delta R_L}{C}$
	mm	μin.	mm	μin.	mm	μin.	mm	μin.			
11	0.013	500	0.025	1000	0.018	700	0.043	1 700	0.59	7400	1.71
					.027	1050	.053	2 100	.48	2400	1.46
					.041	1600	.066	2 600	.38	510	1.31
					.053	2100	.079	3 100	.32	290	1.24
12	0.038	1500	0.074	2900	0.015	600	0.089	3 500	0.83	5700	3.50
					.025	1000	.099	3 900	.74	1800	2.50
					.038	1500	.112	4 400	.66	600	2.00
					.055	2150	.130	5 100	.57	460	1.70
13	0.071	2800	0.117	4600	0.015	600	0.132	5 200	0.89	5800	5.67
					.027	1050	.142	5 600	.82	2200	3.67
					.039	1550	.155	6 100	.75	1200	2.80
					.053	2100	.168	6 600	.70	800	2.33
14	0.107	4200	0.198	7800	0.020	800	0.218	8 600	0.91	5200	6.30
					.030	1200	.228	9 000	.87	1200	4.50
					.043	1700	.241	9 500	.82	500	3.47
					.056	2200	.254	10 000	.78	300	2.90

TABLE XII. - TEST RESULTS FOR THREE-TILTED-LOBE BEARINGS WITH WHOLLY CONVERGING-FILM GEOMETRY

[Offset factor α, 1.0.]

Bearing	Leading-edge entrance wedge thickness, ΔR_L		Preload (ellipticity), a		Minimum radial clearance, $C = R_{PC} - R$		Radial clearance before preload, $C_0 = R_P - R$		Preload coefficient, $\delta = \frac{a}{R_P - R}$	Fractional-frequency-whirl onset speed at zero load, N_W, rpm	Film thickness ratio, $k = 1 + \frac{\Delta R_L}{C}$
	mm	μin.	mm	μin.	mm	μin.	mm	μin.			
15	0.015	600	0.013	500	0.022	850	0.034	1350	0.37	4600	1.71
					.030	1200	.043	1700	.29	1900	1.50
					.044	1750	.057	2250	.22	500	1.34
					.057	2250	.070	2750	.18	200	1.27
16	0.036	1400	0.028	1100	0.017	650	0.046	1800	0.61	9000	3.15
					.024	950	.051	2000	.55	6500	2.47
					.034	1350	.061	2400	.46	5000	2.04
					.050	1950	.076	3000	.37	1700	1.72
17	0.066	2600	0.053	2100	0.015	600	0.069	2700	0.78	7400	5.33
					.025	1000	.079	3100	.68	6500	3.60
					.038	1500	.091	3600	.58	4800	2.73
					.052	2050	.107	4200	.50	4000	2.27
18	0.099	3900	0.079	3100	0.015	600	0.094	3700	0.84	4900	7.50
					.024	950	.102	4000	.77	5000	5.10
					.037	1450	.117	4600	.67	3000	3.69
					.050	1950	.130	5100	.61	1900	3.00

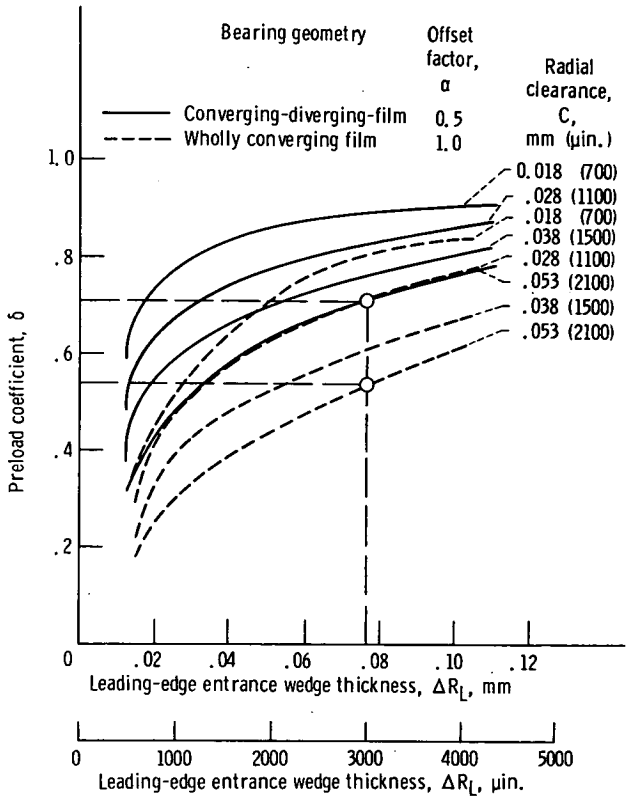

Figure 38. - Preload coefficient as function of leading-edge entrance wedge thickness at various radial clearances for two different bearing lobe configurations.

converging-film bearing, which indicates that a converging-diverging-film bearing might be more stable at $\overline{M}$ values below 0.11 at a ΔR_L of 0.103 millimeter (4050 μin.).

With a converging-diverging-film shape, only a portion of the arc of each lobe (the converging wedge portion) is active in generating load capacity. Increased load capacity and stability can be attained by using more of the arc of each lobe to build up pressure (ref. 12). This is accomplished by tilting the bearing sector on its trailing edge.

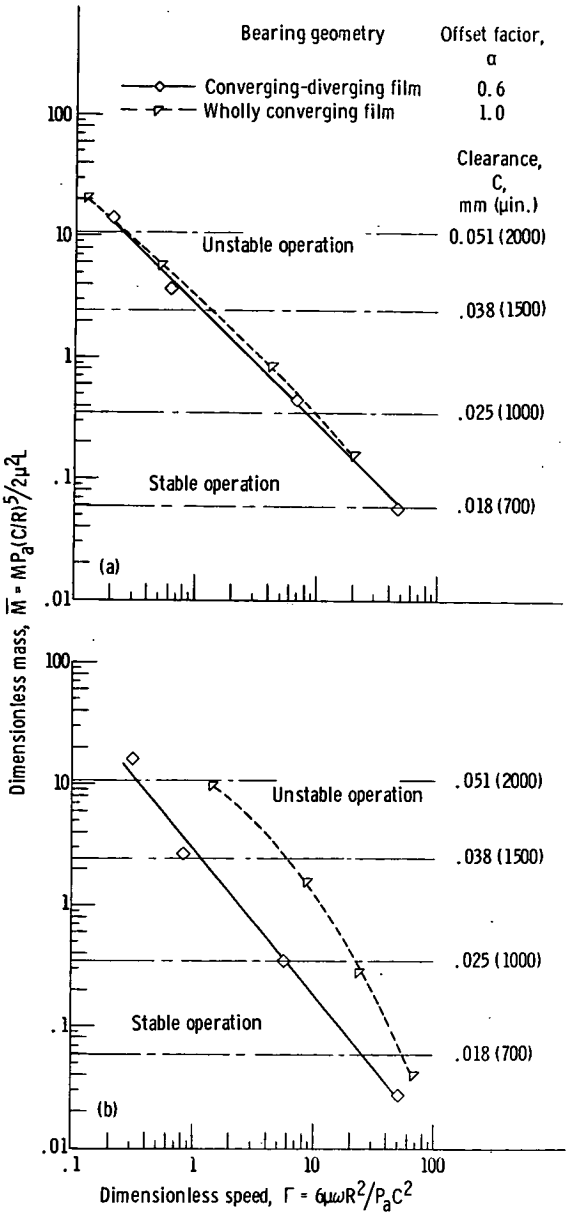

(a) Average leading-edge entrance wedge thickness, 0.014 millimeter (550 μin.).

(b) Average leading-edge entrance wedge thickness, 0.037 millimeter (1450 μin.).

Figure 39. - Effect of bearing configuration on stability of three-lobe bearings at various leading-edge entrance wedge thicknesses.

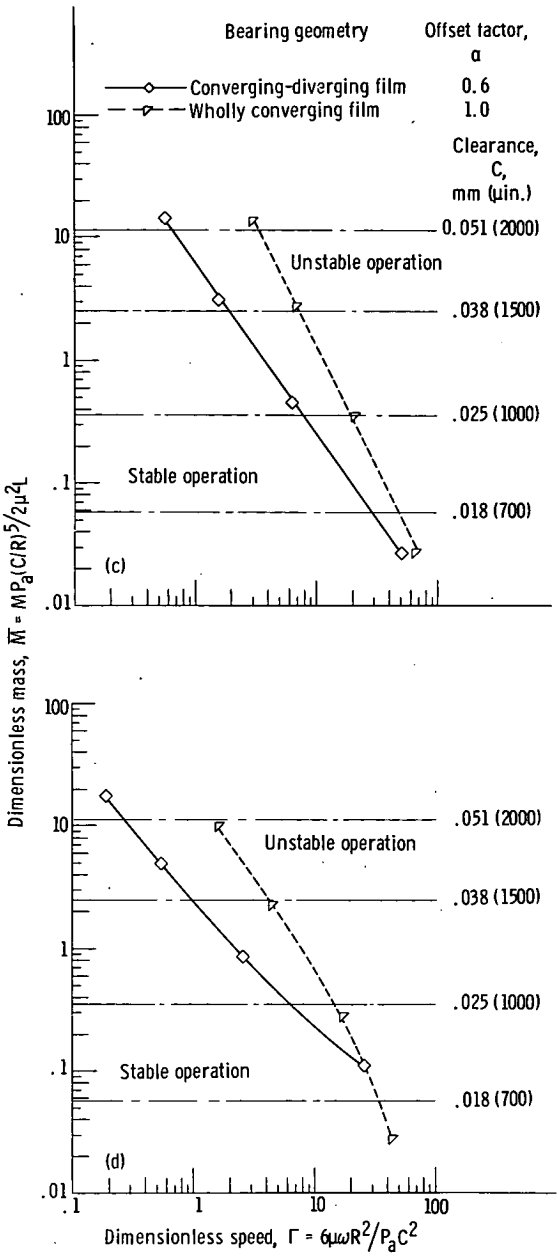

(c) Average leading-edge entrance wedge thickness, 0.014 millimeter (2700 μin.).

(d) Average leading-edge entrance wedge thickness, 0.103 millimeter (4050 μin.).

Figure 39. - Concluded.

Effect of leading-edge entrance wedge thickness on stability. - Figures 40(a) and (b) show the effect of leading-edge entrance wedge thickness ΔR_L on the stability of converging-diverging-film and wholly converging-film bearings, respectively. A maximum in stability exists at a ΔR_L of 0.071 millimeter (2800 μin.) for values of $\overline{M}$ above 0.44 for the converging-diverging-film bearings (fig. 40(a)). Below this value, the bearings with ΔR_L values of 0.013 and 0.107 millimeter (500 and 4200 μin.) were the most stable.

An optimum in stability for the wholly converging-film bearings existed at a ΔR_L of 0.066 millimeter (2600 μin.) (fig. 40(b)) for values of $\overline{M}$ above 0.35. This ΔR_L was near optimum at lower $\overline{M}$ values as well. It is interesting to note that maximum stability for both the converging-diverging-film and the wholly converging-film bearings occurred at almost the same ΔR_L values, namely, 0.071 and 0.066 millimeter (2800 and 2600 μin.),

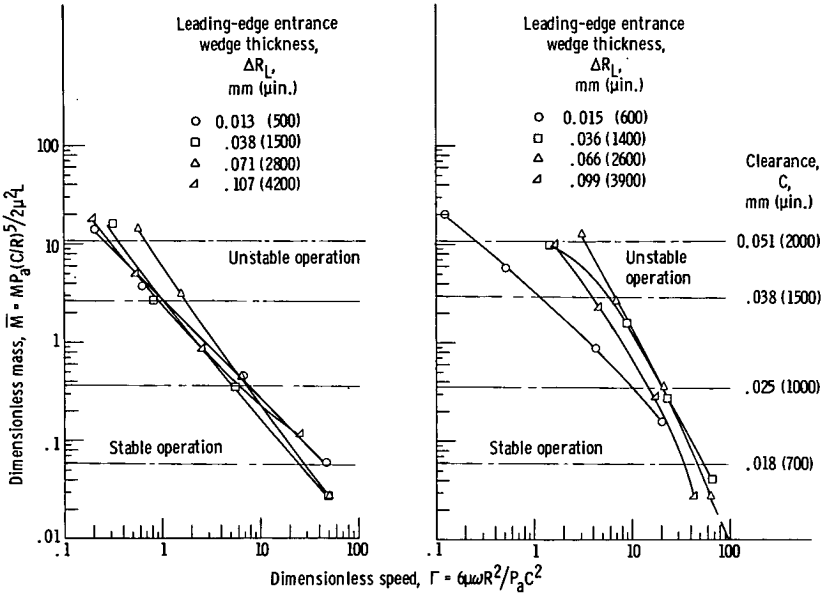

(a) Converging-diverging-film geometry. (b) Wholly converging-film geometry.

Figure 40. - Effect of leading-edge entrance wedge thickness on stability of three-lobe bearing.

respectively, for higher values of $\overline{M}$. Also, there was a considerable gain in stability with the wholly converging-film bearings when the ΔR_L value of 0.015 millimeter (600 μin.) was increased (fig. 40(b)).

Comparison of theoretical and experimental stability data for three-tilted-lobe bearings. - The solid curves shown in figure 41 are from reference 10 and show the theoretical stability threshold of three-lobe bearings that are centrally lobed. The experimental data were plotted by using the parameters of reference 10 and show fair agreement with the theoretical values for the converging-diverging-film bearing, as shown in figure 41(a). Some of the deviation in the experimental data from the theoretical curves might result from the fact that the theoretical curves are based on a centrally lobed configuration, whereas the experimental data were obtained from a noncentral-lobe configuration (fig. 4(c)). This deviation is shown more strikingly in figure 41(b), where the experimental data for a wholly converging-film-geometry bearing (fig. 4(d)) are plotted along with the identical theoretical curves from figure 41(a) for a centrally-lobed bearing configuration. Much of the experimental data shows a more stable bearing than theory predicts for centrally lobed bearings. The scatter of experimental data is more pronounced with the wholly converging film because the preload coefficient δ is not the most desirable parameter to use for a three-sector bearing that is not centrally lobed. The bearing parameters $\overline{M}$ and Γ used in the previous figures give a much better measurement of bearing stability and are not dependent on the manner in which the bearing is tilted.

Three-tilted-lobe bearing design curves. - Whirl onset speed is plotted against radial clearance in figure 42 for four values of ΔR_L for the wholly converging-film bearings. The values of the film thickness ratio $k = 1 + (\Delta R_L/C)$ (table XII) are given for each data point and represent the ratio of inlet to exit film thickness in each sector. Figure 43, obtained from data in figure 42, shows that there is an optimum value of k at any given C and that the optimum is a function of C. It also shows that stability becomes more and more sensitive to k as C increases.

Figure 44 is essentially a repetition of figure 43 except that it was plotted by using two dimensionless parameters, dimensionless speed Γ and film thickness ratio k. It is included because it is more useful as a design tool than the curves of figure 43.

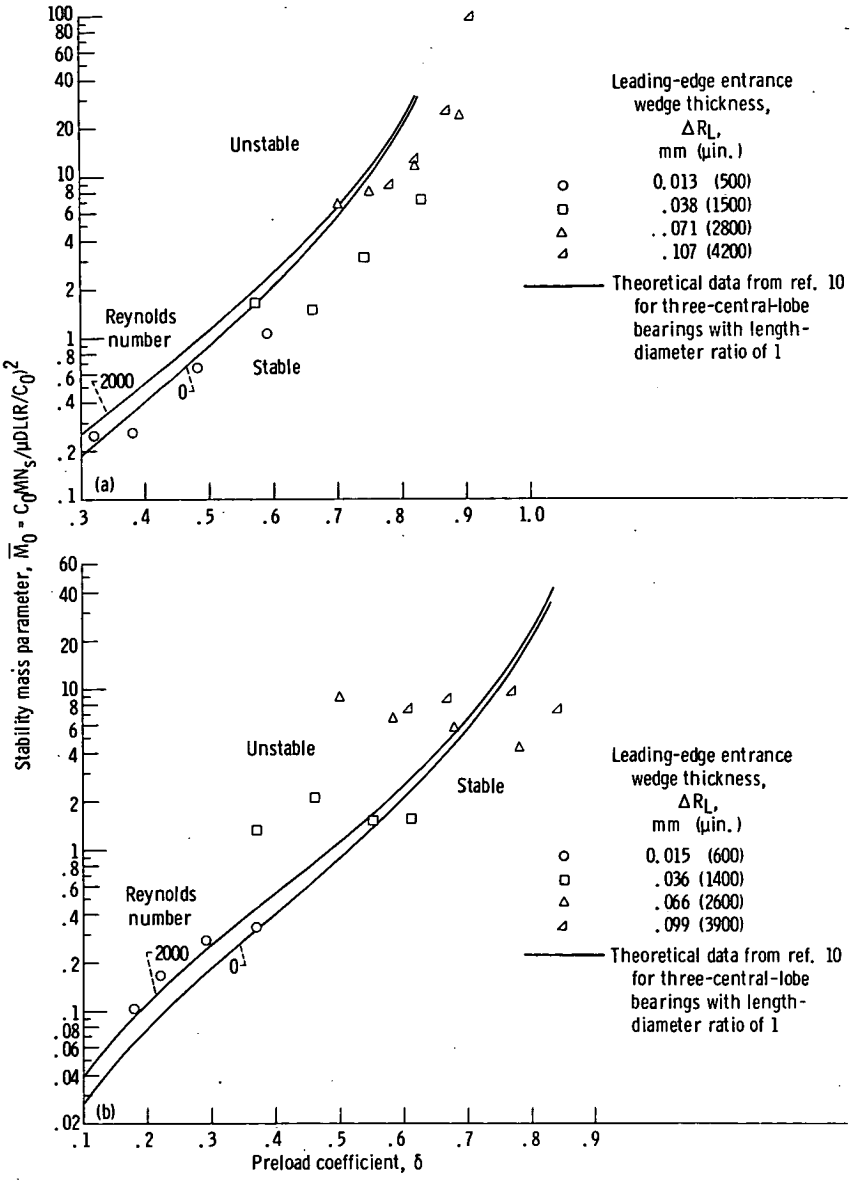

(a) Converging-diverging-film experimental data.

(b) Wholly converging-film experimental data.

Figure 41. - Comparison of theoretical and experimental data for three-lobe bearing using dimensionless parameters of reference 10.

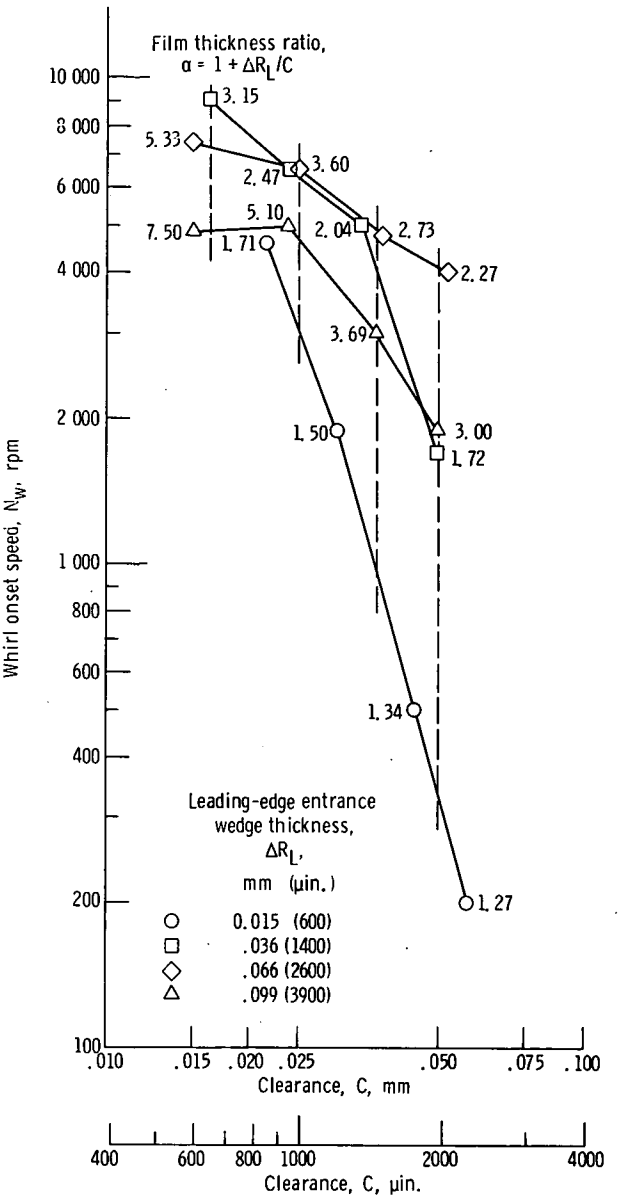

Figure 42. - Whirl onset speed as function of radial clearance for three-lobe wholly converging-film-geometry bearing at various film thickness ratios.

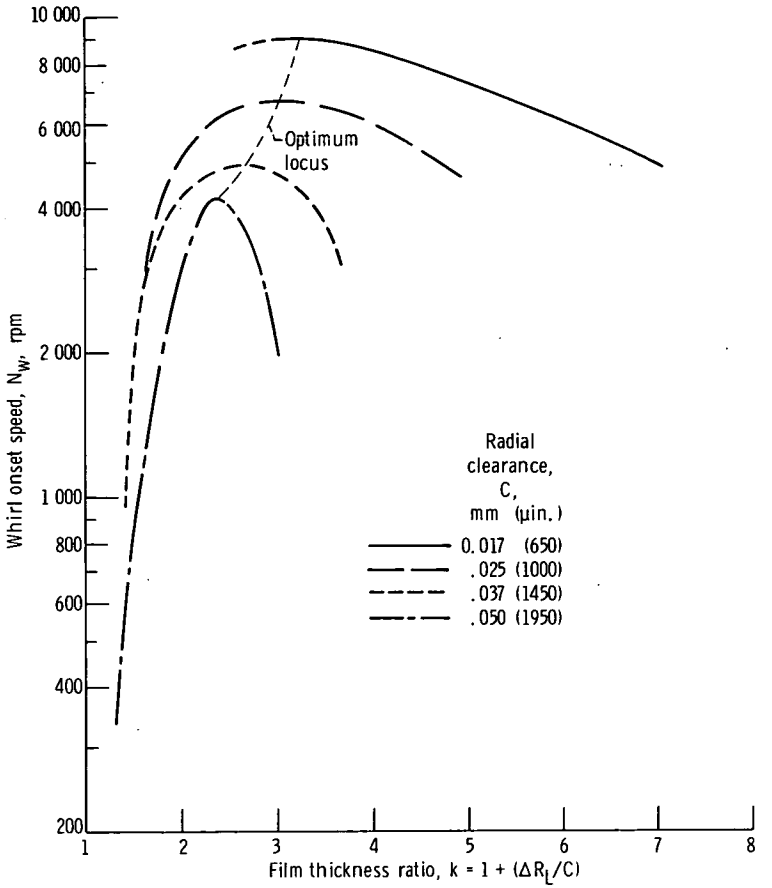

Figure 43. - Whirl onset speed as function of film thickness ratio for wholly converging-film-geometry three-lobe bearing. Offset factor, 1.0.

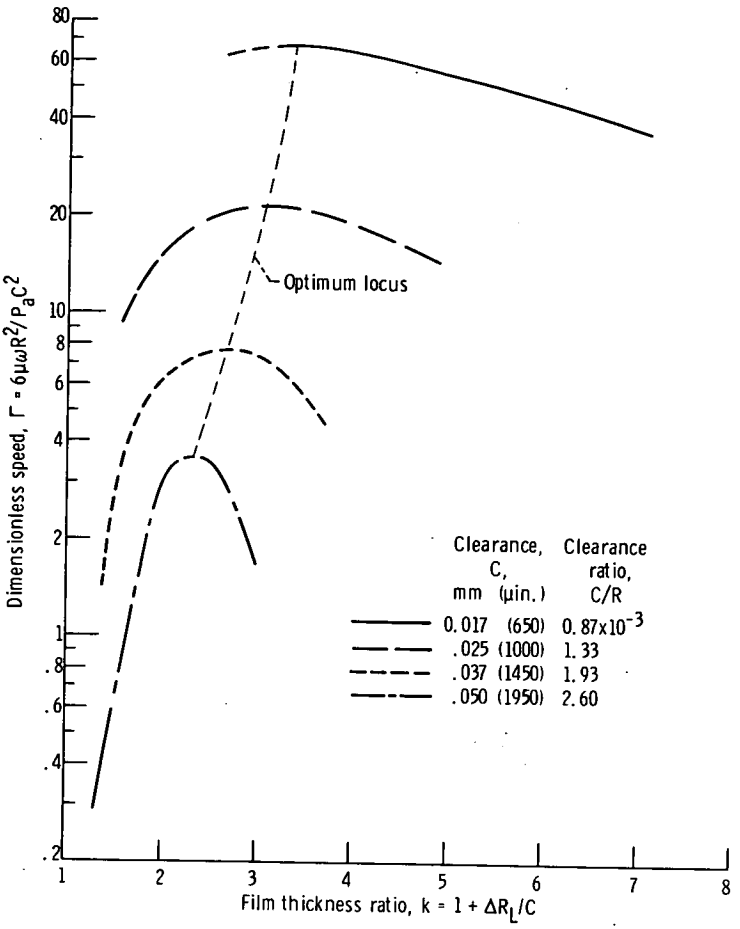

Figure 44. - Dimensionless speed as function of film thickness ratio for wholly converging-film-geometry three-lobe bearing. Offset factor, 1.0.

Three-Lobe-Bearing Geometry of Maximum Stability

The offset factor α of a lobed bearing is defined as the ratio of the arc length from the leading edge of the sector to the line along which the lobe is preloaded radially θ to the arc length of the sector β (figs. 3 and 4). Figure 45 shows a comparison of the stability of three-lobe bearings with various offset factors. Whirl speed is plotted against radial clearance for bearings of three offset factors, 0.5, 0.6, and 1.0. The points for the three-lobe bearing with offset factors of 0.5 and 1.0 cor-

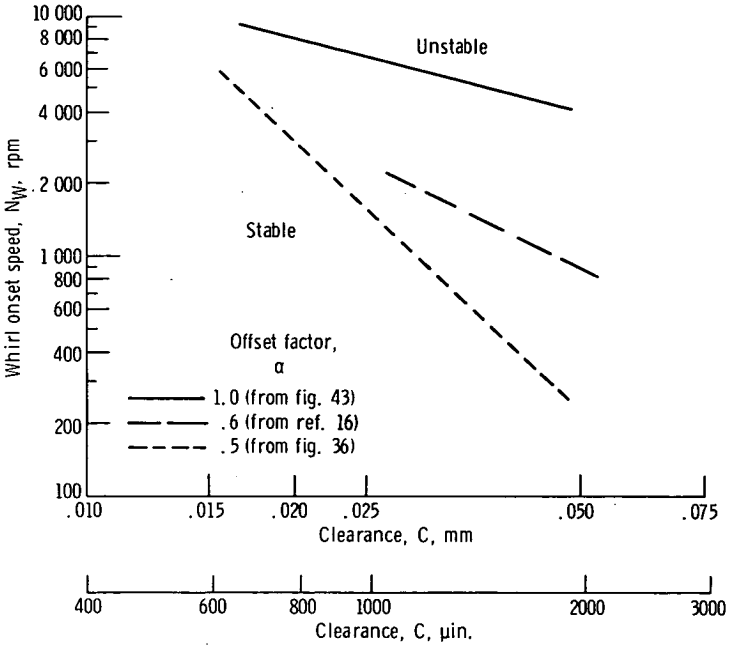

Figure 45. - Comparison of stability of three-lobe bearings at various offset factors.

respond to the points of maximum stability (optimum locus curve) obtained from figures 36 and 43, respectively. The points for the bearings with an offset factor of 0.6 were obtained in a similar manner from the experimental data of this report and reference 16. As the offset factor is increased from 0.5 to 1.0 in figure 45, the curves shift to the upper right at a shallower slope, which indicates an increase in stability and less sensitivity to clearance.

An analytical study of the three-lobe bearing was reported in reference 23, which showed that a maximum in stability for a three-lobe bearing with an $L/D = 1$ occurred at an offset factor of about 0.9. This agrees with the experimental data of figure 45, which show an offset factor of 1.0 to be more stable than an offset factor of 0.5 or 0.6.

Three-Lobe Journals Mated With Plain Bearings

The results of 50 bearing stability tests with three-lobe journals having a range of values of leading-edge entrance wedge thickness ΔR_L from 0.010 to 0.178 millimeter (400 to 7000 μin.) are shown in tables XIII to XV and figures 46 to 51. Twenty-four tests were conducted with ungrooved, three-tilted-lobe journals with an offset factor of 1.0 over a range of ΔR_L values of 0.023 to 0.178 millimeter (900 to 7000 μin.). Radial clearance C ranged from 0.015 to 0.048 millimeter (600 to 1900 μin.), as indicated in table XIII. The results of 22 stability tests on three-tilted-lobe journals with three axial grooves and an offset factor of 1.0 are shown in table XIV. The ΔR_L values ranged from 0.010 to 0.097 millimeter (400 to 3800 μin.), and the radial clearances ranged from 0.015 to 0.048 millimeter (600 to 1900 μin.). Table XV shows the results of tests on an ungrooved, three-lobe central-lobe journal (offset factor of 0.5) at four clearances ranging from 0.017 to 0.047 millimeter (650 to 1850 μin.). These tests were conducted at only one ΔR_L value of 0.023 millimeter (900 μin.).

Effect of offset factor on stability. - Figure 46 shows the experimental results obtained with a converging-diverging film and a wholly converging-film geometry. The figure shows that the wholly converging-film configuration is clearly more stable than the converging-diverging configuration, except at the higher clearance values, approximately 0.048 millimeter (1900 μin.), where their stabilities tend to be equal. Both curves were plotted from data obtained with a leading-edge entrance wedge thickness of 0.023 millimeter (900 μin.), and neither configuration had axial grooves in the journal. With a converging-diverging film shape, only a portion of the arc of each lobe, the converging-wedge portion (see fig. 5(b)), is active in generating load capacity. Increased load capacity and stability can be attained by using more of the arc of each lobe to build up pressure (ref. 12). This is accomplished by tilting the lobe on its trailing edge (fig. 5(a)). Because of the relatively poor stability of the centrally lobed journal compared with that of the tilted-lobe journal, only the tilted-lobe journal was investigated further.

Effect of journal grooving on stability. - Figure 47 shows a comparison of the stability curves for the bearings with a grooved and an ungrooved tilted-lobe journal. The grooved journal configuration was the more stable of the two for values of ΔR_L

TABLE XIII. - TEST RESULTS FOR UNGROOVED THREE-TILTED-LOBE JOURNAL CONFIGURATION

[Offset factor α, 1.0.]

Journal	Leading-edge entrance wedge thickness, ΔR_L		Bearing radial clearance, C		Fractional-frequency-whirl onset speed at zero load, N_W, rpm	Film thickness ratio, $k = 1 + \frac{\Delta R_L}{C}$
	mm	μin.	mm	μin.		
1	0.023	900	0.018	700	5350	2.29
			.031	1200	1100	1.75
			.036	1400	650	1.64
			.048	1900	130	1.47
2	0.046	1800	0.015	600	5400	4.00
			.028	1100	1600	2.64
			.033	1300	1000	2.38
			.046	1800	300	2.00
3	0.066	2600	0.018	700	5330	4.72
			.031	1200	1500	3.16
			.036	1400	1000	2.85
			.048	1900	420	2.37
4	0.097	3800	0.018	700	5400	6.43
			.031	1200	2000	4.17
			.036	1400	1600	3.72
			.048	1900	600	3.00
5	0.132	5200	0.018	700	5200	8.44
			.031	1200	2720	5.33
			.036	1400	1800	4.72
			.048	1900	700	3.74
6	0.178	7000	0.015	600	4800	12.70
			.028	1100	2500	7.37
			.033	1300	1700	6.38
			.046	1800	700	4.89

TABLE XIV. - TEST RESULTS FOR GROOVED THREE-TILTED-LOBE JOURNAL CONFIGURATION

[Offset factor α, 1.0.]

Journal	Leading-edge entrance wedge thickness, ΔR_L		Bearing radial clearance, C		Fractional-frequency-whirl onset speed at zero load, N_W, rpm	Film thickness ratio, $k = 1 + \frac{\Delta R_L}{C}$
	mm	μin.	mm	μin.		
7	0.010	400	0.015	600	4600	1.67
			.022	850	4000	1.47
			.028	1100	2700	1.36
			.033	1300	1500	1.31
			.046	1800	400	1.22
8	0.023	900	0.018	700	4600	2.29
			.024	950	4100	1.95
			.031	1200	3300	1.75
			.036	1400	2600	1.64
			.048	1900	1070	1.47
9	0.046	1800	0.015	600	4700	4.00
			.028	1100	2600	2.64
			.033	1300	1900	2.39
			.046	1800	910	2.00
10	0.066	2600	0.018	700	4100	4.72
			.031	1200	2100	3.16
			.036	1400	1400	2.85
			.048	1900	680	2.37
11	0.097	3800	0.018	700	4200	6.43
			.031	1200	2000	4.17
			.036	1400	1400	3.72
			.048	1900	600	3.00

TABLE XV. - TEST RESULTS FOR UNGROOVED THREE-CENTRAL-LOBE JOURNAL

[Journal 12; offset factor α, 0.5; leading-edge entrance wedge thickness ΔR_L, 0.018 mm (900 μin.).]

Bearing radial clearance, C		Fractional-frequency-whirl onset speed at zero load, N_W, rpm
mm	μin.	
0.017	650	340
.029	1150	190
.034	1350	160
.047	1850	150

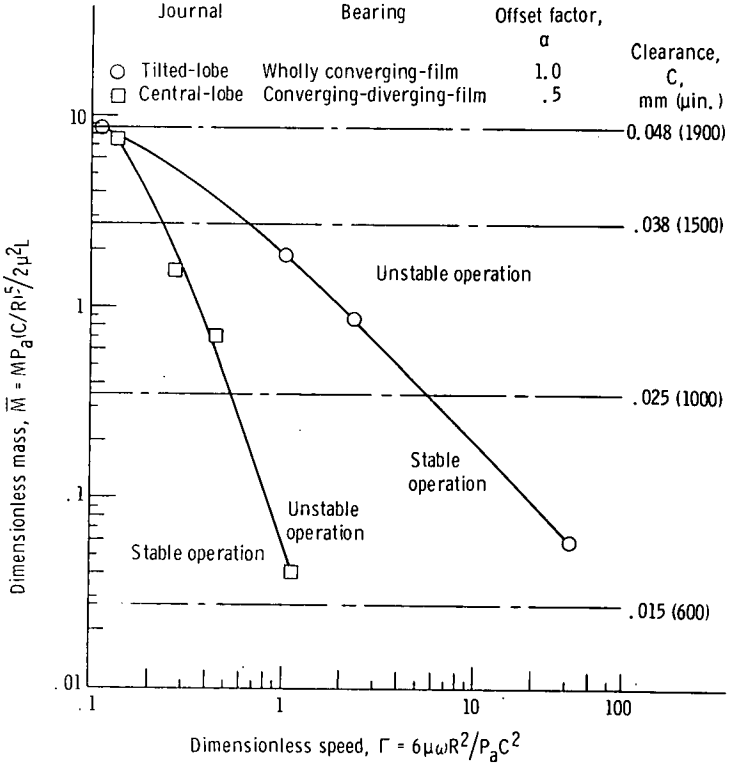

Figure 46. - Comparison of stability of wholly converging-film and converging-diverging-film configurations. Journal leading-edge entrance wedge thickness, 0.023 millimeter (900 μin.); no grooves in journals.

from 0.023 to 0.066 millimeter (900 to 2600 μin.). The difference in stability of the two configurations gradually diminished as ΔR_L was increased, until, at a ΔR_L of 0.097 millimeter (3800 μin.), the two configurations had essentially the same stability characteristics (fig. 47(d)). Evidently a bearing with a large entrance wedge film thickness ΔR_L is better able to feed itself and so is less sensitive to the presence of grooves.

Effect of leading-edge entrance wedge thickness on stability. - Figure 48 shows the effect of leading-edge entrance wedge thickness ΔR_L on the stability of the ungrooved and grooved tilted-lobe journals running in a plain bearing. For ungrooved journals (fig. 48(a)), maximum stability occurred at a ΔR_L of 0.132 millimeter (5200 μin.), as ΔR_L was varied from 0.023 to 0.178 millimeter (900 to 7000 μin.). Stability gradually increased with increased ΔR_L until a value of 0.132 millimeter (5200 μin.) was reached. Further increase in ΔR_L caused a decrease in stability, as shown by the data in figure 48(a).

The grooved journals showed stability characteristics entirely different from those for the ungrooved journals. For the grooved journals (fig. 48(b)), maximum stability occurred at a ΔR_L of 0.023 millimeter (900 μin.), as ΔR_L was varied from 0.010 to 0.097 millimeter (400 to 3800 μin.). This ΔR_L value of 0.023 millimeter (900 μin.) is only about one-sixth that of the optimum ΔR_L for the ungrooved journals (fig. 48(a)). Another difference in stability characteristics of the two different configurations was the manner in which the stability changed with changes in ΔR_L. Whereas the ungrooved journals showed a gradual change in stability with changes in ΔR_L, the stability of the grooved journals (fig. 48(b)) was generally not greatly affected by changes in ΔR_L, except for the abrupt change in stability at a ΔR_L of 0.023 millimeter (900 μin.).

Three-tilted-lobe-journal design curves. - Whirl onset speed is plotted against radial clearance in figure 49(a) for six values of ΔR_L for the grooved journal. The value of the film thickness ratio $k = 1 + (\Delta R_L/C)$, from tables XIII and XIV, is given for each data point and represents the ratio of inlet to exit film thickness in each lobe.

Figure 50, obtained from data in figure 49, shows that there is an optimum value of k at any given C for both the ungrooved and grooved journals and that this optimum is strongly dependent on C. It also shows that stability for both journal types becomes more sensitive to k as C increases. The difference in stability characteristics of the ungrooved and grooved journal configu-

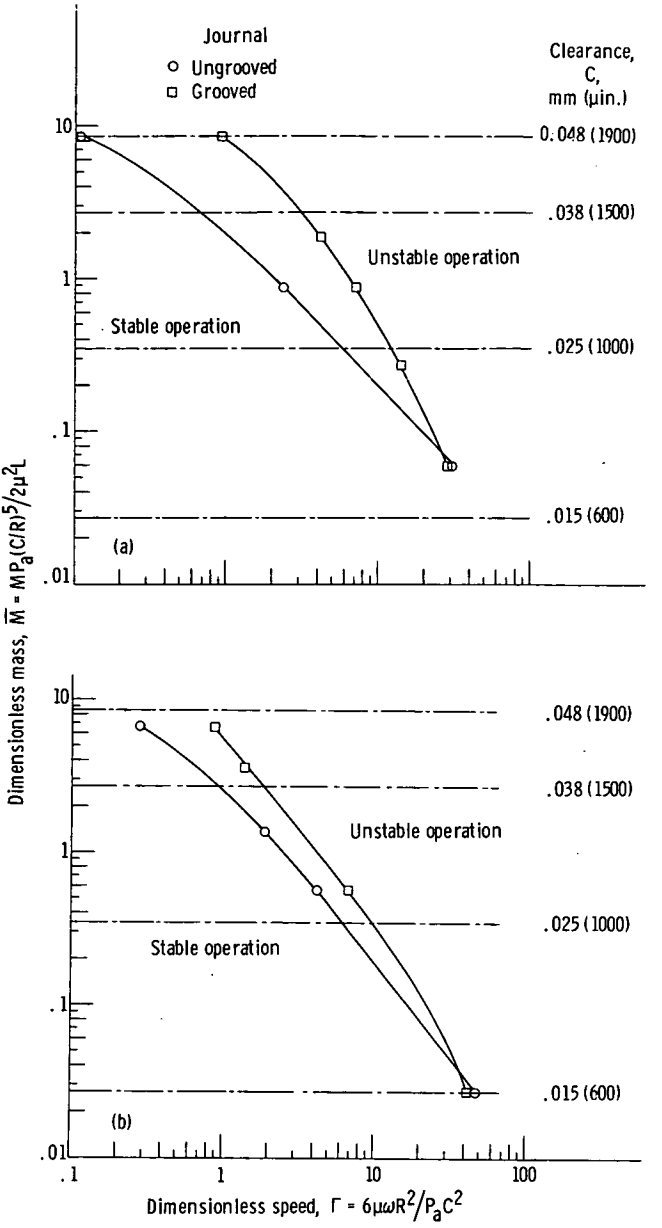

(a) Leading-edge entrance wedge thickness, 0.023 millimeter (900 μin.).

(b) Leading-edge entrance wedge thickness, 0.046 millimeter (1800 μin.).

Figure 47. - Effect of journal grooving on stability of three-tilted-lobe journal configuration at various leading-edge entrance wedge thicknesses. Offset factor, 1.0.

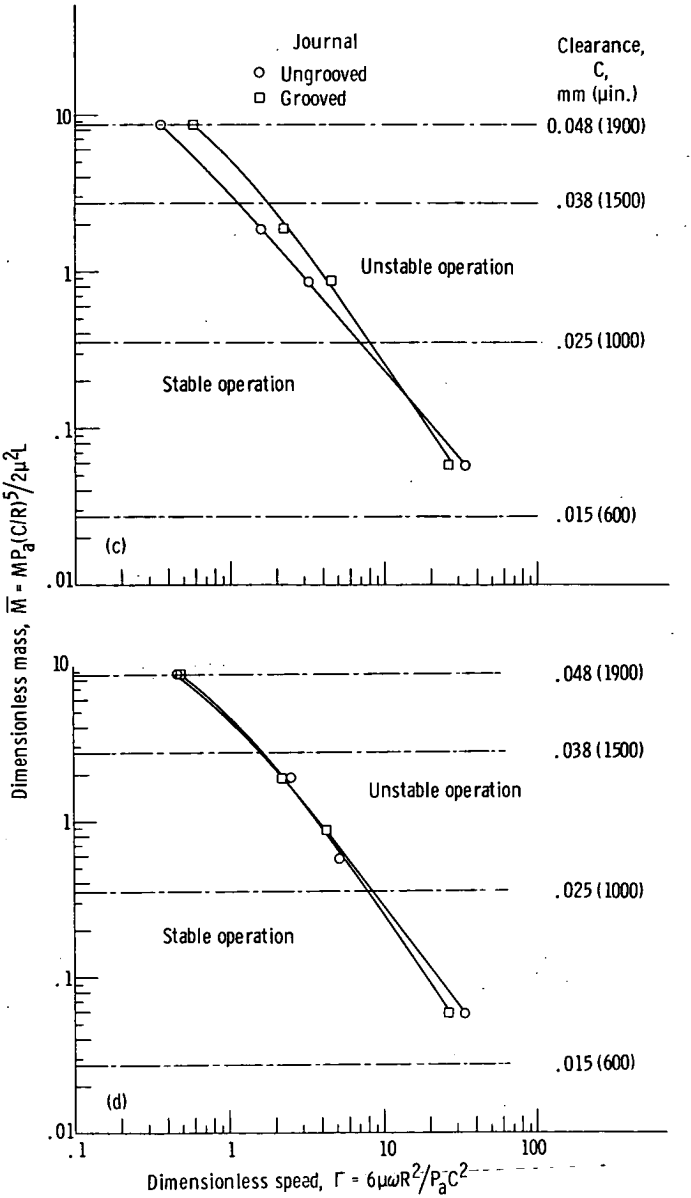

(c) Leading-edge entrance wedge thickness, 0.066 millimeter (2600 μin.).

(d) Leading-edge entrance wedge thickness, 0.097 millimeter (3800 μin.).

Figure 47. - Concluded.

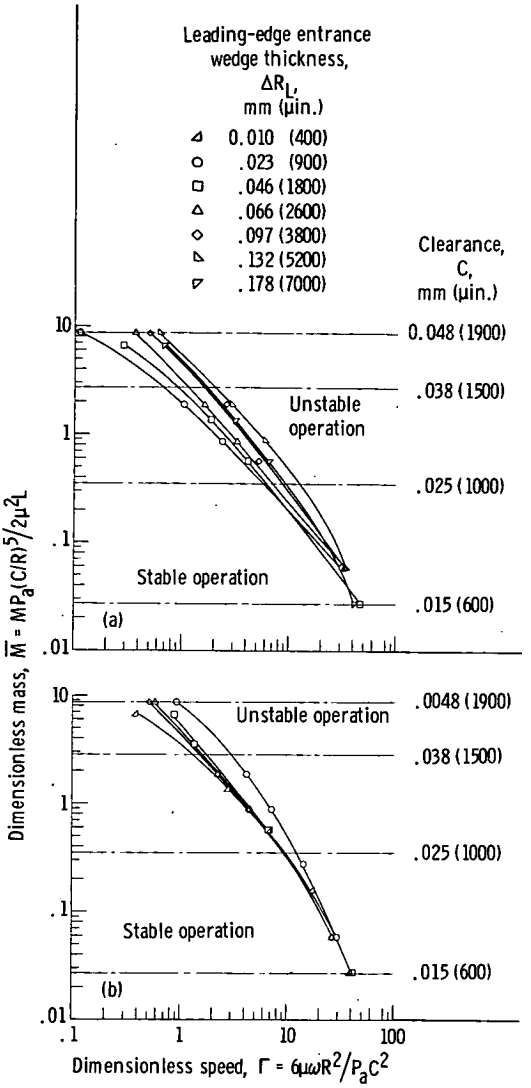

(a) Ungrooved journal.

(b) Grooved journal.

Figure 48. - Effect of leading-edge entrance wedge thickness on stability of plain bearing operating with three-tilted-lobe journal. Offset factor, 1.0.

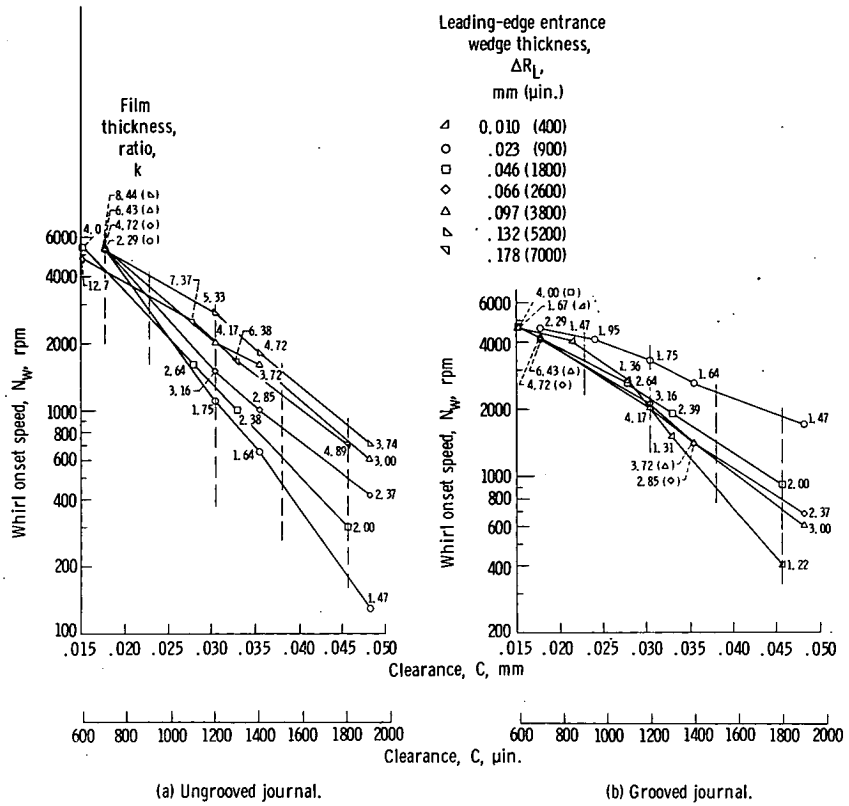

Figure 49. - Whirl onset speed as function of radial clearance for plain bearing operating with three-tilted-lobe journal at various film thickness ratios. Offset factor, 1.0.

rations is apparent in figure 50 when the magnitude and range of k for both configurations are considered. The optimum film thickness ratio k for the ungrooved journal (fig. 50(a)) decreases from 6.7 to 4.0 as the clearance increases from 0.018 to 0.046 millimeter (700 to 1800 μin.), whereas the optimum k for the grooved journal (fig. 50(b)) decreased from 1.92 to 1.55 over a similar clearance range. Except at a clearance of 0.018 millimeter (700 μin.), the stability at optimum k for the grooved journal is greater than that for the ungrooved journal over the range of clearances shown in figure 50. The stability curves for the ungrooved journal (fig. 50(a)), having much flatter peaks than those for the grooved journal (fig. 50(b)), could make the former configuration more desirable for the designer because of its lesser sensitivity to changes in the film thickness ratio, although some sacrifice in stability would result.

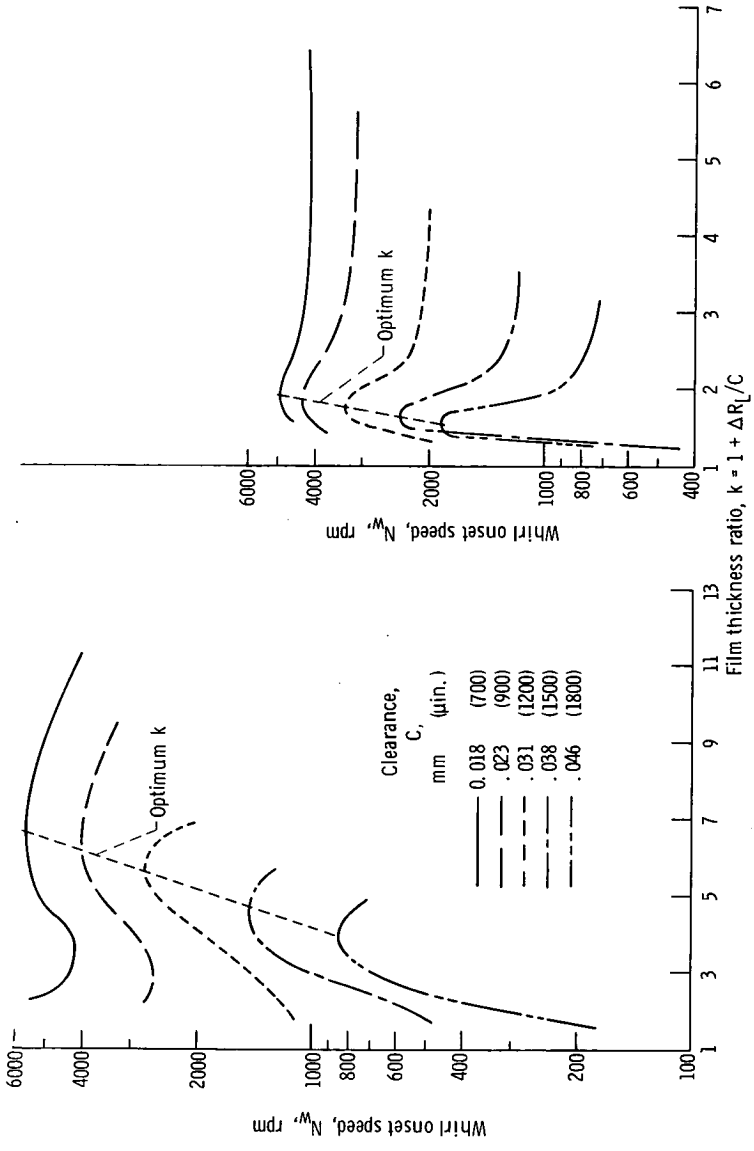

Figure 50. - Whirl onset speed as function of film thickness ratio for plain bearing operating with three-tilted-lobe journal. Offset factor, 1.0.

The reason for the upswing in the 0.018- and 0.023-millimeter- (700- and 900-μin.-) clearance curves for the ungrooved journal (fig. 50(a)), at k values of 2.3 and 2.1, respectively, is not completely clear. The upswing is probably due to slight misalinement of the bearing with the journal. With the tight clearances of 0.018 and 0.023 millimeter (700 and 900 μin.) and the small entrance wedge film thicknesses ΔR_L, which are also present at these small k values (see ref. 22), this misalinement would tend to preload the bearing and give it some added stability. At higher clearances, above 0.023 millimeter (900 μin.), and/or higher ΔR_L values (higher k), this preload would be too small to influence stability. Although these conditions exist for some points at tight clearances for the grooved journals also, there is no upswing effect in figure 50(b). The

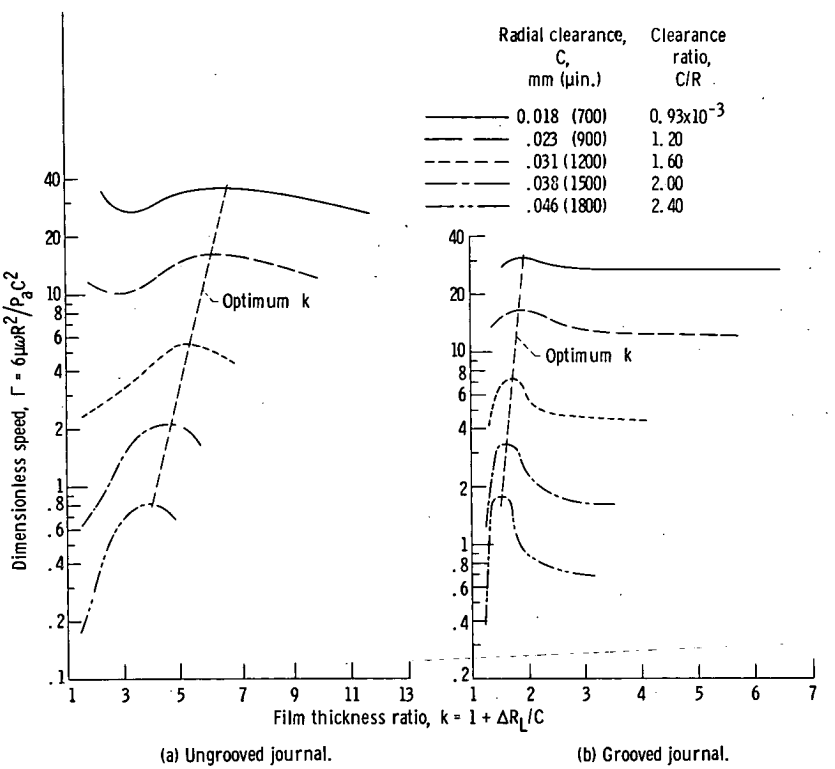

Figure 51. - Dimensionless speed as function of film thickness ratio for plain bearing operating with three-tilted-lobe journal. Offset factor, 1.0.

grooves could have had some effect on the tight clearance values to cancel any advantage in stability gained by preloading due to slight misalinement of the bearing and journal.

Figure 51 is essentially a repetition of figure 50 except that it was plotted by using the dimensionless speed parameter Γ instead of whirl onset speed N_W as the ordinate.

Stability Comparison of Four Three-Lobe Bearing Geometries

Whirl onset speed is plotted against clearance ratio C/R in figure 52 for four different fixed-geometry journal bearings.

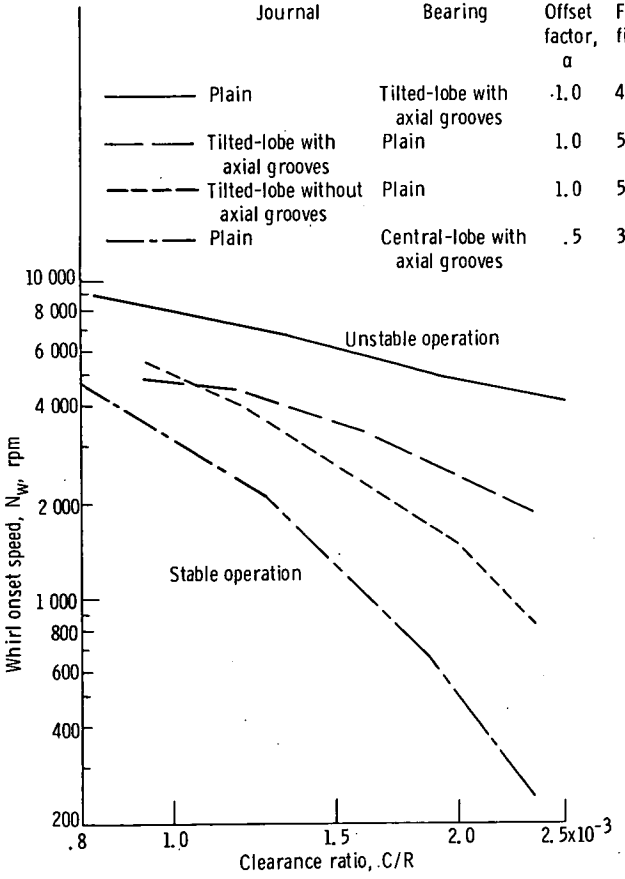

Figure 52. - Stability comparison of four three-lobe bearing geometries.

Two curves represent the stability of a lobed journal running with a plain bearing, and the other two represent a lobed bearing running with a plain journal. The data for the grooved and ungrooved three-tilted-lobe journals running with a plain bearing correspond to the points of maximum stability (optimum k curves) obtained from figure 50. The curve for the three-tilted-lobe bearing (offset factor of 1.0) with three axial grooves running with a plain journal was obtained from figure 43. The curve for the three-central-lobe bearing (offset factor of 0.5) with three axial grooves running with a plain journal was obtained from figure 36.

Figure 52 shows that the four fixed-geometry bearings considered can be generally rated in order of diminishing stability as follows: (1) three-tilted-lobe bearing with grooves (offset factor of 1.0) running with a plain journal; (2) three-tilted-lobe journal with grooves (offset factor of 1.0) running with a plain bearing; (3) three-tilted-lobe, ungrooved journal running with a plain bearing; and (4) three-central-lobe, grooved bearing running with a plain journal.

Finally, it should be mentioned that, in the tests in which the journals had tilted lobes, it was observed that the shaft speed could be increased beyond the point of initial fractional-frequency whirl without the whirl orbit growing excessively. In some cases, a shaft speed that was twice the shaft speed at initial fractional-frequency whirl was reached before any sign of bearing distress (orbit growth or unsteady torque) was observed. This may be one of the best features of the tilted-lobe journal configuration.

Stability Comparison of Five Fixed-Geometry Bearings

Whirl onset speed is plotted against clearance ratio C/R in figure 53 for five different fixed-geometry journal bearings with an L/D of unity. The data for these curves were obtained from optimum locus curves for each bearing. Figure 53 shows that the five fixed-geometry bearings considered can be generally rated in order of diminishing stability as follows: (1) three-tilted-lobe bearing (offset factor of 1.0), (2) herringbone journal mated with a plain bearing, (3) one-segment, three-pad, shrouded Rayleigh step bearing, (4) three-tilted-lobe journal with grooves (offset factor of 1.0) mated with a plain bearing, and

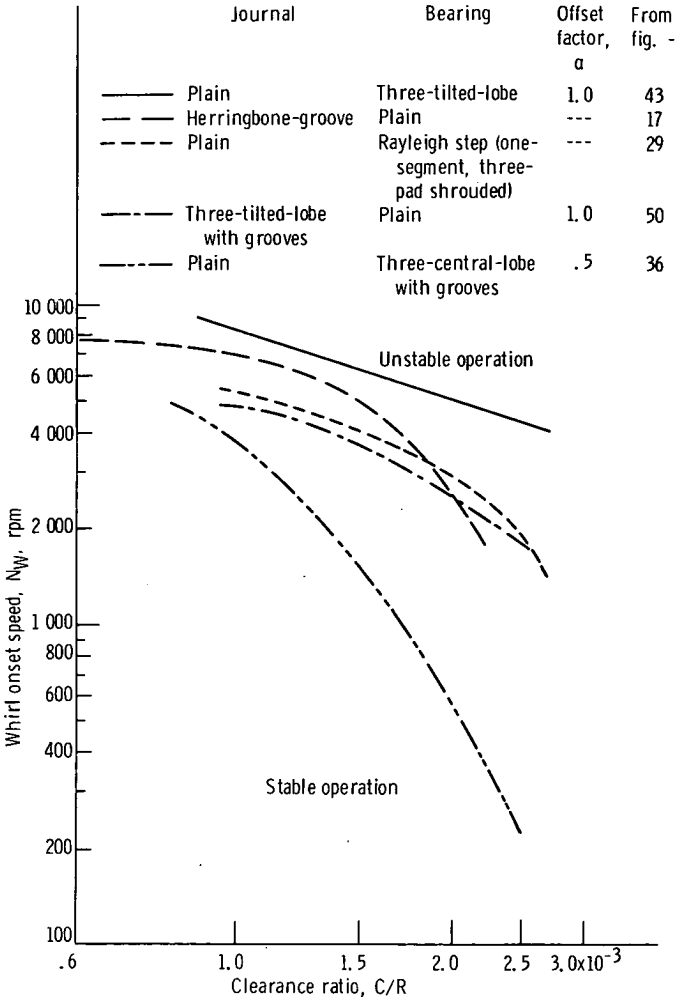

Figure 53. - Stability of five fixed-geometry bearings.

types makes it difficult to rate one above the other. The ratings almost certainly require a qualifying range of clearance to make them worthwhile.

REFERENCES

1. Schuller, Fredrick T.; Anderson, William J.; and Nemeth, Zolton: Experiments with Hydrodynamic Journal Bearings of Various Materials and Designs in Sodium at Temperatures to 800° F. Trans. ASLE, vol. 11, no. 2, Apr. 1968, pp. 140-154.
2. Sternlicht, B.; and Winn, L. W.: Geometry Effects on the Threshold of Half-Frequency Whirl in Self-Acting, Gas-Lubricated Journal Bearings. J. Basic Eng., vol. 86, no. 2, June 1964, pp. 313-320.
3. Malanoski, S. B.: Experiments on an Ultrastable Gas Journal Bearing. J. Lubr. Tech., vol. 89, no. 4, Oct. 1967, pp. 433-438.
4. Cunningham, Robert E.; Fleming, David P.; and Anderson, William J.: Experiments on Stability of Herringbone-Grooved Gas-Lubricated Journal Bearings to High Compressibility Numbers. NASA TN D-4440, 1968.
5. Vohr, J. H.; and Chow, C. Y.: Characteristics of Herringbone-Grooved, Gas-Lubricated Journal Bearings. J. Basic Eng., vol. 87, no. 3, Sept. 1965, pp. 568-578.
6. Hirs, G. G.: The Load Capacity and Stability Characteristics of Hydrodynamic Grooved Journal Bearings. Trans. ASLE, vol. 8, no. 3, July 1965, pp. 296-305.
7. Hamrock, Bernard J.; and Fleming, David P.: Optimization of Self-Acting Herringbone Journal Bearings for Maximum Radial Load Capacity. NASA TN D-6351, 1971.
8. Hamrock, Bernard J.; and Anderson, William J.: Incompressibly Lubricated Rayleigh Step Journal Bearing. I - Zero-Order Perturbation Solution. NASA TN D-4839, 1968.
9. Hamrock, Bernard J.; and Anderson, William J.: Incompressibly Lubricated Rayleigh Step Journal Bearing. II - Infinite-Length Solution. NASA TN D-4873, 1968.
10. Lund, J. W.: Rotor-Bearing Dynamics Design Technology. Part 7: The Three-Lobe Bearing and Floating Ring Bearing. Rep. MTI-67TR47, Mechanical Technology, Inc. (AFAPL-TR-65-45, pt. 7, AD-829895), Feb. 1968.

11. Marsh, Harry: The Stability of Aerodynamic Gas Bearings. Part II: Noncircular Bearings. Ph. D. Dissertation 4525, St. John's College, Cambridge, June 1964.
12. Chadbourne, L. E.; Dobler, F. X.; and Rottler, A. D.: SNAP 50/SPUR Nuclear Mechanical Power Unit Experimental Research and Development Program. Part 2: Bearings. Rep. APS-5249-R, Garrett Corp. (AFAPL-TR-67-34, pt. 2, AD-815583), Dec. 31, 1966.
13. Schuller, Fredrick T.; Fleming, David P.; and Anderson, William J.: Experiments on the Stability of Water Lubricated Herringbone-Groove Journal Bearings. I - Theoretical Considerations and Clearance Effects. NASA TN D-4883, 1968.
14. Schuller, Fredrick T.; Fleming, David P.; and Anderson, William J.: Experiments on the Stability of Water Lubricated Herringbone-Groove Journal Bearings. II - Effects of Configuration and Groove to Ridge Clearance Ratio. NASA TN D-5264, 1969.
15. Schuller, Fredrick T.: Experiments on the Stability of Water-Lubricated Rayleigh Step Hydrodynamic Journal Bearings at Zero Load. NASA TN D-6514, 1971.
16. Schuller, Fredrick T.; and Anderson, William J.: Experiments on the Stability of Water-Lubricated Three-Sector Hydrodynamic Journal Bearings at Zero Load. NASA TN D-5752, 1970.
17. Schuller, Fredrick T.: Experiments on the Stability of Water-Lubricated Three-Lobe Hydrodynamic Journal Bearings at Zero Load. NASA TN D-6315, 1971.
18. Schuller, Fredrick T.: Stability of Water-Lubricated Three-Lobe Journals Mated with Plain Bearings at Zero Load. NASA TN D-6796, 1972.
19. Hamrock, B. J.; and Anderson, W. J.: Rayleigh Step Journal Bearing. Part II - Incompressible Fluid. J. Lubr. Tech., vol. 91, no. 4, Oct. 1969, pp. 641-650.
20. Schuller, Fredrick T.: Lobing Technique for a Multilobed Bearing. NASA Case No. 11, 076, Disclosed Aug. 3, 1967.
21. Lund, J. W., ed.: Design Handbook for Fluid Film Type Bearings. Part III of Rotor-Bearing Dynamics Design Technology. Rep. MTI-65TR14, Mechanical Technology, Inc. (AFAPL TR-65-45, pt. III, AD-466392), May 1965.

22. Boeker, G. F.; and Sternlicht, B.: Investigation of Translatory Fluid Whirl in Vertical Machines. Trans. ASME, vol. 78, no. 1, Jan. 1956, pp. 13-19.
23. Falkenhagen, George L.; and Gunter, Edgar J., Jr.: Non-Linear Transient Analysis of a Rigid Rotor Supported by Non-Circular Bearings. Rep. ME-4040-102-70U, University of Virginia, June 1970.

☆U.S.Government Printing Office: 1973 — 736-990

NATIONAL AERONAUTICS AND SPACE ADMINISTRATION
WASHINGTON, D.C. 20546

OFFICIAL BUSINESS
PENALTY FOR PRIVATE USE $300

SPECIAL FOURTH-CLASS RATE
BOOK

POSTAGE AND FEES PAID
NATIONAL AERONAUTICS AND
SPACE ADMINISTRATION
451

U.S.MAIL

POSTMASTER: If Undeliverable (Section 158 Postal Manual) Do Not Return

"The aeronautical and space activities of the United States shall be conducted so as to contribute . . . to the expansion of human knowledge of phenomena in the atmosphere and space. The Administration shall provide for the widest practicable and appropriate dissemination of information concerning its activities and the results thereof."

—NATIONAL AERONAUTICS AND SPACE ACT OF 1958

NASA SCIENTIFIC AND TECHNICAL PUBLICATIONS

TECHNICAL REPORTS: Scientific and technical information considered important, complete, and a lasting contribution to existing knowledge.

TECHNICAL NOTES: Information less broad in scope but nevertheless of importance as a contribution to existing knowledge.

TECHNICAL MEMORANDUMS: Information receiving limited distribution because of preliminary data, security classification, or other reasons. Also includes conference proceedings with either limited or unlimited distribution.

CONTRACTOR REPORTS: Scientific and technical information generated under a NASA contract or grant and considered an important contribution to existing knowledge.

TECHNICAL TRANSLATIONS: Information published in a foreign language considered to merit NASA distribution in English.

SPECIAL PUBLICATIONS: Information derived from or of value to NASA activities. Publications include final reports of major projects, monographs, data compilations, handbooks, sourcebooks, and special bibliographies.

TECHNOLOGY UTILIZATION PUBLICATIONS: Information on technology used by NASA that may be of particular interest in commercial and other non-aerospace applications. Publications include Tech Briefs, Technology Utilization Reports and Technology Surveys.

Details on the availability of these publications may be obtained from:

SCIENTIFIC AND TECHNICAL INFORMATION OFFICE

NATIONAL AERONAUTICS AND SPACE ADMINISTRATION

Washington, D.C. 20546